

# Confinement of spinons in the XXZ spin-1/2 chain in presence of a transverse magnetic field

Sergei B. Rutkevich

*Fakultät für Mathematik und Naturwissenschaften,  
Bergische Universität Wuppertal, 42097 Wuppertal, Germany.*

(Dated: January 9, 2024)

We study the tuning effect of a transverse magnetic field on the confinement of spinons in the infinite XXZ spin-1/2 chain. The spinon confinement in this model takes place in the gapped antiferromagnetic phase upon application of a staggered longitudinal magnetic field. The tuning transverse magnetic field has mutually orthogonal uniform and staggered components. The energy spectra of the two-spinon bound states (the ‘mesons’) in the confinement regime are analytically calculated in this model using two different perturbative schemes. The first one applies in the extreme anisotropic (Ising) limit and employs the inverse anisotropy constant as a small parameter. The second perturbative scheme, which applies at any anisotropy in the gapped antiferromagnetic domain, exploits the integrability of the XXZ spin chain at zero magnetic field. The small parameters in the second technique are the components of the transverse, and staggered longitudinal magnetic fields. It is shown, that the weak transverse magnetic field mixes the transverse and longitudinal meson modes, and leads to an avoided crossing of their energies upon increase of its strength. The explicit formulas for the two-spinon contribution to the dynamical structure factors of local spin operators are obtained as well in this model in the weak confinement regime for wave-vectors close to the points  $k = 0$  and  $k = \pi$ .

## I. INTRODUCTION

The phenomenon of confinement is commonly associated with high energy physics [1]. The problem of a consistent description of the quark confinement in hadrons in the frame of quantum chromodynamics (QCD) in four-dimensional space-time remains to be one of the most long-standing challenging problems in theoretical physics. The difficulty of this problem stems from the intrinsic non-perturbative nature of the quark confinement, and from the lack of clear understanding of its physical mechanism in QCD in four dimensions.

Confinement of elementary excitations takes place also in certain two-dimensional quantum field theories (QFT) and spin-chain models. It is worth to note, that the confinement in such models is provided by a rather simple and well understood mechanism, which cannot be responsible for the color confinement in the four-dimensional QCD. Nevertheless, studying the confinement in the two-dimensional space-time can give a useful insight into some aspect of the quark confinement in the high energy physics, see e.g. [2, 3]. Note also, that the two-particle bound states of the two-dimensional QFT and spin-chain models in the confinement regime are often referred to as “mesons”, due to the analogy with QCD.

It was shown by ’t Hooft in 1974 [3], that the quarks in two-dimensional QCD with an infinite number of colors are confined forming the mesons, whose masses are exactly determined by the Bethe-Salpeter equation.

In 1978, McCoy and Wu [4] studied the effect of uniform magnetic field  $h$  on the particle content of the Ising field theory (IFT) in the two-dimensional space-time. At zero magnetic field  $h = 0$ , this relativistic field theory

has two degenerate vacua in the ferromagnetic phase due to spontaneous breaking of the  $\mathbb{Z}_2$ -symmetry, and kinks interpolating between these vacua as elementary excitations. McCoy and Wu showed in [4], that the magnetic field  $h > 0$  explicitly breaking the  $\mathbb{Z}_2$ -symmetry of the model Hamiltonian, induces a linear attractive potential acting between neighboring kinks, which were initially free at  $h = 0$ . The strength of the linear attractive potential  $U(x) = f|x|$  is characterized by the positive “string tension”  $f \sim h$ . Treating the two kinks as non-relativistic fermions with dispersion law

$$\omega_0(p) = m_0 + \frac{p^2}{2m_0}, \quad (1)$$

McCoy and Wu obtained [4] for the masses of the “lightest mesons” (the energies of the two-kink bound states with zero total momentum) at small  $h > 0$  the simple formula:

$$E_n = E_0 + \alpha z_n, \quad \text{with } n = 1, 2, 3, \dots, \quad (2)$$

where  $E_0 = 2m_0$ ,  $\alpha = f^{2/3}m_0^{-1/3}$ , and the numbers  $-z_n$  are the zeros of the Airy function,  $\text{Ai}(-z_n) = 0$ .

To our knowledge, the first study of the confinement of magnetic excitations in the spin-chain models was reported by Shiba [5] in 1980. He considered the antiferromagnetic XXZ spin-1/2 chain model in the presence of a staggered longitudinal magnetic field in the limit of the strong uniaxial anisotropy, and calculated the energy spectra of the two-kink bound states (“the Zeeman ladder”) by means of a strong-coupling expansion. Shiba also suggested, that the effective staggered field, that induces the kink confinement, can arise at low

temperatures in the quasi-one-dimensional (1D) uniaxial antiferromagnetic crystals due to a weak interchain interaction in the three-dimensionally ordered antiferromagnetic phase. Note, that since the kinks in the antiferromagnetic XXZ spin chain carry spin  $\pm 1/2$ , they are also often called ‘spinons’. We shall use both terms as synonyms.

The spinon confinement provided by the outlined above physical mechanism was observed later in inelastic neutron scattering [6, 7] and terahertz spectroscopy [8, 9] experiments in the quasi-1D spin-1/2 antiferromagnetic compounds  $\text{BaCo}_2\text{V}_2\text{O}_8$  and  $\text{SrCo}_2\text{V}_2\text{O}_8$  with Heisenberg-Ising (XXZ) anisotropy. However, though Shiba’s theory based on a strong-coupling expansion gives a useful starting point for the understanding of some qualitative features of the spinon confinement in such magnetic crystals, it could not provide a quantitative description of the observed energy spectra of the spinon bound states, since the uniaxial anisotropy in the studied compounds is rather moderate. This is why the experimentally observed energy spectra of the spinon bound states in the confinement regime were usually interpreted in terms of the simple phenomenological McCoy-Wu formula (2) with fitting parameters  $E_0$  and  $\alpha$ , or compared with the results of direct calculations of the energy spectra in the appropriate spin-chain model by means of different numerical techniques [6–8, 10].

In the recent paper [11], we described analytic perturbative calculations of the meson energy spectra in the gapped antiferromagnetic XXZ spin-chain model at any value of the easy-axis anisotropy in the *weak confinement regime*, which is realized in this model in the presence of a weak staggered magnetic field  $h_z$  parallel to the magnetic easy axis  $z$ . Preliminary results of this work were published in [12]. Two different perturbative techniques have been used in [11]. Both techniques exploit the integrability of the XXZ spin-1/2 chain model in the deconfined phase at  $h_z = 0$  and use the staggered magnetic field  $h_z > 0$  in the confinement regime as a small parameter.

The first more rigorous and systematic technique is based on a perturbative analysis of the Bethe-Salpeter equation, which was derived for the XXZ spin-chain model in [11]. For the IFT, the analogous Bethe-Salpeter equation was obtained and studied previously by Fonseca and Zamolodchikov [13, 14].

The second so-called *semiclassical technique* is not rigorous, but rather heuristic and intuitive. It can be viewed as a generalization of McCoy and Wu’s scenario of confinement to systems, in which the kinks in the deconfined phase (i) have a non-quadratic dispersion law, and (ii) are not free, but can interact at short distances. Initially this technique was introduced in [14, 15] in order to interpret the mass spectrum of heavy mesons in the Ising field theory. Later the semiclassical technique was successfully applied to the calculation of the meson energy spectra in different two-dimensional QFT and spin-chain models exhibiting confinement [12, 16–21]. As in the McCoy and Wu picture, the two kinks forming a meson are treated in

this approach as classical particles, that move along the line and attract one another with a linear potential. However, the kinetic energy of these classical particles is now not quadratic in their momenta, but is given by the kink dispersion law in the deconfined phase. The meson energy spectrum in this approach is determined by means of the semiclassical quantization from the Bohr-Sommerfeld quantization rule. If the kinks interact at short distances already in the deconfined phase, their pair interaction is accounted for their non-trivial two-particle scattering phase, which is added in this approach to the left-hand side of the Bohr-Sommerfeld quantization condition.

It was shown in [11], that to leading order in the staggered magnetic field  $h_z$ , the two perturbative techniques outlined above lead to the same result for the meson energy spectra in the antiferromagnetic XXZ spin-chain model.

In this paper, we continue to study kink confinement in the gapped antiferromagnetic XXZ spin chain induced by the longitudinal staggered magnetic field. Here we address the problem of the effect of a weak external transverse magnetic field on the energy spectrum and spin polarization of the meson states. Our interest in this subject is motivated by recent experimental studies [8–10, 22–28] of the influence of external magnetic fields on the magnetic properties of the quasi-1D antiferromagnetic compounds  $\text{BaCo}_2\text{V}_2\text{O}_8$  and  $\text{SrCo}_2\text{V}_2\text{O}_8$ . Besides a number of phase transitions triggered by strong enough magnetic fields, a substantial modification of the magnetic excitations induced by the weak external magnetic fields was observed. It turns out, that the weak longitudinal and transverse uniform external magnetic fields act in a very different way on the meson energy spectra in the confinement regime. It was reported in [8–10], that the weak longitudinal (parallel to the Ising axis) magnetic field leads to a simple Zeeman splitting of the meson energies, which is linear in the applied field. In contrast, the variation of the meson energy spectra with the applied transverse magnetic field measured in  $\text{BaCo}_2\text{V}_2\text{O}_8$  in the inelastic neutron scattering [10] and terahertz spectroscopic experiments [27] displays a rather peculiar non-linear dependence. In particular, it was observed in [10], that the transverse and longitudinal meson modes, which are characterized at zero transverse magnetic field by the  $z$ -projection of the spin  $s = \pm 1$ , and  $s = 0$ , respectively, hybridize upon increase of the applied transverse field. Avoided crossing of the energy curves of different meson modes with increasing transverse field was detected as well.

While the impact of a strong transverse magnetic field on the properties of quasi-1D antiferromagnetic crystals has been thoroughly studied in literature [26, 27, 29–32], the observed effect of a weak transverse field on the magnetic excitations in such crystals in the confinement regime is much less understood and requires theoretical explanations. The goal of this work is to show, that the unusual features of the spin dynamics observed in [10] in  $\text{BaCo}_2\text{V}_2\text{O}_8$  in the presence of the weak transverse

magnetic field can be understood in the frame of properly modified analytic perturbation-theory-technique developed in [11, 12]. Here we apply these techniques to the XXZ spin chain Hamiltonian in the gapped antiferromagnetic phase perturbed not only by the staggered longitudinal, but also by the transverse uniform and transverse staggered magnetic fields. The necessity to account for the effective transverse staggered field stems from the fact, that the latter arises [10, 22] in the magnetic ion chains in the crystal  $\text{BaCo}_2\text{V}_2\text{O}_8$  upon application of an external uniform transverse field due to the non-diagonal  $g_{xy}$ -component of the Landé tensor.

As in the previous papers, [11, 12], we perform perturbative calculations of the meson energy spectra in two different asymptotic regimes: (i) in the extreme anisotropic (Ising) limit, and (ii) at weak magnetic fields at generic values of the anisotropy parameter. In the second regime, the dynamical structure factors (DSF) of the local spin operators are calculated as well. The obtained meson spectra display in both regimes qualitatively similar non-linear dependences on the transverse magnetic field with avoided crossings of the neighboring in energy dispersion curves.

The rest of the paper is organized as follows. In the next section, we describe the Hamiltonian of the XXZ spin chain perturbed by magnetic fields of different nature: staggered and uniform, transverse and longitudinal. We recall there also the well-known discrete-symmetry properties of the XXZ spin chain at zero magnetic field. Section III contains the perturbative calculation of the meson energy spectra in the XXZ spin chain in the limit of strong anisotropy  $\Delta \rightarrow -\infty$  for arbitrary fixed values of the staggered longitudinal and mutually orthogonal staggered and uniform transverse magnetic fields.

In Secs. IV-X, the anisotropy parameter is taken at a generic value in the domain  $\Delta < -1$ , corresponding to the gapped antiferromagnetic phase. In these sections, exploiting integrability of the XXZ spin chain at zero magnetic field, we use the components of the applied magnetic fields as small parameters in perturbative calculations, which are performed in two steps. First, we keep the staggered longitudinal field at zero value, and study in Secs. IV, V, and VI, the effect of the weak transverse uniform and staggered magnetic fields on the ground states, one-, and two-kink excitations, respectively. Next, we switch on the weak staggered longitudinal magnetic field inducing the confinement of kinks, which become coupled into the meson bound states. In Section VII, we describe, how the classification and symmetry properties of the resulting meson states are effected by the presence of the mutually orthogonal uniform and staggered transverse magnetic fields. The meson energy spectra for this magnetic field configuration are studied in Secs. VIII, IX by means of the semiclassical perturbative technique [12]. The effect of the weak transverse magnetic fields on the DSF of local spin operators in the confinement regime is studied in Section X. The obtained analytical results are compared in Section XI with the re-

sults of the inelastic neutron scattering experiments on the antiferromagnetic crystals  $\text{BaCo}_2\text{V}_2\text{O}_8$  reported by Faure *et al.* [10]. Concluding remarks are presented in Section XII. Finally, there are two Appendixes. In Appendix A, we collect the well-known explicit formulas for the two-kink scattering amplitudes and for the two-kink form factors of the spin operators. Appendix B contains the details of some technical calculations relegated from Section IX.

## II. MODEL

In this section, we introduce several Hamiltonians of the XXZ spin-1/2 chain model, which is deformed in different ways by external magnetic fields. The models defined by these Hamiltonians will be studied in the subsequent sections by means of different perturbative techniques.

The most general Hamiltonian of the infinite XXZ spin-1/2 chain in the presence of both uniform and staggered magnetic fields can be written in the form:

$$\mathcal{H}_{XXZ} = \mathcal{H}_0 + V, \quad (3)$$

where

$$\mathcal{H}_0 = -\frac{1}{2} \sum_{j=-\infty}^{\infty} (\sigma_j^x \sigma_{j+1}^x + \sigma_j^y \sigma_{j+1}^y + \Delta \sigma_j^z \sigma_{j+1}^z), \quad (4)$$

$$V = - \sum_{j=-\infty}^{\infty} \sum_{\mathbf{a}=x,y,z} [(-1)^j h_{1\mathbf{a}} + h_{2\mathbf{a}}] \sigma_j^{\mathbf{a}}. \quad (5)$$

Here the index  $j$  enumerates the spin-chain sites,  $\sigma_j^{\mathbf{a}}$  are the Pauli matrices,  $\mathbf{a} = x, y, z$ , and  $\Delta$  is the anisotropy parameter. The “-” sign in front of the right-hand side in (4) is the subject of convention, since it can be changed to “+” by a certain unitary transformation of the Hamiltonian, see equations (259), (262) below. In our choice of this sign we follow the convention widely accepted in the literature devoted to the algebraic approach to the XXZ spin-chain model, see e.g. [33, 34]. The anisotropy constant will be taken throughout this paper in the interval  $\Delta < -1$ , and parametrized in the usual way:

$$\Delta = (q + q^{-1})/2 = -\cosh \eta, \quad (6)$$

$$q = -\exp(-\eta) \in (-1, 0), \quad \eta > 0. \quad (7)$$

We will use also the notation  $S^{\mathbf{a}}$  for the projection of the total spin operator on the  $\mathbf{a}$ -axis:

$$S^{\mathbf{a}} = \frac{1}{2} \sum_{j=-\infty}^{\infty} \sigma_j^{\mathbf{a}}. \quad (8)$$

The XXZ spin chain at zero magnetic field defined by the Hamiltonian (4) is integrable. In the gapped antiferromagnetic phase at  $\Delta < -1$ , it has two ground states

$|vac\rangle^{(1)}$  and  $|vac\rangle^{(0)}$ , which display Néel-type order:

$${}^{(1)}\langle vac|\sigma_j^z|vac\rangle^{(1)} = (-1)^j \bar{\sigma}, \quad (9)$$

$${}^{(0)}\langle vac|\sigma_j^z|vac\rangle^{(0)} = -(-1)^j \bar{\sigma}, \quad (10)$$

with the staggered spontaneous magnetization [35–37]

$$\bar{\sigma}(\eta) = \prod_{n=1}^{\infty} \left( \frac{1 - e^{-2n\eta}}{1 + e^{-2n\eta}} \right)^2. \quad (11)$$

The elementary excitations in this regime are the kinks interpolating between these two vacuums.

The XXZ spin chain (3) remains also integrable, if solely the longitudinal uniform magnetic field  $h_{2z}$  is applied. In the presence of any other magnetic field  $h_{ia}$ , with  $i \neq 2$ , and  $\mathbf{a} \neq z$ , model (3) becomes non-integrable. In the latter case, it can be studied either by direct numerical methods, or by different analytic perturbative techniques.

The confinement regime in model (3) takes place upon application of the staggered longitudinal magnetic field  $h_{1z} > 0$ . In the case, when all other components  $h_{ia}$  in (5) are zero, the meson energy spectra in model (3) were studied in [5, 11, 12]. It was shown in [11], that the meson states  $|\pi_{s,\iota,n}(P)\rangle$  in this case can be classified by the quasimomentum  $P \in [0, \pi)$ , the spin  $s = 0, \pm 1$ , the parity  $\iota = 0, \pm$ , and the natural number  $n = 1, 2, \dots$ . The quantum numbers  $\iota$  and  $s$  are not independent:  $\iota = 0$  for  $s = \pm 1$ , and  $\iota = \pm$ , for  $s = 0$ . The meson states  $|\pi_{s,\iota,n}(P)\rangle$  satisfy the following equations (see equations (125) in [11]):

$$\mathcal{H}_1(h_{1z})|\pi_{s,\iota,n}(P)\rangle = E_{\iota,n}(P)|\pi_{s,\iota,n}(P)\rangle, \quad (12a)$$

$$T_1^2|\pi_{s,\iota,n}(P)\rangle = e^{2iP}|\pi_{s,\iota,n}(P)\rangle, \quad (12b)$$

$$S^z|\pi_{s,\iota,n}(P)\rangle = s|\pi_{s,\iota,n}(P)\rangle. \quad (12c)$$

Here  $T_1$  is the one-site translation operator defined below by equation (20), and the Hamiltonian  $\mathcal{H}_1(h_{1z})$  is defined as follows:

$$\mathcal{H}_1(h_{1z}) = \mathcal{H}_0 - \sum_{j=-\infty}^{\infty} [(-1)^j h_{1z} \sigma_j^z + c(h_{1z})]. \quad (13)$$

The constant  $c(h_{1z})$  in the right-hand side is chosen in such a way, that the ground-state energy of the Hamiltonian (13) vanishes.

It is easy to understand, how the application of the uniform longitudinal magnetic field  $h_{2z}$  effects the meson energy spectra. Really, since

$$[S^z, \mathcal{H}_1(h_{1z})] = 0,$$

the Hamiltonian

$$\mathcal{H}_2(h_{1z}, h_{2z}) = \mathcal{H}_1(h_{1z}) - 2h_{2z} S^z \quad (14)$$

has the same set of eigenstates, as  $\mathcal{H}_1(h_{1z})$ , and

$$\mathcal{H}_2(h_{1z}, h_{2z})|\pi_{s,\iota,n}(P)\rangle = [E_{\iota,n}(P) - 2h_{2z}s]|\pi_{s,\iota,n}(P)\rangle. \quad (15)$$

Therefore, the uniform longitudinal magnetic field  $h_{2z}$  has no effect on the energies of the meson modes with  $s = 0$ , while the two modes with  $s = \pm 1$ , which were degenerate in energy at  $h_{2z} = 0$ , get the linear Zeeman splitting at  $h_{2z} > 0$ . Such longitudinal field dependences of the meson modes energies were indeed observed in the neutron scattering [10] and high-resolution terahertz spectroscopic [9] experiments on the compound  $\text{BaCo}_2\text{V}_2\text{O}_8$ .

In the rest of this paper we will concentrate on the case of the zero uniform longitudinal magnetic field in the Hamiltonian (3)-(5),  $h_{2z} = 0$ . The subsequent analysis of the tuning effect of the transverse magnetic field on the spinon confinement will be limited to the case, in which the uniform and staggered transverse magnetic fields are mutually orthogonal. The reason is twofold. First, the classification of the meson states and perturbative calculations of their energy spectra become easier in this case. Second, according to [10, 22], it is relevant to the experimental situation in the compound  $\text{BaCo}_2\text{V}_2\text{O}_8$ .

So, in the study of the spinon confinement, we will restrict our attention in this paper to the Hamiltonian (3)-(5) with  $h_{2z} = h_{1x} = h_{2y} = 0$ . In order to simplify notations, we rewrite this Hamiltonian in the equivalent form:

$$\mathcal{H}(\Delta, \mathbf{h}_t, h_z) = \mathcal{H}_0(\Delta) + V_t(\mathbf{h}_t) + V_l(h_z), \quad (16)$$

$$V_t(\mathbf{h}_t) = - \sum_{j=-\infty}^{\infty} [h_2 \sigma_j^x + (-1)^j h_1 \sigma_j^y], \quad (17)$$

$$V_l(h_z) = -h_z \sum_{j=-\infty}^{\infty} (-1)^j \sigma_j^z. \quad (18)$$

where  $\mathbf{h}_t = h_2 \mathbf{e}_x + h_1 \mathbf{e}_y$ .

To conclude this section, we describe, following essentially Lukyanov and Terras [34], the set of the discrete-symmetry operators, which will be important for the subsequent analysis.

The Hamiltonians (3) and (16) act in the vector space  $\mathcal{L} = \otimes_{j=-\infty}^{\infty} \mathbb{C}_j^2$  spanned by the basis states

$$|\mathcal{E}\rangle = \otimes_{j=-\infty}^{\infty} e_{j,s_j} = \dots \otimes e_{-1,s_{-1}} \otimes e_{0,s_0} \otimes e_{1,s_1} \otimes \dots, \quad (19)$$

with  $s_j = \pm 1$ , such that

$$\sigma_j^z |\mathcal{E}\rangle = s_j |\mathcal{E}\rangle.$$

The discrete-symmetry operators are defined by their action on the basis vectors  $|\mathcal{E}\rangle$  as follows.

1. The translation (shift) operator by one chain site  $T_1$ :

$$T_1 |\mathcal{E}\rangle = \otimes_{j=-\infty}^{\infty} e_{j,s_{j+1}}. \quad (20)$$

2. ‘Charge conjugation operators’  $\mathbb{C}_a = \otimes_{j=-\infty}^{\infty} \sigma_j^a$ , with  $\mathbf{a} = x, y, z$ . In particular, the operator  $\mathbb{C}_x$  acts on the basis state (19) as:

$$\mathbb{C}_x |\mathcal{E}\rangle = \otimes_{j=-\infty}^{\infty} e_{j,-s_j}.$$

3. We shall use two modified translation operators by one chain site:

$$\tilde{T}_1 = T_1 \mathbb{C}_x, \quad (21)$$

$$\check{T}_1 = T_1 \mathbb{C}_y. \quad (22)$$

4. The time inversion is the anti-unitary operators  $\mathbb{T}$ , that acts trivially on the basis states:  $\mathbb{T}|\mathfrak{E}\rangle = |\mathfrak{E}\rangle$ . The following equality

$$\mathbb{T}(c|\psi\rangle) = c^* \mathbb{T}|\psi\rangle, \quad (23)$$

holds for any  $|\psi\rangle \in \mathcal{L}$ , and a complex number  $c$ .

5. Two spatial reflection operators  $\mathbb{P}_{ev}$ , and  $\mathbb{P}_{odd} = T_1 \mathbb{P}_{ev}$ :

$$\mathbb{P}_{odd}|\mathfrak{E}\rangle = \otimes_{j=-\infty}^{\infty} e_{j,s-j}, \quad (24)$$

$$\mathbb{P}_{ev}|\mathfrak{E}\rangle = \otimes_{j=-\infty}^{\infty} e_{j,s_{1-j}}. \quad (25)$$

These operators act on the Pauli matrices as follows:

$$T_1^{-1} \sigma_j^a T_1 = \sigma_{j+1}^a, \quad (26a)$$

$$\mathbb{C}_x \sigma_j^a \mathbb{C}_x = e^{i\pi d_a} \sigma_j^a, \quad (26b)$$

$$\mathbb{C}_y \sigma_j^a \mathbb{C}_y = e^{i\pi \check{d}_a} \sigma_j^a, \quad (26c)$$

$$\tilde{T}_1^{-1} \sigma_j^a \tilde{T}_1 = e^{i\pi d_a} \sigma_{j+1}^a, \quad (26d)$$

$$\check{T}_1^{-1} \sigma_j^a \check{T}_1 = e^{i\pi \check{d}_a} \sigma_{j+1}^a, \quad (26e)$$

$$\mathbb{T} \sigma_j^x \mathbb{T} = \sigma_j^x, \quad \mathbb{T} \sigma_j^y \mathbb{T} = -\sigma_j^y, \quad \mathbb{T} \sigma_j^z \mathbb{T} = \sigma_j^z, \quad (26f)$$

$$\mathbb{P}_{odd} \sigma_j^a \mathbb{P}_{odd} = \sigma_{-j}^a, \quad \mathbb{P}_{ev} \sigma_j^a \mathbb{P}_{ev} = \sigma_{1-j}^a, \quad (26g)$$

where  $d_x = 0$ ,  $d_y = d_z = 1$ ,  $\check{d}_y = 0$ , and  $\check{d}_x = \check{d}_z = 1$ .

The Hamiltonian  $\mathcal{H}_0$  of the infinite XXZ spin chain at zero magnetic field commutes with the operator  $S^z$ , and with all discrete symmetry operators listed above. In the antiferromagnetic phase  $\Delta < -1$ , some of these symmetries are spontaneously broken, and the two ground states  $|vac\rangle^{(1)}$ ,  $|vac\rangle^{(0)}$  of the Hamiltonian  $\mathcal{H}_0$  have the following properties:

$$\mathcal{H}_0 |vac\rangle^{(\mu)} = E_{vac}^{(0)} |vac\rangle^{(\mu)}, \quad (27a)$$

$$\langle {}^{(1)}vac | \sigma_0^z | vac \rangle^{(1)} = \bar{\sigma} = - \langle {}^{(0)}vac | \sigma_0^z | vac \rangle^{(0)}, \quad (27b)$$

$$T_1 |vac\rangle^{(\mu)} = |vac\rangle^{(1-\mu)}, \quad (27c)$$

$$\mathbb{C}_x |vac\rangle^{(\mu)} = |vac\rangle^{(1-\mu)}, \quad (27d)$$

$$\mathbb{P}_{ev} |vac\rangle^{(\mu)} = |vac\rangle^{(1-\mu)}, \quad (27e)$$

$$\mathbb{C}_x \mathbb{T} |vac\rangle^{(\mu)} = |vac\rangle^{(1-\mu)}, \quad (27f)$$

$$\tilde{T}_1 |vac\rangle^{(\mu)} = |vac\rangle^{(\mu)}, \quad (27g)$$

$$\mathbb{T} |vac\rangle^{(\mu)} = |vac\rangle^{(\mu)}, \quad (27h)$$

$$\mathbb{P}_{odd} |vac\rangle^{(\mu)} = |vac\rangle^{(\mu)}, \quad (27i)$$

where  $\mu = 0, 1$ . The ground state energy  $E_{vac}^{(0)}$  of the Hamiltonian  $\mathcal{H}_0$  is proportional to the number of sites in the spin chain, which becomes infinite in the thermodynamic limit.

### III. ISING LIMIT $\Delta \rightarrow -\infty$

In this section we describe the perturbative calculation of the meson energy spectra in the confinement regime for the model defined by the Hamiltonian (16) in the strong-anisotropy (Ising) limit  $-\Delta \gg 1$  to linear order in  $|\Delta|^{-1}$ . To this end, we use the strong-coupling expansion method developed by Ishimura and Shiba [38]. Though the strong-anisotropy condition  $|\Delta|^{-1} \ll 1$  is not satisfied in real quasi-1D antiferromagnetic crystals, the results obtained by means of the strong-coupling expansion provide a useful insight into the qualitative picture of the spinon confinement tuned by transverse magnetic field.

In the Ising limit  $\Delta \rightarrow -\infty$ , it is convenient to rescale the Hamiltonian (16) and to add to it a suitable (infinite in the thermodynamic limit) constant:

$$\begin{aligned} \mathcal{H}_I(\varepsilon, \mathbf{h}_t, h_z) &= |\Delta|^{-1} \mathcal{H}(\Delta, \mathbf{h}_t, h_z) + Const \\ &= \mathcal{H}_I^{(0)} + \varepsilon V_I, \end{aligned} \quad (28)$$

where

$$\mathcal{H}_I^{(0)} = \frac{1}{2} \sum_{j=-\infty}^{\infty} (\sigma_j^z \sigma_{j+1}^z + 1), \quad (29)$$

$$V_I = - \sum_{j=-\infty}^{\infty} (\sigma_j^+ \sigma_{j+1}^- + \sigma_j^- \sigma_{j+1}^+) \quad (30)$$

$$\begin{aligned} &- \sum_{j=-\infty}^{\infty} [h_2 \sigma_j^x + h_1 (-1)^j \sigma_j^y] \\ &- h_z \sum_{j=-\infty}^{\infty} [(-1)^j \sigma_j^z - 1]. \end{aligned}$$

Here  $\varepsilon = |\Delta|^{-1}$  is the small parameter, and  $\sigma_j^{\pm} = \frac{1}{2}(\sigma_j^x \pm i\sigma_j^y)$ .

At  $\varepsilon = 0$ , the Hamiltonian (28) has two Néel vacua  $|0\rangle^{(\mu)}$ ,  $\mu = 0, 1$ , with zero energy:

$$\mathcal{H}_I^{(0)} |0\rangle^{(\mu)} = 0, \quad \mu = 0, 1, \quad (31)$$

where

$$|0\rangle^{(1)} : \quad \dots \downarrow \begin{array}{c} 0 \\ \uparrow \\ 1 \end{array} \begin{array}{c} 1 \\ \downarrow \\ 2 \end{array} \downarrow \uparrow \downarrow \dots, \quad (32a)$$

$$|0\rangle^{(0)} : \quad \dots \uparrow \begin{array}{c} 0 \\ \downarrow \\ 1 \end{array} \begin{array}{c} 1 \\ \uparrow \\ 2 \end{array} \uparrow \downarrow \uparrow \dots \quad (32b)$$

#### A. One-kink sector

Let us consider the localized kink states  $|\mathbf{K}_{\mu\nu}(j)\rangle$ , which interpolate between vacua  $|0\rangle^{(\mu)}$  to the left, and  $|0\rangle^{(\nu)}$  to the right of the bond  $(j, j+1)$ . For example, the state  $|\mathbf{K}_{10}(2)\rangle$  looks like as follows:

$$|\mathbf{K}_{10}(2)\rangle : \quad \dots \downarrow \begin{array}{c} 0 \\ \uparrow \\ 1 \end{array} \downarrow \begin{array}{c} 1 \\ \uparrow \\ 2 \end{array} \begin{array}{c} 3 \\ \uparrow \\ 2 \end{array} \downarrow \uparrow \dots \quad (33)$$

The states  $|\mathbf{K}_{\mu\nu}(j)\rangle$  are the eigenvectors of the zero-order Hamiltonian (29), which are characterized by the same (unit) eigenvalue:

$$\mathcal{H}_I^{(0)}|\mathbf{K}_{\mu\nu}(j)\rangle = |\mathbf{K}_{\mu\nu}(j)\rangle, \quad (34)$$

and are normalized by the condition

$$\langle \mathbf{K}_{\nu\mu}(j)|\mathbf{K}_{\mu'\nu'}(j')\rangle = \delta_{\mu\mu'}\delta_{\nu\nu'}\delta_{jj'}. \quad (35)$$

They transform under the action of the operators  $T_1$ ,  $\mathbb{C}_x$ , and  $\tilde{T}_1$  in the following way:

$$T_1|\mathbf{K}_{\mu\nu}(j)\rangle = |\mathbf{K}_{\nu\mu}(j-1)\rangle, \quad (36)$$

$$\mathbb{C}_x|\mathbf{K}_{\mu\nu}(j)\rangle = |\mathbf{K}_{\nu\mu}(j)\rangle, \quad (37)$$

$$\tilde{T}_1|\mathbf{K}_{\mu\nu}(j)\rangle = |\mathbf{K}_{\mu\nu}(j-1)\rangle. \quad (38)$$

Denote by  $\mathcal{P}^{(1)}$  the projection operator onto the subspace  $\mathcal{L}^{(1)}$  of the one-kink states, and by  $\mathcal{H}_1(\varepsilon, \mathbf{h}_t, h_z)$  the restriction of the Hamiltonian  $\mathcal{H}_I(\varepsilon, \mathbf{h}_t, h_z)$  to  $\mathcal{L}^{(1)}$ :

$$\mathcal{H}_1(\varepsilon, \mathbf{h}_t, h_z) = \mathcal{P}^{(1)}\mathcal{H}_I(\varepsilon, \mathbf{h}_t, h_z)\mathcal{P}^{(1)}. \quad (39)$$

The Hamiltonian (39) acts at  $h_z = 0$  on the basis localized kink states  $|\mathbf{K}_{\mu\nu}(j)\rangle$  as follows:

$$\begin{aligned} \mathcal{H}_1(\varepsilon, \mathbf{h}_t, 0)|\mathbf{K}_{\mu\nu}(j)\rangle &= |\mathbf{K}_{\mu\nu}(j)\rangle \\ &- \varepsilon[|\mathbf{K}_{\mu\nu}(j+2)\rangle + |\mathbf{K}_{\mu\nu}(j-2)\rangle] \\ &- \varepsilon h_2[|\mathbf{K}_{\mu\nu}(j+1)\rangle + |\mathbf{K}_{\mu\nu}(j-1)\rangle] \\ &- i(-1)^\mu \varepsilon h_1[|\mathbf{K}_{\mu\nu}(j+1)\rangle - |\mathbf{K}_{\mu\nu}(j-1)\rangle]. \end{aligned} \quad (40)$$

The one-kink Bloch states

$$|K_{\mu\nu}^I(p)\rangle = e^{ip} \sum_{j=-\infty}^{\infty} e^{ijp} |\mathbf{K}_{\mu\nu}(j)\rangle \quad (41)$$

with  $p \in (-\pi, \pi)$  diagonalize the Hamiltonian  $\mathcal{H}_1(\varepsilon, \mathbf{h}_t, 0)$  and the modified translation operator  $\tilde{T}_1$ :

$$\mathcal{H}_1 \Big|_{h_z=0} |K_{\mu\nu}^I(p)\rangle = \omega_{\mu\nu}(\varepsilon, p, \mathbf{h}_t) |K_{\mu\nu}^I(p)\rangle, \quad (42)$$

$$\tilde{T}_1 |K_{\mu\nu}^I(p)\rangle = e^{ip} |K_{\mu\nu}^I(p)\rangle. \quad (43)$$

where

$$\begin{aligned} \omega_{\mu\nu}(\varepsilon, p, \mathbf{h}_t) &= 1 - 2\varepsilon \cos(2p) \\ &- 2\varepsilon [h_2 \cos p + (-1)^\mu h_1 \sin p] \end{aligned} \quad (44)$$

is the kink dispersion law.

## B. Two-kink sector

The two-kink subspace  $\mathcal{L}^{(2)}$  is spanned by the basis of localized states  $|\mathbf{K}_{\mu\nu}(j_1)\mathbf{K}_{\nu\mu}(j_2)\rangle$ , with  $j_1 < j_2$ . Denote by  $\mathcal{P}^{(2)}$  the projection operator onto this subspace, and by  $\mathcal{H}_2(\varepsilon, \mathbf{h}_t, h_z)$  the restriction of the Hamiltonian to  $\mathcal{L}^{(2)}$ :

$$\mathcal{H}_2(\varepsilon, \mathbf{h}_t, h_z) = \mathcal{P}^{(2)}\mathcal{H}_I(\varepsilon, \mathbf{h}_t, h_z)\mathcal{P}^{(2)}. \quad (45)$$

Let us define the Bloch state  $|\Psi(P)\rangle$  in the subspace  $\mathcal{L}^{(2)}$  as follows:

$$|\Psi(P)\rangle = \sum_{j_1=-\infty}^{\infty} e^{iPj_1} \sum_{j=1}^{\infty} e^{iPj/2} \psi(j) |\mathbf{K}_{10}(j_1)\mathbf{K}_{01}(j_1+j)\rangle. \quad (46)$$

Due to (38), it satisfies equation

$$\tilde{T}_1 |\Psi(P)\rangle = e^{iP} |\Psi(P)\rangle. \quad (47)$$

We require also, that the Bloch state  $|\Psi(P)\rangle$  is the eigenstate of the reduced Hamiltonian (45):

$$\mathcal{H}_2(\varepsilon, \mathbf{h}_1, h_z) |\Psi(P)\rangle = E(P) |\Psi(P)\rangle, \quad (48)$$

with the eigenvalue

$$E(P) = 2 + \varepsilon \Lambda(P). \quad (49)$$

Due to (46)-(49) the wave function  $\psi(j)$  must satisfy the fourth order linear difference equation at  $j \in \mathbb{N}$ :

$$\begin{aligned} (2h_z j - \Lambda)\psi(j) - 2 \cos P [\psi(j+2) + \psi(j-2)] \\ - 2h_2 \cos \frac{P}{2} [\psi(j+1) + \psi(j-1)] \\ + 2ih_1 \cos \frac{P}{2} [\psi(j+1) - \psi(j-1)] = 0. \end{aligned} \quad (50)$$

Its solution must satisfy the Dirichlet boundary condition at the left boundary:

$$\psi(-1) = \psi(0) = 0, \quad (51)$$

and vanish at  $j \rightarrow +\infty$ .

For the theory of linear difference equations see the monograph by G. Teschl [39].

### 1. Exact solution of the discrete Sturm-Liouville problem

The discrete Sturm-Liouville problem (50), (51) can be solved exactly. Indeed, let us define the generating function  $\phi(z)$  of the complex variable  $z$

$$\phi(z) = \sum_{j=1}^{\infty} \psi(j) z^j. \quad (52)$$

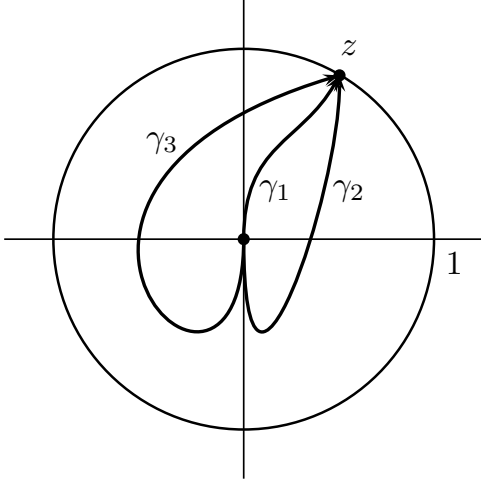
The Taylor series (52) must converge at  $|z| \leq 1$ .

Equations (50), (51) lead to the following first-order linear ordinary differential equation for the generating function  $\phi(z)$ :

$$\begin{aligned} (-\Lambda + 2h_z z \partial_z) \phi(z) + \epsilon_I(z|P) \phi(z) \\ = -2 \cos P [\psi(1) z^{-1} + \psi(2)] \\ - 2(h_2 - ih_1) \psi(1) \cos \frac{P}{2}, \end{aligned} \quad (53)$$

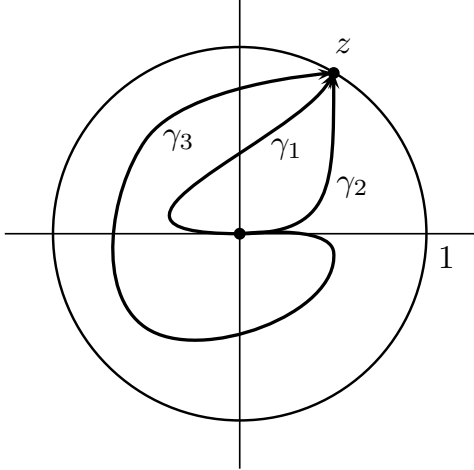
where

$$\begin{aligned} \epsilon_I(z|P) &= -2(z^2 + z^{-2}) \cos P \\ &- 2[h_2(z + z^{-1}) + ih_1(z - z^{-1})] \cos \frac{P}{2}, \end{aligned} \quad (54)$$



$\cos P > 0$

(a)



$\cos P < 0$

(b)

FIG. 1: Integration paths  $\gamma_1$ ,  $\gamma_2$ , and  $\gamma_3$  in (56) connecting the points  $w = 0$  and  $w = z$  in the  $w$ -complex plane: (a) for  $\cos P > 0$ , (b) for  $\cos P < 0$ .

and

$$\psi(1) = \phi'(0), \quad \psi(2) = \frac{\phi''(0)}{2}. \quad (55)$$

Besides, the generating function  $\phi(z)$  must vanish at the origin due to (51):  $\phi(0) = 0$ . The appropriate partial

solution of the differential equation (53) reads:

$$\begin{aligned} \phi(z) = & -\frac{1}{h_z} \int_0^z \frac{dw}{w} \exp \left\{ \frac{i}{2h_z} [\mathcal{F}_I(w|\Lambda) - \mathcal{F}_I(z|\Lambda)] \right\} \\ & \times \left[ \psi(1) \left( (h_2 - ih_1) \cos \frac{P}{2} + \frac{\cos P}{w} \right) + \psi(2) \cos P \right], \end{aligned} \quad (56)$$

where

$$\begin{aligned} \mathcal{F}_I(z|\Lambda) = & i \left[ \Lambda \ln z + (z^2 - z^{-2}) \cos P \right. \\ & \left. + 2h_2(z - z^{-1}) \cos \frac{P}{2} + 2ih_1(z + z^{-1}) \cos \frac{P}{2} \right]. \end{aligned} \quad (57)$$

Note, that

$$iz\mathcal{F}'_I(z|\Lambda) = \epsilon_I(z|P) - \Lambda. \quad (58)$$

The integrand in the integral in the right-hand side of (56) has the essential singularity at  $w = 0$ , that arises from the second order pole of the function  $\mathcal{F}_I(w|\Lambda)$  determined by (57):

$$\mathcal{F}_I(w|\Lambda) = -i \frac{\cos P}{w^2} + O(w^{-1}). \quad (59)$$

The integral in (56) converges, if the integration path approaches the origin  $w = 0$  along the line  $\text{Re} \frac{\cos P}{w^2} < 0$ . Depending on the sign of  $\cos P$ , the appropriate allowed integration path in (56) approaches the origin either along the imaginary axis for  $\cos P > 0$ , or along the real axis for  $\cos P < 0$ , see Figure 1. In both cases, the integrals in the right-hand side of (56) performed along the topologically non-equivalent paths  $\gamma_1$ ,  $\gamma_2$  and  $\gamma_3$  shown in Figure 1 must give the same result. This leads to two constraints

$$\begin{aligned} \int_{C_j} \frac{dw}{w} \exp \left\{ \frac{i}{2h_z} [\mathcal{F}_I(w|\Lambda)] \right\} \\ \times \left[ \psi(1) \left( (h_2 - ih_1) \cos \frac{P}{2} + \frac{\cos P}{w} \right) + \psi(2) \cos P \right] = 0, \end{aligned} \quad (60)$$

where  $j = 1, 2$ , and the integration contours  $C_1 = \gamma_2 - \gamma_1$ ,  $C_2 = \gamma_1 - \gamma_3$  are shown in Figure 2.

Let us introduce notations:  $f_1(w) = 1$ ,  $f_2(w) = w^{-1}$ ,

$$\langle \dots \rangle_j = \int_{C_j} \frac{dw}{w} \dots \exp \left\{ \frac{i}{2h_z} [\mathcal{F}_I(w|\Lambda)] \right\}, \quad (61)$$

with  $j = 1, 2$ , and

$$W_{ji} = \langle f_i \rangle_j. \quad (62)$$

Then, constraints (60) can be written as a system of two linear uniform equations on the parameters  $Y_1$  and  $Y_2$ :

$$\begin{aligned} W_{11}Y_1 + W_{12}Y_2 = 0, \\ W_{21}Y_1 + W_{22}Y_2 = 0, \end{aligned} \quad (63)$$

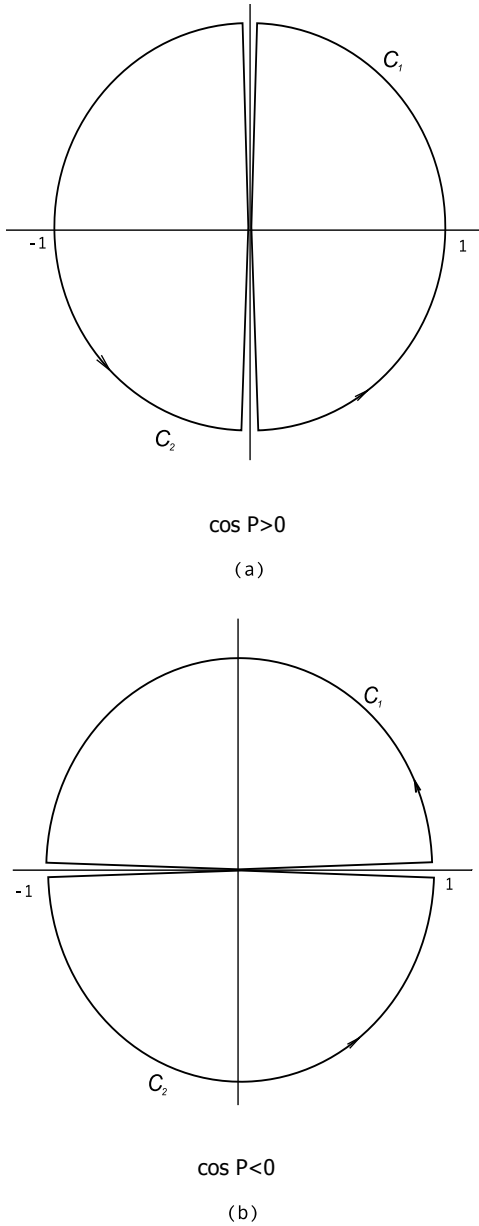


FIG. 2: Integration contours  $C_1$  and  $C_2$  in (60), (61): (a) for  $\cos P > 0$ , (b) for  $\cos P < 0$ .

where

$$Y_1 = \psi(1)(h_2 - ih_1) \cos \frac{P}{2} + \psi(2) \cos P, \quad (64)$$

$$Y_2 = \psi(1) \cos P.$$

This system has non-trivial solutions provided the following equality holds:

$$W_{11}W_{22} - W_{12}W_{21} = 0. \quad (65)$$

For given values of  $h_1, h_2, h_z$ , and  $P$ , the solutions of the transcendent equation (65) on the parameter  $\Lambda$  determine the discrete spectrum  $\{\Lambda_n\}_{n=1}^{\infty}$ , of the Sturm-Liouville problem (50), (51). This completes calculation

of the meson energy spectra for the model (16) in the Ising limit  $\Delta \rightarrow -\infty$  to the linear order in the small parameter  $\varepsilon = 1/|\Delta|$ :

$$E_n(P, \Delta, \mathbf{h}_t, h_z) = 2 + \varepsilon \Lambda_n(P, \mathbf{h}_t, h_z) + O(\varepsilon^2). \quad (66)$$

## 2. Limit $\mathbf{h}_t = 0$

In the limit  $\mathbf{h}_t = 0$ , the reduction of the function (57) to the form

$$\mathcal{F}_I(z|\Lambda) \Big|_{\mathbf{h}_t=0} = i [\Lambda \ln z + (z^2 - z^{-2}) \cos P] \quad (67)$$

leads to the following equalities:

$$W_{21} = W_{11} \exp\left(-\frac{i\Lambda\pi}{2h_z}\right), \quad W_{12} = -W_{22} \exp\left(\frac{i\Lambda\pi}{2h_z}\right),$$

and equation (65) simplifies to:

$$2W_{11}W_{22} = 0. \quad (68)$$

Furthermore, the integrals  $W_{11}, W_{22}$  admit at  $\mathbf{h}_t = 0$  the explicit representations in terms of the Bessel function:

$$\frac{W_{11}}{\pi i} = \begin{cases} J_\nu\left(\frac{\cos P}{h_z}\right), & \text{for } \cos P > 0, \\ \exp\left(-\frac{i\pi\Lambda}{4h_z}\right) J_\nu\left(\frac{-\cos P}{h_z}\right), & \text{for } \cos P < 0, \end{cases} \quad (69)$$

$$\frac{W_{22}}{\pi i} = \begin{cases} -\exp\left(-\frac{i\pi\Lambda}{2h_z}\right) J_{\nu-1/2}\left(\frac{\cos P}{h_z}\right), & \text{for } \cos P > 0, \\ i \exp\left(\frac{i\pi\Lambda}{4h_z}\right) J_{\nu-1/2}\left(\frac{-\cos P}{h_z}\right), & \text{for } \cos P < 0, \end{cases} \quad (70)$$

where  $\nu = -\frac{\Lambda}{4h_z}$ . Accordingly, the dispersion laws of the meson states at  $\mathbf{h}_t = 0$  in the Ising limit  $\Delta \rightarrow -\infty$  are determined by the solutions of the equation:

$$J_{-\frac{\Lambda}{4h_z}}\left(\frac{|\cos P|}{h_z}\right) J_{-\frac{1}{2}-\frac{\Lambda}{4h_z}}\left(\frac{|\cos P|}{h_z}\right) = 0 \quad (71)$$

in agreement with [12]. It was shown in [12], that the dispersion laws of the mesons with zero  $z$ -projection  $s = 0$  of the spin are determined by solutions of equation

$$J_{-\frac{\Lambda}{4h_z}}\left(\frac{|\cos P|}{h_z}\right) = 0, \quad (72)$$

while the energies of the mesons with  $s = \pm 1$  is determined by solutions of equation

$$J_{-\frac{1}{2}-\frac{\Lambda}{4h_z}}\left(\frac{|\cos P|}{h_z}\right) = 0. \quad (73)$$



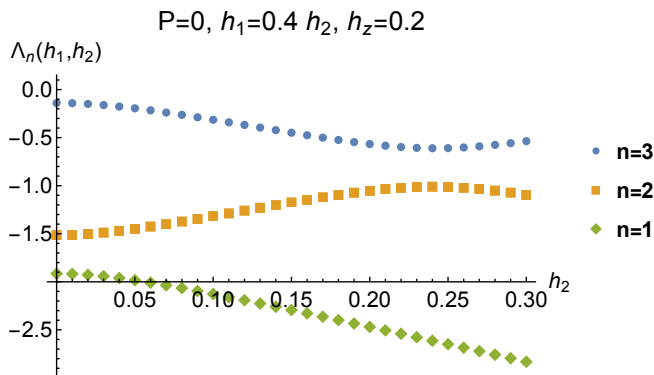


FIG. 3: The energies of three lightest mesons versus  $h_2$  due to (65) and (66) at  $h_1 = 0.4 h_2$  and fixed  $P = 0$ , and  $h_z = 0.2$ .

### 3. Meson energy spectra in the Ising limit at $\mathbf{h}_t \neq 0$

Application of the transverse magnetic field  $\mathbf{h}_t$  breaks conservation of the  $z$ -projection of the total spin and leads to the hybridization of the meson modes with  $s = 0$ , and  $s = \pm 1$ .

Obtained results are illustrated in Figure 3, which displays the evolution of the energies of three lightest meson modes with increasing transverse magnetic field  $h_2$  at the fixed ratio  $h_1/h_2 = 0.4$ , and fixed  $P = 0$  and  $h_z = 0.2$ . Hybridization of the first longitudinal and the second transverse modes leads to the avoided crossing of their dispersion curves, that takes place at  $h_2 \approx 0.25$  for the chosen values of other parameters.

The described above qualitative evolution of the meson energies with increasing transverse magnetic field was indeed observed by Faure *et al.* [10] in the inelastic neutron scattering experiments in the crystal  $\text{BaCo}_2\text{V}_2\text{O}_8$ , see Figure 3 in [10]. However, Faure *et al.* give the value  $\varepsilon = 0.53$  for the inverse anisotropy parameter  $\varepsilon = |\Delta|^{-1}$  in this crystal, which is far from the strong anisotropic regime  $\varepsilon \ll 1$ . Therefore, the results obtained above in the limit  $\varepsilon \rightarrow 0$  cannot describe quantitatively the experimentally relevant regime.

In subsequent Secs. IV-IX, we will present the alternative perturbative scheme, which is free from the above shortcoming. It applies to the whole interval of the anisotropy constant  $\Delta < -1$ , and exploits the staggered longitudinal magnetic field  $h_z$  as a small parameter. In the more simple case of zero transverse magnetic field, this perturbative technique was already used for calculation of the meson dispersion laws in the XXZ spin chain in papers [11, 12]. However, at  $\mathbf{h}_t = 0$ , one could benefit from the fact, that the XXZ model at  $h_z = 0$  is integrable. This is not the case anymore in presence of the transverse magnetic field  $\mathbf{h}_t \neq 0$ . To overcome this difficulty, we perform the perturbative calculations in two steps, as it was noticed in the Introduction. First, in Secs. IV-VI we concentrate on the deconfinement regime at  $h_z = 0$ , and determine the deformations of the antiferromagnetic

vacua, one-, and two-kink excitations by the weak transverse magnetic field having both uniform and staggered components. Then the weak staggered longitudinal field  $h_z$  is switched on inducing the kink confinement. The energies of their bound states in this regime are calculated in Secs. VII, IX following the strategy developed in [11, 12].

## IV. GROUND-STATE ENERGY AT $h_z = 0$

Let us return to the Hamiltonian (3), and put in it  $h_{1z} = h_{2z} = 0$ . At non-zero  $h_{ix}, h_{iy}$ ,  $i = 1, 2$ , the interaction term  $V$  given by (5) does not commute with the total spin operator  $S^z$ , and with all listed in (27) discrete symmetry operators, except of  $\mathbb{P}_{odd}$ , and  $\mathbb{C}_x \mathbb{T}$ :

$$\mathbb{P}_{odd} V = V \mathbb{P}_{odd}, \quad (74)$$

$$\mathbb{C}_x \mathbb{T} V = V \mathbb{T} \mathbb{C}_x. \quad (75)$$

It follows from equations (27f) and (75), that the application of the transverse magnetic fields  $h_{ix}, h_{iy}$ ,  $i = 1, 2$  does not lift the degeneracy between the two deformed antiferromagnetic vacua  $|Vac(\mathbf{h}_t)\rangle^{(1)}$  and  $|Vac(\mathbf{h}_t)\rangle^{(0)}$ ,

$$(\mathcal{H}_0 + V)|Vac(\mathbf{h}_t)\rangle^{(1)} = E_{vac}(\mathbf{h}_t)|Vac(\mathbf{h}_t)\rangle^{(1)},$$

$$(\mathcal{H}_0 + V)|Vac(\mathbf{h}_t)\rangle^{(0)} = E_{vac}(\mathbf{h}_t)|Vac(\mathbf{h}_t)\rangle^{(0)},$$

$$\mathbb{C}_x \mathbb{T} |Vac(\mathbf{h}_t)\rangle^{(\mu)} = |Vac(\mathbf{h}_t)\rangle^{(1-\mu)}, \quad \mu = 0, 1,$$

where  $\mathbf{h}_t = \langle h_{1x}, h_{2x}, h_{1y}, h_{2y} \rangle$ .

The ground-state energy  $E_{vac}(\mathbf{h}_t)$  admits the Rayleigh-Schrödinger expansion in the components of the transverse magnetic field. The leading correction to the ground state energy  $E_{vac}^{(0)}$  is of the second order. In the two-kink approximation, it can be written as [40]:

$$E_{vac}^{(2)}(\mathbf{h}_t) = - \sum_{s=\pm 1/2} \int_{-\pi/2}^{\pi/2} \frac{dp_1}{\pi} \int_{-\pi/2}^{p_1} \frac{dp_2}{\pi} \frac{1}{\omega(p_1) + \omega(p_2)} \quad (76)$$

$$^{(1)} \langle vac | V | K_{10}(p_1) K_{01}(p_2) \rangle_{ss}$$

$$\times {}_{ss} \langle K_{10}(p_2) K_{01}(p_1) | V | vac \rangle^{(1)}.$$

Here  $|K_{10}(p_1) K_{01}(p_2)\rangle_{s_1 s_2}$  denotes the two-kink Bloch state characterized by the quasimomenta  $p_1, p_2$  and spins  $s_1, s_2$  of two kinks. Some properties of these states are collected in Appendix A. The kink dispersion law  $\omega(p)$  is explicitly known due to Johnson, Krinsky, and McCoy [41]:

$$\omega(p, \eta) = I \sqrt{1 - k^2 \cos^2 p}, \quad (77)$$

where

$$I = \frac{2K}{\pi} \sinh \eta, \quad (78)$$

and  $K [K']$  is the complete elliptic integral of modulus  $k$  [ $k' = \sqrt{1 - k^2}$ ] such that

$$\frac{K'}{K} = \frac{\eta}{\pi}. \quad (79)$$

The perturbing operator  $V$  can be represented as

$$V = \sum_{m=-\infty}^{\infty} \tilde{T}_1^{-2m} v_0 \tilde{T}_1^{2m}, \quad (80)$$

where

$$v_0 = -[(h_{1x} + h_{2x})\sigma_0^x + (h_{1y} + h_{2y})\sigma_0^y] \\ - [(-h_{1x} + h_{2x})\sigma_1^x + (-h_{1y} + h_{2y})\sigma_1^y].$$

After substitution of (80) into (76) and summation over  $m$  using equality (A1a), one obtains in the thermodynamic limit

$$\lim_{N \rightarrow \infty} \frac{E_{vac}^{(2)}(\mathfrak{h}_t)}{N} = -\frac{1}{2} \sum_{s=\pm 1/2} \int_{-\pi/2}^{\pi/2} \frac{dp}{\pi} \frac{1}{2\omega(p)} \times \quad (81)$$

$${}^{(1)}\langle vac|v_0|K_{10}(p)K_{01}(-p)\rangle_{ss} \\ \times {}_{ss}\langle K_{10}(-p)K_{01}(p)|v_0|vac\rangle^{(1)},$$

where  $N$  is the number of sites in the spin chain. The matrix elements of the operator  $v_0$  in the right-hand side can be expressed in terms of the two-kink form factors  $X^0(\xi_1, \xi_2)$ ,  $X^1(\xi_1, \xi_2)$  given in equations (A9) in Appendix A:

$${}^{(1)}\langle vac|v_0|K_{10}(p)K_{01}(-p)\rangle_{-1/2, -1/2} = \\ -\frac{\sinh \eta}{\omega(p)} \{ (h_{1x} - ih_{1y})[X^1(\xi, \xi^{-1}) - X^0(\xi, \xi^{-1})] \\ + (h_{2x} - ih_{2y})[X^1(\xi, \xi^{-1}) + X^0(\xi, \xi^{-1})] \}, \\ {}^{(1)}\langle vac|v_0|K_{10}(p)K_{01}(-p)\rangle_{1/2, 1/2} = \\ \frac{\sinh \eta}{\omega(p)} \{ (h_{1x} + ih_{1y})[X^1(\xi, \xi^{-1}) - X^0(\xi, \xi^{-1})] \\ - (h_{2x} + ih_{2y})[X^1(\xi, \xi^{-1}) + X^0(\xi, \xi^{-1})] \},$$

where

$$\xi := \xi(p) = -ie^{i\alpha(p)}, \quad (82)$$

and  $\alpha$  is the kink rapidity corresponding to the momentum  $p$ . Note, that the kink momentum  $p$  and energy  $\omega$  can be parametrized in terms of the Jacobi elliptic functions of the rapidity variable  $\alpha$ :

$$p(\alpha) = -\frac{\pi}{2} + \text{am} \left( \frac{2K\alpha}{\pi}, k \right), \quad (83)$$

$$\omega(\alpha) = I \text{dn} \left( \frac{2K\alpha}{\pi}, k \right) = \sinh \eta \frac{dp(\alpha)}{d\alpha}. \quad (84)$$

Let us proceed to the polar coordinates in the magnetic field components:

$$h_{1x} = h_1 \cos \varphi_1, \quad h_{1y} = h_1 \sin \varphi_1, \quad (85)$$

$$h_{2x} = h_2 \cos \varphi_2, \quad h_{2y} = h_2 \sin \varphi_2. \quad (86)$$

The second order correction (81) then can be represented in the form

$$\lim_{N \rightarrow \infty} \frac{E_{vac}^{(2)}(\mathfrak{h}_t)}{N} = -\frac{\chi_1}{2} h_1^2 - \frac{\chi_2}{2} h_2^2 \quad (87)$$

where  $\chi_1$  and  $\chi_2$  are the magnetic susceptibilities corresponding to the staggered and uniform transverse magnetic fields, respectively:

$$\chi_1 = \frac{A_+^2}{A_-^2} \chi_2, \quad (88)$$

$$\chi_2 = \frac{\sinh \eta}{\pi} \int_0^\pi \frac{dp}{\omega^2(p)} |X^1(\xi, \xi^{-1}) + X^0(\xi, \xi^{-1})|^2, \quad (89)$$

with  $\xi$  given by (82), and

$$A_+(\eta) = 2\vartheta_4(0|e^{-\eta}) \vartheta_2(i\eta/\pi|e^{-4\eta}), \quad (90)$$

$$A_-(\eta) = 2\vartheta_3(0|e^{-\eta}) \vartheta_2(i\eta/\pi|e^{-4\eta}).$$

Here  $\vartheta_i(u|p)$ , with  $i = 1, 2, 3, 4$ , denotes the elliptic theta-functions defined by equations (A17).

Note, that the ratio  $A_+^2/A_-^2$  is equal to the complementary elliptic modulus  $k'$ :

$$\frac{A_+^2}{A_-^2} = \left[ \frac{\vartheta_4(0|e^{-\eta})}{\vartheta_3(0|e^{-\eta})} \right]^2 = \left[ \frac{\vartheta_2(0|e^{-\pi^2/\eta})}{\vartheta_3(0|e^{-\pi^2/\eta})} \right]^2 \\ = k'(\eta) = \sqrt{1 - k(\eta)^2}.$$

## V. FIRST ORDER CORRECTION TO THE KINK ENERGY AT $h_z = 0$

At zero magnetic field, the XXZ model is determined by the Hamiltonian (4). At  $\Delta < -1$ , the infinite chain (4) has two antiferromagnetic ground states  $|vac\rangle^{(1)}$ , and  $|vac\rangle^{(0)}$ . The one-kink subspace  $\mathcal{L}^{(1)}$  has two topological sectors  $\mathcal{L}_{10}^{(1)}$  and  $\mathcal{L}_{01}^{(1)}$ , which are spanned by the basis vectors  $|K_{10}(p)\rangle_s$ , and  $|K_{01}(p)\rangle_s$ , respectively, with  $p \in (0, \pi)$ , and  $s = \pm 1/2$ . The defining equations for these one-kink Bloch states read:

$$\tilde{T}_1 |K_{\mu\nu}(p)\rangle_s = e^{ip} |K_{\mu\nu}(p)\rangle_{-s}, \quad (91a)$$

$$S^z |K_{\mu\nu}(p)\rangle_s = s |K_{\mu\nu}(p)\rangle_s, \quad (91b)$$

$$(\mathcal{H}_0 - E_{vac}^{(0)}) |K_{\mu\nu}(p)\rangle_s = \omega(p) |K_{\mu\nu}(p)\rangle_s, \quad (91c)$$

$${}_s\langle K_{\nu\mu}(p) | K_{\mu'\nu'}(p') \rangle_{s'} = \pi \delta_{\mu\mu'} \delta_{\nu\nu'} \delta_{s,s'} \delta(p - p'), \quad (91d)$$

where  $\omega(p)$  is given by (77). Note also the relation [11]

$$|K_{\mu\nu}(p + \pi)\rangle_s = \varkappa(\mu, s) |K_{\mu\nu}(p)\rangle_s, \quad (92)$$

where  $\varkappa(0, 1/2) = \varkappa(1, -1/2) = 1$ , and  $\varkappa(1, 1/2) = \varkappa(0, -1/2) = -1$ . Formula (92) allows one to extend the above definition of the one-kink states  $|K_{\mu\nu}(p)\rangle_s$  from the interval  $p \in (0, \pi)$  to the whole real axis of the momentum  $p \in \mathbb{R}$ . All one-kink Bloch states  $|K_{\mu\nu}(p)\rangle_s$  have the same dispersion law (77).

If  $h_{1z} = h_{2z} = 0$ , application of the weak transverse uniform and staggered magnetic fields  $\mathfrak{h}_t = (h_{1x}, h_{2x}, h_{1y}, h_{2y})$  deform the two antiferromagnetic ground states  $|vac\rangle^{(\mu)}$ , with  $\mu = 0, 1$  into the vacua  $|Vac(\mathfrak{h}_t)\rangle^{(\mu)}$ , which remain degenerate in energy. The

lowest in energy excitations form the subspace  $\mathcal{L}^{(1)}$ , which splits into two sectors  $\mathcal{L}_{10}^{(1)}$  and  $\mathcal{L}_{01}^{(1)}$  formed by kink Bloch states  $|\mathbb{K}_{\mu\nu}(p|\mathfrak{h}_t)\rangle_a$ , interpolating between the two antiferromagnetic vacua. These kink Bloch states are defined as solutions of the eigenvalue problem:

$$T_1^2 |\mathbb{K}_{\mu\nu}(p|\mathfrak{h}_t)\rangle_a = e^{2ip} |\mathbb{K}_{\mu\nu}(p|\mathfrak{h}_t)\rangle_a, \quad (93)$$

$$[\mathcal{H}_0 + V - E_{vac}(\mathfrak{h}_t)] |\mathbb{K}_{\mu\nu}(p|\mathfrak{h}_t)\rangle_a \quad (94)$$

$$= \Omega_{\mu\nu}^{(a)}(p|\mathfrak{h}_t) |\mathbb{K}_{\mu\nu}(p|\mathfrak{h}_t)\rangle_a,$$

with  $a = 1, 2$  and  $p \in (0, \pi)$ .

Note, that we have used the two-site translation operator  $T_1^2$  in (93) [instead of the one-site modified translation  $\tilde{T}_1$  in equation (91a)] in order to define the kink quasi-momentum  $p$ . The reason is that the operator  $\tilde{T}_1$  does not commute with  $V$  for generic values of the transverse magnetic field components at  $h_{1z} = h_{2z} = 0$ .

The one-kink Bloch states  $|\mathbb{K}_{\mu\nu}(p|\mathfrak{h}_t)\rangle_a$  admit a Taylor expansion in powers of the components of the applied transverse magnetic field. The standard Rayleigh-Schrödinger perturbation theory arguments [40] yield:

$$|\mathbb{K}_{\mu\nu}(p|\mathfrak{h}_t)\rangle_a \quad (95)$$

$$= U_{a1} |K_{\mu\nu}(p)\rangle_{1/2} + U_{a2} |K_{\mu\nu}(p)\rangle_{-1/2} + O(|\mathfrak{h}_t|),$$

$$\Omega_{\mu\nu}^{(a)}(p|\mathfrak{h}_t) = \omega(p) + \delta\Omega_{\mu\nu}^{(a)}(p|\mathfrak{h}_t) + O(|\mathfrak{h}_t|^2), \quad (96)$$

where  $\delta\Omega_{\mu\nu}^{(a)}(p|\mathfrak{h}_t) \sim \mathfrak{h}_t$ . The matrix elements of the  $2 \times 2$  unitary matrix  $U_{ab}$  are, generally speaking, different for the topological sectors  $\mathcal{L}_{10}^{(1)}$  and  $\mathcal{L}_{01}^{(1)}$ , depend on the kink momentum  $p \in (0, \pi)$ , and on the orientation in the  $xy$ -plane of the applied transverse magnetic fields, but do not depend on  $|\mathfrak{h}_t|$ . In order to determine  $\delta\Omega_{\mu\nu}^{(a)}(p)$  and  $U_{ab}$ , one has to diagonalize the matrix  ${}_s\langle K_{\nu\mu}(p)|V|K_{\mu\nu}(p')\rangle_{s'}$ , which can be written as:

$${}_s\langle K_{\nu\mu}(p)|V|K_{\mu\nu}(p')\rangle_{s'} = \pi\delta(p-p')\mathcal{V}_{ss'}(p), \quad (97)$$

where the Hermitian  $2 \times 2$  matrix  $\mathcal{V}_{ss'}(p)$  is defined by the relation

$$\begin{aligned} \mathcal{V}_{ss'}(p) &= {}_s\langle K_{\nu\mu}(p)|v_0|K_{\mu\nu}(p)\rangle_{s'} \quad (98) \\ &= \frac{\sinh \eta}{\omega(p)} \delta_{-s,s'} {}_s\langle K_{\nu\mu}(\xi)|v_0|\mathcal{K}_{\mu\nu}(\xi)\rangle_{s'}. \end{aligned}$$

In the second line  $|\mathcal{K}_{\mu\nu}(\xi)\rangle_s$  denotes the kink state parametrised by the multiplicative spectral parameter  $\xi(\alpha) = -ie^{i\alpha}$ . This state differs from  $|K_{\mu\nu}(p)\rangle_s$  by the numerical factor  $\sqrt{p'(\alpha)}$ :

$$|\mathcal{K}_{\mu\nu}(\xi)\rangle_s = \sqrt{\frac{\omega(p)}{\sinh \eta}} |K_{\mu\nu}(p)\rangle_s. \quad (99)$$

Using (26d) and the crossing relation [33]

$$\begin{aligned} &{}_s\langle \mathcal{K}_{\nu\mu}(\xi')|\sigma_0^a|\mathcal{K}_{\mu\nu}(\xi)\rangle_s \quad (100) \\ &= {}^{(\nu)}\langle vac|\sigma_0^a|\mathcal{K}_{\nu\mu}(-q\xi')\mathcal{K}_{\mu\nu}(\xi)\rangle_{-s',s}, \end{aligned}$$

with  $\mathbf{a} = x, y, z$ , the non-zero matrix elements in the second line of (98) can be expressed in terms of the two-kink form factors  $X^0(\xi_1, \xi_2), X^1(\xi_1, \xi_2)$  of the spin operators  $\sigma_0^\pm$  described in Appendix A:

$${}_{-1/2}\langle \mathcal{K}_{01}(\xi)|v_0|\mathcal{K}_{10}(\xi)\rangle_{1/2} \quad (101)$$

$$\begin{aligned} &= -(h_1 e^{i\varphi_1} + h_2 e^{i\varphi_2}) X^1(e^{-\eta}\xi, \xi) \\ &- (-h_1 e^{i\varphi_1} + h_2 e^{i\varphi_2}) X^0(e^{-\eta}\xi, \xi), \end{aligned}$$

$${}_{1/2}\langle \mathcal{K}_{01}(\xi)|v_0|\mathcal{K}_{10}(\xi)\rangle_{-1/2} \quad (102)$$

$$\begin{aligned} &= -(h_1 e^{-i\varphi_1} + h_2 e^{-i\varphi_2}) X^0(e^{-\eta}\xi, \xi) \\ &- (-h_1 e^{-i\varphi_1} + h_2 e^{-i\varphi_2}) X^1(e^{-\eta}\xi, \xi), \end{aligned}$$

$${}_{-1/2}\langle \mathcal{K}_{10}(\xi)|v_0|\mathcal{K}_{01}(\xi)\rangle_{1/2} \quad (103)$$

$$\begin{aligned} &= -(h_1 e^{i\varphi_1} + h_2 e^{i\varphi_2}) X^0(e^{-\eta}\xi, \xi) \\ &- (-h_1 e^{i\varphi_1} + h_2 e^{i\varphi_2}) X^1(e^{-\eta}\xi, \xi), \end{aligned}$$

$${}_{1/2}\langle \mathcal{K}_{10}(\xi)|v_0|\mathcal{K}_{01}(\xi)\rangle_{-1/2} \quad (104)$$

$$\begin{aligned} &= -(h_1 e^{-i\varphi_1} + h_2 e^{-i\varphi_2}) X^1(e^{-\eta}\xi, \xi) \\ &- (-h_1 e^{-i\varphi_1} + h_2 e^{-i\varphi_2}) X^0(e^{-\eta}\xi, \xi). \end{aligned}$$

The following explicit formulas hold for the form factors  $X^{0,1}(e^{-\eta}\xi, \xi)$  that stand in the above expressions:

$$X^1(e^{-\eta}\xi, \xi) + X^0(e^{-\eta}\xi, \xi) = A_+ \cos[p(\alpha)], \quad (105)$$

$$X^1(e^{-\eta}\xi, \xi) - X^0(e^{-\eta}\xi, \xi) = iA_- \sin[p(\alpha)], \quad (106)$$

where  $p(\alpha)$  is the kink momentum parametrized by the rapidity variable according to equation (83), and the amplitudes  $A_\pm(\eta)$  are given by (90).

As the result, the matrix elements  $\mathcal{V}_{s,s'}(p)$  in the case  $\mu = 1, \nu = 0$  reduce to the form:

$$\mathcal{V}_{1/2,-1/2}(p) = \frac{\sinh \eta}{\omega(p)} [ie^{-i\varphi_1} h_1 A_- \sin p - e^{-i\varphi_2} h_2 A_+ \cos p],$$

$$\mathcal{V}_{-1/2,1/2}(p) = \frac{\sinh \eta}{\omega(p)} [-ie^{i\varphi_1} h_1 A_- \sin p - e^{i\varphi_2} h_2 A_+ \cos p],$$

$$\mathcal{V}_{1/2,1/2}(p) = \mathcal{V}_{-1/2,-1/2}(p) = 0.$$

In the case  $\mu = 0, \nu = 1$ , the matrix elements  $\mathcal{V}_{s,s'}(p)$  read instead:

$$\mathcal{V}_{1/2,-1/2}(p) = \frac{\sinh \eta}{\omega(p)} [-ie^{-i\varphi_1} h_1 A_- \sin p - e^{-i\varphi_2} h_2 A_+ \cos p],$$

$$\mathcal{V}_{-1/2,1/2}(p) = \frac{\sinh \eta}{\omega(p)} [ie^{i\varphi_1} h_1 A_- \sin p - e^{i\varphi_2} h_2 A_+ \cos p],$$

$$\mathcal{V}_{1/2,1/2}(p) = \mathcal{V}_{-1/2,-1/2}(p) = 0.$$

Diagonalization of the matrix  $\mathcal{V}_{ss'}(p)$  allows one to determine the kink dispersion law to the first order in  $|\mathfrak{h}_t|$ :

$$\Omega_{10}^{(a)}(p|\mathfrak{h}_t) = \omega(p) \pm \frac{\sinh \eta}{\omega(p)} \quad (107)$$

$$\begin{aligned} &\times [(h_1 A_- \sin p)^2 + (h_2 A_+ \cos p)^2 \\ &- h_1 h_2 A_+ A_- \sin(2p) \sin(\varphi_1 - \varphi_2)]^{1/2} + O(|\mathfrak{h}_t|^2), \end{aligned}$$

$$\Omega_{01}^{(a)}(p|\mathfrak{h}_t) = \Omega_{10}^{(a)}(-p|\mathfrak{h}_t), \quad (108)$$

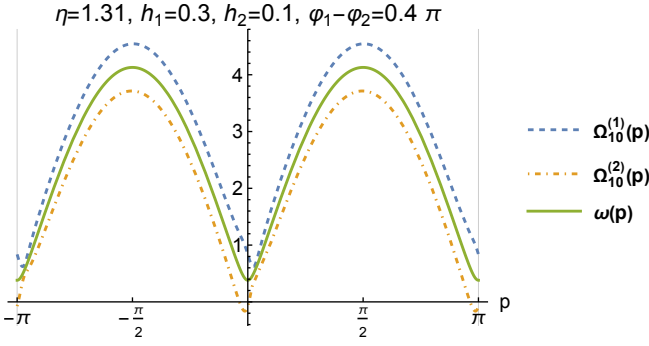


FIG. 4: Dashed blue and dot-dashed orange lines: dispersion laws (107) of kinks perturbed by transverse magnetic fields. Solid green line: kink dispersion law (77) at zero magnetic field.

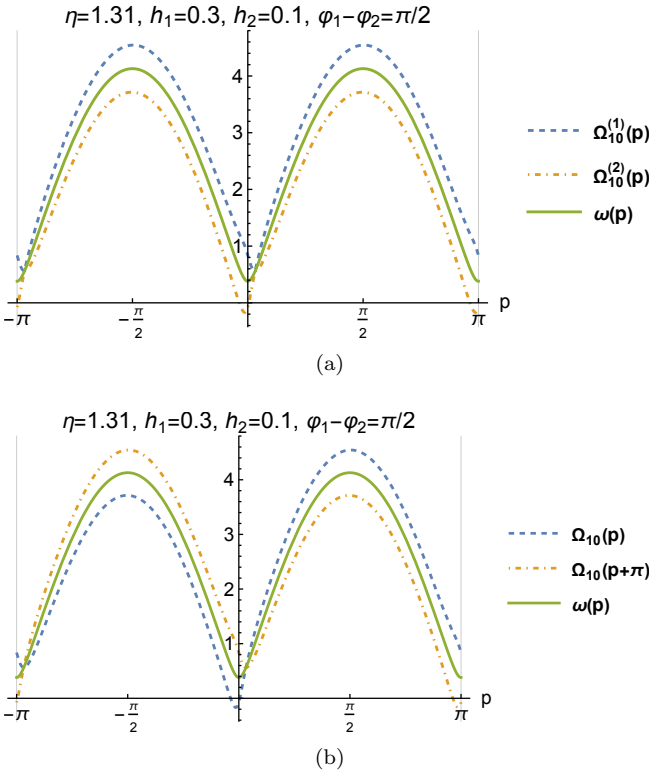


FIG. 5: Dashed blue and dot-dashed orange lines: dispersion laws [(109) in (a), and (118) in (b)] of kinks perturbed by the mutually orthogonal transverse staggered and uniform magnetic fields. Solid green line: the kink dispersion law (77) at zero magnetic field.

with  $a = 1, 2$ , and  $p \in (0, \pi)$ .

Figure 4 illustrates the dispersion laws (107) of two kink modes  $\Omega_{10}^{(a)}(p|\mathbf{h}_t)$ ,  $a = 1, 2$ , in the topological sector  $\mathcal{L}_{10}^{(1)}$  at  $\eta = 1.31$ ,  $h_1 = 0.3$ ,  $h_2 = 0.1$ , and  $\varphi_1 - \varphi_2 = 0.4\pi$ . These large enough values of the magnetic fields  $h_1$  and  $h_2$  have been chosen in order to provide a sufficient separation of three dispersion curves in Figure 4. The draw-

back of this choice is that the kink frequency  $\Omega_{10}^{(2)}(p)$  vanishes and becomes negative at certain values of  $p$ . This does not happen at small values of the transverse magnetic fields required by the applicability of the Rayleigh-Schrödinger perturbation theory.

At generic mutual orientations and strengths of the transverse uniform and staggered magnetic fields, the degeneracy between the two kink modes  $\Omega_{10}^{(1)}(p)$  and  $\Omega_{10}^{(2)}(p)$  is lifted at all  $p$ . The situation is different, however, in two cases: (i) if the staggered and uniform transverse magnetic fields are mutually orthogonal; (ii) if either the staggered, or the uniform transverse magnetic field vanishes.

Let us address the first case, and put  $\varphi_1 - \varphi_2 = \pi/2$  in equations (107), (108), which reduce then to the form:

$$\Omega_{10}^{(a)}(p|\mathbf{h}_t) = \omega(p) \pm \frac{\sinh \eta}{\omega(p)} \quad (109)$$

$$\times |h_1 A_- \sin p - h_2 A_+ \cos p| + O(|\mathbf{h}_t|^2),$$

$$\Omega_{01}^{(a)}(p|\mathbf{h}_t) = \Omega_{10}^{(a)}(-p|\mathbf{h}_t), \quad (110)$$

with  $p \in (0, \pi)$ .

As one can see from Figure 5a, the gap between the two modes  $\Omega_{10}^{(1)}(p|\mathbf{h}_t)$ , and  $\Omega_{10}^{(2)}(p|\mathbf{h}_t)$  vanishes at a certain value of the kink momentum  $p$ . The physical reason of this partly restored degeneracy is the additional symmetry of the Hamiltonian. Indeed, at  $h_{1z} = h_{2z} = 0$ ,  $\varphi_1 = \pi/2$  and  $\varphi_2 = 0$ , the interaction operator (5) reduces to the operator  $V_t(\mathbf{h}_t)$  given by (17):

$$V \Big|_{h_{1z}=h_{2z}=0, \varphi_1=\pi/2, \varphi_2=0} = V_t(\mathbf{h}_t),$$

where  $\mathbf{h}_t = h_2 \mathbf{e}_x + h_1 \mathbf{e}_y$ . The latter operator commutes with the modified translation  $\tilde{T}_1$ :

$$[V_t(\mathbf{h}_t), \tilde{T}_1] = 0. \quad (111)$$

This allows us to redefine the kink quasi-momentum by means of the relation

$$\tilde{T}_1 |\mathbb{K}_{\mu\nu}(p|\mathbf{h}_t)\rangle = e^{ip} |\mathbb{K}_{\mu\nu}(p|\mathbf{h}_t)\rangle, \quad (112)$$

instead of (93), and to let the kink quasi-momentum run through the whole interval  $p \in (0, 2\pi)$  in equation (112). As a result, one can consider only the single one-kink mode in the extended Brillouin zone  $p \in (-\pi, \pi)$  in each topological sector  $\mathcal{L}_{10}^{(1)}$  and  $\mathcal{L}_{01}^{(1)}$ . The one-kink states  $|\mathbb{K}_{\mu\nu}(p|\mathbf{h}_t)\rangle$  with  $p \in (0, 2\pi)$  form the basis in the one-kink subspace  $\mathcal{L}_{\mu\nu}^{(1)}$ . These basis states will be normalized by the condition

$$\langle \mathbb{K}_{\nu\mu}(p|\mathbf{h}_t) | \mathbb{K}_{\mu'\nu'}(p'|\mathbf{h}_t) \rangle = 2\pi \delta_{\mu\mu'} \delta_{\nu\nu'} \delta(p - p'),$$

with  $p, p' \in (0, 2\pi)$ , and  $\mu \neq \nu$ .

In the limit  $\mathbf{h}_t \rightarrow 0$ , the one-kink states  $|\mathbb{K}_{\mu\nu}(p|\mathbf{h}_t)\rangle$  can be related with the previously introduced states

$|K_{\mu\nu}(p)\rangle_s$ . Really, it follows from (91a) and (112), that we can put without loss of generality

$$\lim_{\mathbf{h}_t \rightarrow 0} |\mathbb{K}_{\mu\nu}(p|\mathbf{h}_t)\rangle = |K_{\mu\nu}(p)\rangle_{1/2} + |K_{\mu\nu}(p)\rangle_{-1/2}, \quad (113)$$

for  $0 < p < \pi$ . For these one-kink state we shall use the notation  $|K_{\mu\nu}(p)\rangle$ :

$$|K_{\mu\nu}(p)\rangle := \lim_{\mathbf{h}_t \rightarrow 0} |\mathbb{K}_{\mu\nu}(p|\mathbf{h}_t)\rangle. \quad (114)$$

Exploiting equation (92), we can extend formula (113) from the interval  $p \in (0, \pi)$  to the whole real axis  $p \in \mathbb{R}$ . In particular, we get this way:

$$|K_{10}(p + \pi)\rangle = -|K_{10}(p)\rangle_{1/2} + |K_{10}(p)\rangle_{-1/2}, \quad (115)$$

$$|K_{01}(p + \pi)\rangle = |K_{01}(p)\rangle_{1/2} - |K_{01}(p)\rangle_{-1/2}. \quad (116)$$

The Bloch states  $|\mathbb{K}_{\mu\nu}(p|\mathbf{h}_t)\rangle$  are the eigenstates of the Hamiltonian  $(\mathcal{H}_0 + V_t)$ :

$$[\mathcal{H}_0 + V_t - E_{vac}(\mathbf{h}_t)]|\mathbb{K}_{\mu\nu}(p|\mathbf{h}_t)\rangle = \Omega_{\mu\nu}(p|\mathbf{h}_t)|\mathbb{K}_{\mu\nu}(p|\mathbf{h}_t)\rangle. \quad (117)$$

Their dispersion laws  $\Omega_{\mu\nu}(p|\mathbf{h}_t)$  are the  $2\pi$ -periodical functions of  $p$ . To the first order in  $\mathbf{h}_t$  these functions read as:

$$\Omega_{10}(p|\mathbf{h}_t) = \omega(p) + \delta\Omega_{10}(p|\mathbf{h}_t) + O(|\mathbf{h}_t|^2), \quad (118)$$

$$\Omega_{01}(p|\mathbf{h}_t) = \omega(p) + \delta\Omega_{01}(p|\mathbf{h}_t) + O(|\mathbf{h}_t|^2),$$

where

$$\delta\Omega_{10}(p|\mathbf{h}_t) = \frac{\sinh \eta}{\omega(p)} (h_1 A_- \sin p - h_2 A_+ \cos p), \quad (119)$$

$$\delta\Omega_{01}(p|\mathbf{h}_t) = \delta\Omega_{10}(-p|\mathbf{h}_t).$$

The plot of the function  $\Omega_{10}(p|\mathbf{h}_t)$  at  $\eta = 1.31$ ,  $h_1 = 0.3$ ,  $h_2 = 0.1$  is shown in Figure 5b.

The situation is very similar in the second case, when either the staggered, or the uniform transverse magnetic field vanishes. At  $h_{2x} > 0$ ,  $h_{1x} = h_{1y} = h_{2y} = 0$ , and, as well, at  $h_{1x} = h_{2y} = h_{2x} = 0$ ,  $h_{1y} > 0$ , the interaction term  $V_t$  commutes with  $\tilde{T}_1$ , and one can use (112) in order to define the kink quasi-momentum  $p \in (-\pi, \pi)$ . Accordingly, one can still use equations (118), (119) to determine the kink dispersion laws in the extended Brillouin zone  $p \in (-\pi, \pi)$ .

## VI. TWO-KINK STATES AT $h_z = 0$ , $\mathbf{h}_t \neq 0$

The two-kink subspace  $\mathcal{L}^{(2)}$  is the direct sum of two subspaces

$$\mathcal{L}^{(2)} = \mathcal{L}_{11}^{(2)} \oplus \mathcal{L}_{00}^{(2)}.$$

At a generic  $\mathbf{h}_t \neq 0$ , the basis in the first subspace  $\mathcal{L}_{11}^{(2)}$  is formed by the vectors  $|\mathbb{K}_{10}(p_1|\mathbf{h}_t)\mathbb{K}_{01}(p_2|\mathbf{h}_t)\rangle_{a_1, a_2}$ , and the basis in the second space  $\mathcal{L}_{00}^{(2)}$  is formed by the vectors

$|\mathbb{K}_{01}(p_1|\mathbf{h}_t)\mathbb{K}_{10}(p_2|\mathbf{h}_t)\rangle_{a_1, a_2}$ . In both bases  $a_i = 1, 2$ , and  $0 < p_2 < p_1 < \pi$ .

These basis states must satisfy the following relations:

$$T_1^2 |\mathbb{K}_{\mu\nu}(p_1|\mathbf{h}_t)\mathbb{K}_{\nu\mu}(p_2|\mathbf{h}_t)\rangle_{a_1, a_2} = \quad (120)$$

$$e^{2i(p_1+p_2)} |\mathbb{K}_{\mu\nu}(p_1|\mathbf{h}_t)\mathbb{K}_{\nu\mu}(p_2|\mathbf{h}_t)\rangle_{a_1, a_2},$$

$$[\mathcal{H}_0 + V_t - E_{vac}(\mathbf{h}_t)]|\mathbb{K}_{\mu\nu}(p_1|\mathbf{h}_t)\mathbb{K}_{\nu\mu}(p_2|\mathbf{h}_t)\rangle_{a_1, a_2} = \quad (121)$$

$$[\Omega_{\mu\nu}^{(a_1)}(p_1|\mathbf{h}_t) + \Omega_{\nu\mu}^{(a_2)}(p_2|\mathbf{h}_t)]|\mathbb{K}_{\mu\nu}(p_1|\mathbf{h}_t)\mathbb{K}_{\nu\mu}(p_2|\mathbf{h}_t)\rangle_{a_1, a_2},$$

where  $\Omega_{\mu\nu}^{(a)}(p|\mathbf{h}_t)$  are the kink dispersion laws determined by equations (107), (108).

If the transverse staggered and uniform magnetic fields are mutually orthogonal, we can parametrize them by the two-component vector  $\mathbf{h}_t = \mathbf{e}_x h_2 + \mathbf{e}_y h_1$ . In this case a different, more convenient classification of two-kink basis Bloch states is possible. Since equation (111) holds at  $\varphi_1 = \pi/2$  and  $\varphi_2 = 0$ , we can define in this case the alternative basis of the two-kink states by the relations:

$$\tilde{T}_1 |\mathbb{K}_{\mu\nu}(p_1|\mathbf{h}_t)\mathbb{K}_{\nu\mu}(p_2|\mathbf{h}_t)\rangle \quad (122a)$$

$$= e^{i(p_1+p_2)} |\mathbb{K}_{\mu\nu}(p_1|\mathbf{h}_t)\mathbb{K}_{\nu\mu}(p_2|\mathbf{h}_t)\rangle,$$

$$[\mathcal{H}_0 + V_t - E_{vac}(\mathbf{h}_t)]|\mathbb{K}_{\mu\nu}(p_1|\mathbf{h}_t)\mathbb{K}_{\nu\mu}(p_2|\mathbf{h}_t)\rangle \quad (122b)$$

$$= [\Omega_{\mu\nu}(p_1|\mathbf{h}_t) + \Omega_{\nu\mu}(p_2|\mathbf{h}_t)]|\mathbb{K}_{\mu\nu}(p_1|\mathbf{h}_t)\mathbb{K}_{\nu\mu}(p_2|\mathbf{h}_t)\rangle,$$

$$\langle \mathbb{K}_{\mu\nu}(p_2|\mathbf{h}_t)\mathbb{K}_{\nu\mu}(p_1|\mathbf{h}_t) | \mathbb{K}_{\mu\nu}(p'_1|\mathbf{h}_t)\mathbb{K}_{\nu\mu}(p'_2|\mathbf{h}_t) \rangle \quad (122c)$$

$$= 4\pi^2 \delta(p_1 - p'_1) \delta(p_2 - p'_2),$$

where  $0 < p_2 < p_1 < 2\pi$ , and  $0 < p'_2 < p'_1 < 2\pi$ .

We shall use the following notation for the two-kink states at  $\mathbf{h}_t = 0$ :

$$|K_{\mu\nu}(p_1)K_{\nu\mu}(p_2)\rangle := \lim_{\mathbf{h}_t \rightarrow 0} |\mathbb{K}_{\mu\nu}(p_1|\mathbf{h}_t)\mathbb{K}_{\nu\mu}(p_2|\mathbf{h}_t)\rangle \quad (123)$$

These two-kink basis states can be related with the two-kink basis states  $|K_{\mu\nu}(p_1)K_{\nu\mu}(p_2)\rangle_{s_1, s_2}$  characterized by the  $z$ -projections of the kink spins  $s_1, s_2$ . Namely,

$$|K_{\mu\nu}(p_1)K_{\nu\mu}(p_2)\rangle \quad (124)$$

$$= \sum_{s_1 = \pm 1/2} \sum_{s_2 = \pm 1/2} |K_{\mu\nu}(p_1)K_{\nu\mu}(p_2)\rangle_{s_1, s_2},$$

for  $\langle p_1, p_2 \rangle \in \Gamma_1$ , where the triangular region  $\Gamma_1$  is shown in Figure 6. By means of equalities (A3), one can extend formula (124) to the three other triangular regions  $\Gamma_2, \Gamma_3, \Gamma_4$  in Figure 6. Extension of equation (124) from the region  $\Gamma_1$  into the region  $\Gamma_5$  can be performed, in turn, by means of the Faddeev-Zamolodchikov commutation relation

$$|K_{\mu\nu}(p_1)K_{\nu\mu}(p_2)\rangle_{s_1 s_2} = \sum_{s'_1, s'_2 = \pm 1/2} S_{s_1 s_2}^{s'_1 s'_2}(p_1, p_2) \quad (125)$$

$$\times |K_{\mu\nu}(p_2)K_{\nu\mu}(p_1)\rangle_{s'_2 s'_1},$$

applied to the right-hand side of (124). Finally, exploiting again equality (A3), one can extend formula (124)

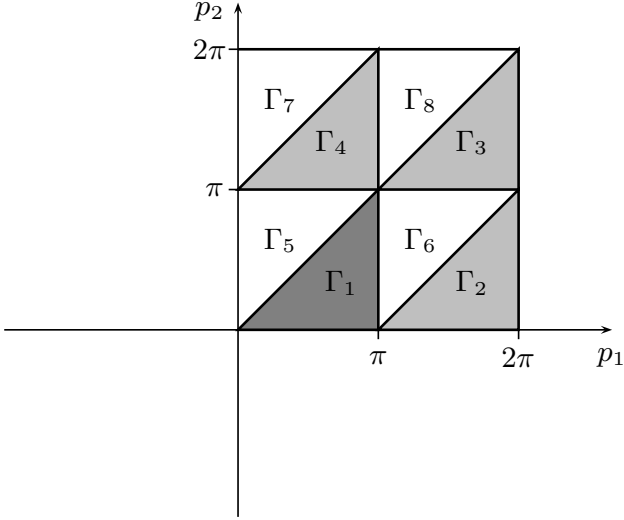


FIG. 6: Triangular regions in the plane of momenta  $p_1, p_2$ , which parametrize the two-kink states.

from the triangular region  $\Gamma_5$  into the regions  $\Gamma_6$ ,  $\Gamma_7$ , and  $\Gamma_8$  shown in Figure 6. As the result, equation (124) allows one to determine the two-kink basis state  $|K_{\mu\nu}(p_1)K_{\nu\mu}(p_2)\rangle$  for any real  $\langle p_1, p_2 \rangle \in \mathbb{R}^2$ .

In the basis (124), the Faddeev-Zamolodchikov commutations relations (125) reduce to the form:

$$\begin{aligned} & |K_{\mu\nu}(p_1)K_{\nu\mu}(p_2)\rangle \\ &= \frac{w_0(p_1, p_2) + w_+(p_1, p_2)}{2} |K_{\mu\nu}(p_2)K_{\nu\mu}(p_1)\rangle \\ &+ \frac{-w_0(p_1, p_2) + w_+(p_1, p_2)}{2} |K_{\mu\nu}(p_2 + \pi)K_{\nu\mu}(p_1 + \pi)\rangle, \end{aligned} \quad (126)$$

where the scattering amplitudes  $w_0(p_1, p_2)$  and  $w_+(p_1, p_2)$  are given by equations (A6a) in Appendix A. The commutation relation (126) holds for any  $p_1, p_2 \in \mathbb{R}$ . The projector operator  $\mathcal{P}_{\mu\mu}^{(2)}$  on the subspace  $\mathcal{L}_{\mu\mu}^{(2)}$  can be written at  $\mathbf{h}_t = 0$  as:

$$\begin{aligned} \mathcal{P}_{\mu\mu}^{(2)} &= \sum_{\substack{s_1=\pm 1/2 \\ s_2=\pm 1/2}} \iint_{\Gamma_1} \frac{dp_1 dp_2}{\pi^2} |K_{\mu\nu}(p_1)K_{\nu\mu}(p_2)\rangle_{s_1 s_2} \\ &\quad \times {}_{s_2 s_1} \langle K_{\mu\nu}(p_2)K_{\nu\mu}(p_1) | \\ &= \frac{1}{2} \int_0^{2\pi} \frac{dp_1}{2\pi} \int_0^{2\pi} \frac{dp_2}{2\pi} |K_{\mu\nu}(p_1)K_{\nu\mu}(p_2)\rangle \\ &\quad \times \langle K_{\mu\nu}(p_2)K_{\nu\mu}(p_1) |. \end{aligned} \quad (128)$$

Application of a small enough, but finite transverse magnetic field  $\mathbf{h}_t = h_2 \mathbf{e}_x + h_1 \mathbf{e}_y$  not only modifies the dispersion laws of kinks due to (117)-(119), but also effects their mutual scattering.

Let us consider for given  $P$  and  $E$  all solutions of the equations

$$\begin{aligned} \exp[i(p_1 + p_2)] &= \exp(iP), \\ \Omega_{\mu\nu}(p_1) + \Omega_{\nu\mu}(p_2) &= E, \end{aligned} \quad (129)$$

lying in the interval  $\langle p_1, p_2 \rangle \in (0, 2\pi)$ . We denote such a solution  $\langle p_{1,in}, p_{2,in} \rangle$ , if

$$\partial_{p_1} \Omega_{\mu\nu}(p_1) - \partial_{p_2} \Omega_{\nu\mu}(p_2) > 0 \quad (130)$$

at this solution, and use the notation  $\langle p_{1,out}, p_{2,out} \rangle$  for the solutions, in which the opposite inequality

$$\partial_{p_1} \Omega_{\mu\nu}(p_1) - \partial_{p_2} \Omega_{\nu\mu}(p_2) < 0 \quad (131)$$

holds. If there are  $m$  in- and out- solutions of equations (129), we distinguish them by the index  $i = 1, \dots, m$ . Using these notations, the elastic two-kink scattering can be characterized by the scattering matrix  $W_{i'}^i(E, P | \mathbf{h}_t)$  by means of the following ‘‘deformed Faddeev-Zamolodchikov commutation relation’’:

$$\begin{aligned} & |\mathbb{K}_{\mu\nu}(p_{1,in}^i | \mathbf{h}_t) \mathbb{K}_{\nu\mu}(p_{2,in}^i | \mathbf{h}_t)\rangle \\ &= \sum_{i'=1}^m W_{i'}^i(E, P | \mathbf{h}_t) |\mathbb{K}_{\mu\nu}(p_{1,out}^{i'} | \mathbf{h}_t) \mathbb{K}_{\nu\mu}(p_{2,out}^{i'} | \mathbf{h}_t)\rangle. \end{aligned} \quad (132)$$

Of course, at  $\mathbf{h}_t \neq 0$ , the  $n$ -particle scattering matrices with  $n > 2$  do not factorize in the two-particle ones, since the transverse magnetic field breaks integrability of the XXZ spin-chain model.

At a small  $|\mathbf{h}_t|$ , the scattering matrix  $W_{i'}^i(E, P | \mathbf{h}_t)$  should analytically depend on  $h_1, h_2$ , and the initial terms of its Taylor expansion in these parameters could be, in principal, determined by means of the standard perturbation theory. At  $\mathbf{h}_t = 0$ , equation (132) must reduce to (126).

Using equation (132), one can extend definition of the two-kink basis states  $|\mathbb{K}_{\mu\nu}(p_1 | \mathbf{h}_t) \mathbb{K}_{\nu\mu}(p_2 | \mathbf{h}_t)\rangle$  from the triangular region  $0 < p_2 < p_1 < 2\pi$  to the square  $p_1, p_2 \in (0, 2\pi)$ . Subsequent application of the periodicity relation

$$\begin{aligned} |\mathbb{K}_{\mu\nu}(p_1 | \mathbf{h}_t) \mathbb{K}_{\nu\mu}(p_2 | \mathbf{h}_t)\rangle &= |\mathbb{K}_{\mu\nu}(p_1 + 2\pi | \mathbf{h}_t) \mathbb{K}_{\nu\mu}(p_2 | \mathbf{h}_t)\rangle \\ &= |\mathbb{K}_{\mu\nu}(p_1 | \mathbf{h}_t) \mathbb{K}_{\nu\mu}(p_2 + 2\pi | \mathbf{h}_t)\rangle \end{aligned}$$

allows one to define such two-kink Bloch states for any real  $\langle p_1, p_2 \rangle \in \mathbb{R}^2$ .

It is natural to expect, that the projector operator  $\mathcal{P}_{\mu\mu}^{(2)}(\mathbf{h}_t)$  onto the two-kink subspace  $\mathcal{L}_{\mu\mu}^{(2)}(\mathbf{h}_t)$  admits at a small enough, but finite  $\mathbf{h}_t = h_2 \mathbf{e}_x + h_1 \mathbf{e}_y$  the representations

$$\begin{aligned} \mathcal{P}_{\mu\mu}^{(2)}(\mathbf{h}_t) &= \int_0^{2\pi} \frac{dp_1}{2\pi} \int_0^{2\pi} \frac{dp_2}{2\pi} |\mathbb{K}_{\mu\nu}(p_1 | \mathbf{h}_t) \mathbb{K}_{\nu\mu}(p_2 | \mathbf{h}_t)\rangle \\ &\quad \times \langle \mathbb{K}_{\mu\nu}(p_2 | \mathbf{h}_t) \mathbb{K}_{\nu\mu}(p_1 | \mathbf{h}_t) | \\ &= \frac{1}{2} \int_0^{2\pi} \frac{dp_1}{2\pi} \int_0^{2\pi} \frac{dp_2}{2\pi} |\mathbb{K}_{\mu\nu}(p_1 | \mathbf{h}_t) \mathbb{K}_{\nu\mu}(p_2 | \mathbf{h}_t)\rangle \\ &\quad \times \langle \mathbb{K}_{\mu\nu}(p_2 | \mathbf{h}_t) \mathbb{K}_{\nu\mu}(p_1 | \mathbf{h}_t) |, \end{aligned} \quad (133)$$

which are analogous to (127), (128).

## VII. MESON STATES AT $h_z > 0$

Proceeding to the XXZ spin-chain model (3) with non-zero staggered longitudinal magnetic field, we will restrict our attention to the case of the Hamiltonian (16), in which the staggered and uniform transverse fields are mutually orthogonal.

The first reason in favor of this choice is that the Hamiltonian (16) commutes with the modified translation operator (21):

$$[\mathcal{H}(\Delta, \mathbf{h}_t, h_z), \tilde{T}_1] = 0. \quad (134)$$

This makes the perturbative analysis of the kink-confinement in model (16) more simple, than in the original one (3). The second reason is that the XXZ model with mutually orthogonal staggered and uniform transverse magnetic fields has been used by Faure *et al.* [10] for the interpretation of their results of the neutron scattering study of the meson energy spectra in the quasi-one-dimensional magnetic crystal  $\text{BaCo}_2\text{V}_2\text{O}_8$  in the kink confinement regime in the presence of the external uniform transverse magnetic field. The effective staggered transverse magnetic field orthogonal to the applied external uniform transverse field is induced in this compound due to the off-diagonal components of the anisotropic  $g$ -tensor [22].

The application of the longitudinal staggered magnetic field  $h_z$  explicitly breaks the  $\mathbb{Z}_2$  symmetry of the model decreasing the energy of the vacuum  $|\text{Vac}(\mathbf{h}_t, h_z)\rangle^{(1)}$ , which becomes the true ground state, and increasing the energy of the vacuum  $|\text{Vac}(\mathbf{h}_t, h_z)\rangle^{(0)}$ , which becomes metastable. The true (and also, the false) vacuum  $|\text{Vac}(\mathbf{h}_t, h_z)\rangle^{(1)}$  remains invariant with respect to the action of modified translation operator:

$$\tilde{T}_1|\text{Vac}(\mathbf{h}_t, h_z)\rangle^{(1)} = |\text{Vac}(\mathbf{h}_t, h_z)\rangle^{(1)}. \quad (135)$$

The margin between the energies of the true and false vacuums opened by the staggered longitudinal field  $h_z$  leads to the confinement of kinks  $|\mathbb{K}_{\mu\nu}(p|\mathbf{h}_t)\rangle$  into the meson bound states  $|\pi_n(P|\mathbf{h}_t, h_z)\rangle$ . The defining relations for these meson bound states read:

$$\tilde{T}_1|\pi_n(P|\mathbf{h}_t, h_z)\rangle = e^{iP}|\pi_n(P|\mathbf{h}_t, h_z)\rangle, \quad (136a)$$

$$(\mathcal{H} + C)|\pi_n(P|\mathbf{h}_t, h_z)\rangle = E_n(P|\mathbf{h}_t, h_z)|\pi_n(P|\mathbf{h}_t, h_z)\rangle, \quad (136b)$$

where the Hamiltonian  $\mathcal{H}$  is given by (16),  $E_n(P|\mathbf{h}_t, h_z)$  is dispersion law of the  $n$ -th meson mode,  $0 < P < 2\pi$ ,  $n = 1, 2, \dots$ , and the numerical constant  $C$  is chosen in such a way, that

$$(\mathcal{H} + C)|\text{Vac}(\mathbf{h}_t, h_z)\rangle^{(1)} = 0.$$

At  $h_z = 0$ , the meson states  $|\pi_n(P|\mathbf{h}_t, h_z)\rangle$  decouple into some linear combinations of two-kink states:

$$|\pi_n(P|\mathbf{h}_t, 0)\rangle \rightarrow |\mathbb{K}_{10}(p_1|\mathbf{h}_t)\mathbb{K}_{01}(p_2|\mathbf{h}_t)\rangle,$$

with  $\exp[i(p_1 + p_2)] = \exp(iP)$ .

On the other hand, it will be shown later, that at  $\mathbf{h}_t = 0$ , the meson states  $|\pi_n(P|\mathbf{h}_t, h_z)\rangle$  transform into the meson states  $|\pi_{s,\iota,m}(P|h_z)\rangle$  with  $s = \pm 1$ ,  $\iota = 0, \pm$ , introduced in [11]. Namely, for  $0 < P < \pi$  and odd  $n = 2m - 1$ :

$$|\pi_{2m-1}(P|\mathbf{0}, h_z)\rangle \cong |\pi_{1,0,m}(P|h_z)\rangle + |\pi_{-1,0,m}(P|h_z)\rangle, \quad (137)$$

$$|\pi_{2m-1}(P + \pi|\mathbf{0}, h_z)\rangle \cong |\pi_{1,0,m}(P|h_z)\rangle - |\pi_{-1,0,m}(P|h_z)\rangle,$$

while for  $0 < P < \pi$  and even  $n = 2m$ :

$$|\pi_{2m}(P|\mathbf{0}, h_z)\rangle \cong |\pi_{0,+,m}(P|h_z)\rangle, \quad (138)$$

$$|\pi_{2m}(P + \pi|\mathbf{0}, h_z)\rangle \cong |\pi_{0,-,m}(P|h_z)\rangle,$$

where  $\cong$  denotes the equality up to some numerical factor, and  $m = 1, 2, \dots$

It follows from (136a) and (136b), that the meson dispersion law  $E_n(P|\mathbf{h}_t, h_z)$  is the  $2\pi$ -periodical function of the meson momentum  $P$ , and we can set without loss of generality:

$$|\pi_n(P + 2\pi l|\mathbf{h}_t, h_z)\rangle = |\pi_n(P|\mathbf{h}_t, h_z)\rangle, \quad (139)$$

for  $l \in \mathbb{Z}$ . The function  $E_n(P|\mathbf{h}_t, h_z)$  is also even with respect to the  $P$ -inversion:

$$E_n(P|\mathbf{h}_t, h_z) = E_n(-P|\mathbf{h}_t, h_z).$$

As in the previously studied case [11]  $\mathbf{h}_t = 0$ , the eigenvalue problem (136) is very difficult, since the interaction term  $V_1(h_z)$  given by (18) does not conserve the number of kinks. The key simplification is achieved by means of the two-kink approximation [11], which implies replacement of the exact eigenvalue problem (136) by its projection onto the two-kink subspace  $\mathcal{L}_{11}^{(2)}(\mathbf{h}_t)$ :

$$\tilde{T}_1|\tilde{\pi}_n(P|\mathbf{h}_t, h_z)\rangle = e^{iP}|\tilde{\pi}_n(P|\mathbf{h}_t, h_z)\rangle, \quad (140a)$$

$$\mathcal{H}^{(2)}|\tilde{\pi}_n(P|\mathbf{h}_t, h_z)\rangle = \tilde{E}_n(P|\mathbf{h}_t, h_z)|\tilde{\pi}_n(P|\mathbf{h}_t, h_z)\rangle, \quad (140b)$$

where  $|\tilde{\pi}_n(P|\mathbf{h}_t, h_z)\rangle \in \mathcal{L}_{11}^{(2)}(\mathbf{h}_t)$ , and

$$\mathcal{H}^{(2)} = \mathcal{P}_{11}^{(2)}(\mathbf{h}_t)\mathcal{H}\mathcal{P}_{11}^{(2)}(\mathbf{h}_t). \quad (141)$$

Tildes in  $\tilde{\pi}_n(P|\mathbf{h}_t, h_z)$ ,  $\tilde{E}_n(P|\mathbf{h}_t, h_z)$  distinguish solutions of equations (140) from those of the exact eigenvalue problem (136). The meson states  $|\tilde{\pi}_n(P|\mathbf{h}_t, h_z)\rangle$  will be normalized by the condition

$$\langle \tilde{\pi}_n(P|\mathbf{h}_t, h_z) | \tilde{\pi}_{n'}(P'|\mathbf{h}_t, h_z) \rangle = 2\pi \delta_{nn'} \delta(P - P'), \quad (142)$$

for  $0 < P, P' < 2\pi$ . These states form a basis in the two-kink subspace  $\mathcal{L}_{11}^{(2)}(\mathbf{h}_t)$ , and the projector (133) on this subspace admits the expansion:

$$\mathcal{P}_{11}^{(2)}(\mathbf{h}_t) = \sum_{n=1}^{\infty} \int_0^{2\pi} \frac{dP}{2\pi} |\tilde{\pi}_n(P|\mathbf{h}_t, h_z)\rangle \langle \tilde{\pi}_n(P|\mathbf{h}_t, h_z)|. \quad (143)$$

The two-kink meson state  $|\tilde{\pi}_n(P|\mathbf{h}_t, h_z)\rangle$  can be characterized by the wave-function:

$$\begin{aligned} \Phi_n(p_1, p_2|P, \mathbf{h}_t, h_z) = & \quad (144) \\ \langle \mathbb{K}_{10}(p_2|\mathbf{h}_t)\mathbb{K}_{01}(p_1|\mathbf{h}_t)|\tilde{\pi}_n(P|\mathbf{h}_t, h_z)\rangle, \end{aligned}$$

It follows also from (122a), (140a), that

$$\Phi_n(p_1, p_2|P, \mathbf{h}_t, h_z) = e^{i(P-p_1-p_2)}\Phi_n(p_1, p_2|P, \mathbf{h}_t, h_z). \quad (145)$$

For  $(p_1+p_2), P \in (0, 2\pi)$ , this allows one to represent the meson wave function  $\Phi_n(p_1, p_2|P, \mathbf{h}_t, h_z)$  in the form

$$\begin{aligned} \Phi_n(p_1, p_2|P, \mathbf{h}_t, h_z) = & 2\pi \delta(p_1 + p_2 - P) \quad (146) \\ & \times \phi_n\left(\frac{p_1 - p_2}{2}|P, \mathbf{h}_t, h_z\right). \end{aligned}$$

The reduced wave function  $\phi_n(p|P, \mathbf{h}_t, h_z)$  in the right-hand side is the  $2\pi$ -periodical function of  $p$ . The normalization conditions following from (142) reads:

$$\int_{-\pi}^{\pi} \frac{dp}{2\pi} \phi_n^*(p|P, \mathbf{h}_t, h_z) \phi_{n'}(p|P, \mathbf{h}_t, h_z) = 2\delta_{nn'}. \quad (147)$$

By means of the procedure described in [11], one can show, that this function must solve the Bethe-Salpeter integral equation:

$$\begin{aligned} [\mathcal{E}(p|P) - \tilde{E}_n(P)]\phi_n(p|P) = & \frac{h_z}{2} \int_{-\pi}^{\pi} \frac{dp'}{2\pi} \phi_n(p'|P) \quad (148) \\ & \times \langle \mathbb{K}_{10}(p_2)\mathbb{K}_{01}(p_1)|(\sigma_0^z - \langle \sigma_0^z \rangle)|\mathbb{K}_{10}(p'_1)\mathbb{K}_{01}(p'_2)\rangle, \end{aligned}$$

where

$$\mathcal{E}(p|P, \mathbf{h}_t) = \Omega_{10}(p_1|\mathbf{h}_t) + \Omega_{01}(p_2|\mathbf{h}_t) \quad (149)$$

$$\begin{aligned} & = \epsilon(p|P) + \delta\mathcal{E}(p|P, \mathbf{h}_t) + O(|\mathbf{h}_t|^2), \\ \epsilon(p|P) = & \omega(P/2 + p) + \omega(P/2 - p), \quad (150) \end{aligned}$$

$$\delta\mathcal{E}(p|P, \mathbf{h}_t) = \delta\Omega_{10}(p + P/2|\mathbf{h}_t) + \delta\Omega_{01}(-p + P/2|\mathbf{h}_t), \quad (151)$$

$$\langle \sigma_0^z \rangle = {}^{(1)}\langle \text{Vac}(\mathbf{h}_t, 0)|\sigma_0^z|\text{Vac}(\mathbf{h}_t, 0)\rangle^{(1)}, \quad (152)$$

$\delta\Omega_{\mu\nu}(p|\mathbf{h}_t)$  are given by (119), and  $p_{1,2} = P/2 \pm p, p'_{1,2} = P/2 \pm p'$ . We have omitted the explicit dependencies of functions in equation (148) on  $\mathbf{h}_t$  and  $h_z$ .

The function  $\epsilon(p|P)$  defined by (150) determines the effective kinetic energy of the relative motion of two kinks at zero magnetic field. It satisfies a number of symmetry relations

$$\begin{aligned} \epsilon(p|P) = \epsilon(p|P + 2\pi) = \epsilon(-p|P) = \epsilon(p| - P) \quad (153) \\ = \epsilon(p + \pi|P) = \epsilon(p - \pi/2|P - \pi), \end{aligned}$$

following directly from (150), (77). Application of the transverse magnetic field  $\mathbf{h}_t$  deforms the effective kinetic energy to the function  $\mathcal{E}(p|P, \mathbf{h}_t)$  defined by (149), which is much less symmetric, than  $\epsilon(p|P)$ . The linear part

$\delta\mathcal{E}(p|P, \mathbf{h}_t)$  of this deformation satisfies relations

$$\delta\mathcal{E}(p|P, \mathbf{h}_t) = \delta\mathcal{E}(p|P + 2\pi, \mathbf{h}_t), \quad (154)$$

$$\delta\mathcal{E}(p + \pi|P, \mathbf{h}_t) = -\delta\mathcal{E}(p|P, \mathbf{h}_t), \quad (155)$$

$$\delta\mathcal{E}(-p|P, \mathbf{h}_t) \neq \delta\mathcal{E}(p|P, \mathbf{h}_t), \quad (156)$$

$$\delta\mathcal{E}(p|\pi, \mathbf{h}_t) = 0, \quad (157)$$

that follow from (151), (119). From (157) and  $2\pi$ -periodicity of the effective kinetic energy in  $P$ , we get:

$$\mathcal{E}(p|P, \mathbf{h}_t) = \epsilon(p|P) + O(|\mathbf{h}_t|^2) \quad (158)$$

at  $P = \pi + 2\pi n$ , with  $n \in \mathbb{Z}$ .

In the limit  $\mathbf{h}_t = 0$ , equation (148) reduces to the form

$$\begin{aligned} [\epsilon(p|P) - \tilde{E}_n(P)]\phi_n(p|P) = & \frac{h_z}{2} \int_{-\pi}^{\pi} \frac{dp'}{2\pi} \phi_n(p'|P) \quad (159) \\ & \times \langle K_{10}(p_2)K_{01}(p_1)|(\sigma_0^z - \bar{\sigma})|K_{10}(p'_1)K_{01}(p'_2)\rangle, \end{aligned}$$

where  $\bar{\sigma}$  is the staggered spontaneous magnetization at zero magnetic field given by (11), and the two-kink basis states  $|K_{10}(p_1)K_{01}(p_2)\rangle$  are defined by (123).

It follows from (126), and (144), that the reduced wave function  $\phi_n(p|P, \mathbf{h}_t, h_z)$  satisfies at  $\mathbf{h}_t = 0$  the reflection property:

$$\begin{aligned} \phi_n(p|P) = & \frac{w_0^* + w_+^*}{2} \phi_n(-p|P) \quad (160) \\ & + \frac{-w_0^* + w_+^*}{2} \phi_n(-p + \pi|P), \end{aligned}$$

where

$$\begin{aligned} w_0 = & w_0(p + P/2, -p + P/2), \quad (161) \\ w_+ = & w_+(p + P/2, -p + P/2) \end{aligned}$$

are the two-kink scattering amplitudes (A6a).

Let us show, that the integral equation (159) represents in the compact form all three Bethe-Salpeter equations (230) of paper [11], which were derived there for the wave-functions of the mesons with different spins  $s = 0, \pm 1$ , and parities  $\iota = 0, \pm$ . Really, using equation (124), the integral kernel in the second line of (159) can be rewritten as

$$\begin{aligned} \langle K_{10}(p_2)K_{01}(p_1)|(\sigma_0^z - \bar{\sigma})|K_{10}(p'_1)K_{01}(p'_2)\rangle = & \quad (162) \\ 4\bar{\sigma} \left[ e^{i(p'-p)}G_0(p, p'|P) + G_+(p, p'|P) \right], \end{aligned}$$

where  $G_0(p, p'|P)$  and  $G_+(p, p'|P)$  were defined by equations (112) and (228) in [11], respectively. Since due to equation (233) in [11], the kernels  $G_0(p, p'|P)$  and  $G_+(p, p'|P)$  are  $\pi$ -periodic functions of the variables  $p$  and  $p'$ , the integral equation (159) decouples in two separate equations for the meson wave functions  $\phi_n(p|P)$  with different transformation properties upon the translation  $p \rightarrow p + \pi$ . Namely, the  $\pi$ -antiperiodic solution of



(159) satisfies equations

$$\phi_n(p + \pi|P) = -\phi_n(p|P), \quad (163)$$

$$\begin{aligned} & [\epsilon(p|P) - \tilde{E}_n(P)] e^{ip} \phi_n(p|P) \\ &= 2h_z \bar{\sigma} \int_{-\pi/2}^{\pi/2} \frac{dp'}{\pi} e^{ip'} \phi_n(p'|P) G_0(p, p'|P), \end{aligned} \quad (164)$$

whereas for the  $\pi$ -periodic solution of (159) we get instead:

$$\phi_n(p + \pi|P) = \phi_n(p|P), \quad (165)$$

$$\begin{aligned} & [\epsilon(p|P) - \tilde{E}_n(P)] \phi_n(p|P) \\ &= 2h_z \bar{\sigma} \int_{-\pi/2}^{\pi/2} \frac{dp'}{\pi} \phi_n(p'|P) G_+(p, p'|P). \end{aligned} \quad (166)$$

Finally, it follows from the equality

$$G_+(p, p'|P + \pi) = G_-(p + \pi/2, p' + \pi/2|P),$$

that the  $\pi$ -periodic solution  $\phi_n(p|P + \pi)$  of the integral equation (159) must satisfy equalities

$$\phi_n(p + \pi|P + \pi) = \phi_n(p|P + \pi), \quad (167)$$

$$\begin{aligned} & [\epsilon(p|P) - \tilde{E}_n(P + \pi)] \phi_n(p|P + \pi) \\ &= 2h_z \bar{\sigma} \int_{-\pi/2}^{\pi/2} \frac{dp'}{\pi} \phi_n(p'|P + \pi) G_-(p, p'|P). \end{aligned} \quad (168)$$

Equations (164), (166), and (168) coincide with the Bethe-Salpeter equation (230) derived in [11] for the cases  $\iota = 0, +, -$ , respectively.

The most consistent, but technically demanding approach for the calculation of the meson energy spectrum in model (16) in the presence of the transverse magnetic field  $\mathbf{h}_t \neq 0$  requires the perturbative solution of the Bethe-Salpeter equation (148). In the case  $\mathbf{h}_t = 0$ , this strategy was realized in [11]. In what follows, we shall use the less rigorous, but more simple heuristic semiclassical approach.

To conclude this section, let us comment on the two-kink approximation (140), (141), which is essential in derivation of the Bethe-Salpeter equation (148) and will be implicitly exploited in the subsequent semiclassical calculations. The same approximation was used by Fonseca and Zamolodchikov [13, 14] in derivation of the Bethe-Salpeter equation for the Ising field theory. The kink confinement in this model is induced by the uniform magnetic field  $h > 0$ . It was shown in [14], that in the case of the IFT, the two-kink approximation is asymptotically exact in the weak confinement regime at  $h \rightarrow +0$ , and the leading ‘multi-kink’ correction (the correction beyond the two-kink approximation) to the meson masses is quadratic in  $h$ . In analogy with IFT, we expect, that exact meson energies  $E_n(P|\mathbf{h}_t, h_z)$  coincide with their two-kink approximations  $\tilde{E}_n(P|\mathbf{h}_t, h_z)$  to the linear order in  $h_z \rightarrow 0$ , and

$$E_n(P|\mathbf{h}_t, h_z) - \tilde{E}_n(P|\mathbf{h}_t, h_z) = O(h_z^2). \quad (169)$$

Since the subsequent perturbative analysis of the meson energy spectra will be restricted to the linear order in  $h_z$ , we will neglect the difference (169) and drop tildes in  $\tilde{E}_n(P|\mathbf{h}_t, h_z)$ .

## VIII. HEURISTIC APPROACH TO THE KINK CONFINEMENT PROBLEM

It turns out, that even in the frame of the heuristic approach, the perturbative calculations of the meson energy spectra for the model (16)-(18) remain rather involved. By this reason, we present in this section an informal non-technical introduction to our heuristic semiclassical approach, which will be applied in Section IX for the calculation of the meson energy spectra.

We start from the more simple case studied in [11] of the XXZ model (16)-(18) in a weak staggered longitudinal field  $h_z > 0$ , and zero transverse field  $\mathbf{h}_t = 0$ .

At the first step, one treats the two kinks in the spin chain as classical spinless particles moving along the line and attracting one another with a linear potential. Their Hamiltonian is taken in the form

$$H(x_1, x_2, p_1, p_2) = \omega(p_1) + \omega(p_2) + f \cdot (x_2 - x_1), \quad (170)$$

where  $\omega(p)$  is the kink dispersion law (77), and  $f = 2h_z \bar{\sigma}$  is the string tension. The kink spatial coordinates  $x_1, x_2 \in \mathbb{R}$  are subjected to the constraint

$$-\infty < x_1 < x_2 < \infty, \quad (171)$$

that results from the local ‘‘hard-sphere interaction’’ of two particles.

After the canonical transformation

$$X = \frac{x_1 + x_2}{2}, \quad x = x_1 - x_2, \quad (172a)$$

$$P = p_1 + p_2, \quad p = \frac{p_1 - p_2}{2}, \quad (172b)$$

the Hamiltonian (170) takes the form

$$H(p, x|P) = \epsilon(p|P) - f x, \quad (173)$$

where  $\epsilon(p|P)$  is given by (150), and  $x < 0$ . The effective kinetic energy of two kinks  $\epsilon(p|P)$  is a  $\pi$ -periodical even function of  $p$ . At small enough absolute values of the total momentum

$$|P| < P_c(\eta), \quad (174)$$

with

$$P_c(\eta) = \arccos \frac{1 - k'(\eta)}{1 + k'(\eta)}, \quad (175)$$

it monotonically increases with  $p$  in the interval  $(0, \pi/2)$ , as it is shown in Figure 7.

The total energy-momentum conservation laws read:

$$\epsilon(p(t)|P) - f x(t) = E = \text{const}, \quad (176)$$

$$P(t) = \text{const}. \quad (177)$$

The classical evolution in the “center of mass frame” in the time interval between two successive particle collisions is determined by the canonical equations of motion:

$$\dot{X}(t) = \frac{\partial \epsilon(p|P)}{\partial P}, \quad (178a)$$

$$\dot{P}(t) = 0, \quad (178b)$$

$$\dot{x}(t) = \frac{\partial \epsilon(p|P)}{\partial p}, \quad (178c)$$

$$\dot{p}(t) = f. \quad (178d)$$

If the condition (174) is satisfied, and the energy  $E$  of two particles lies in the interval  $\epsilon(0|P) < E < \epsilon(\pi/2|P)$ , the momentum  $p$  characterising their relative motion varies in the lacuna  $-p_a < p < p_a$  shown in Figure 7. The functions  $x(t)$  and  $p(t)$  are periodical in  $t$  with the period  $t_1 = 2p_a/f$ , and

$$p(t) = -p_a + \{t/t_1\} t_1 f, \quad \text{at } t > 0, \quad (179)$$

where  $\{z\}$  denotes the fractional part of  $z$ . Figure 8 illustrates the world paths  $x_1(t) < x_2(t)$  of two particles for the simple Hamiltonian dynamics determined by equations (172), and (178).

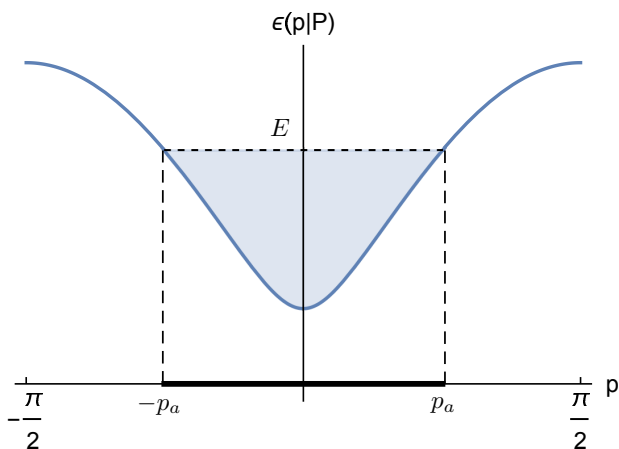


FIG. 7: The  $p$ -dependence of the effective kinetic energy  $\epsilon(p|P)$  determined by (150) at a fixed  $P$  satisfying (174). The kinematically allowed region  $(-p_a, p_a)$  of the momentum  $p$  for the given energy  $E$  of two particles is shown as well.

The second step of the calculation of the meson energy spectra  $E_n(P)$  in our heuristic approach requires quantization of the simple two-particle Hamiltonian dynamics described above. Two approximate quantization schemes have been used in [11]. The canonical quantization is appropriate for calculations of energies of ‘lightest’ mesons with small  $n = 1, 2, \dots$ , while the semiclassical quantization procedure is best suited for calculation of energies of highly excited mesons with  $n \gg 1$ . It turns out, however, the obtained in [11] predictions for the masses of the lightest mesons in the XXZ spin-chain model perturbed

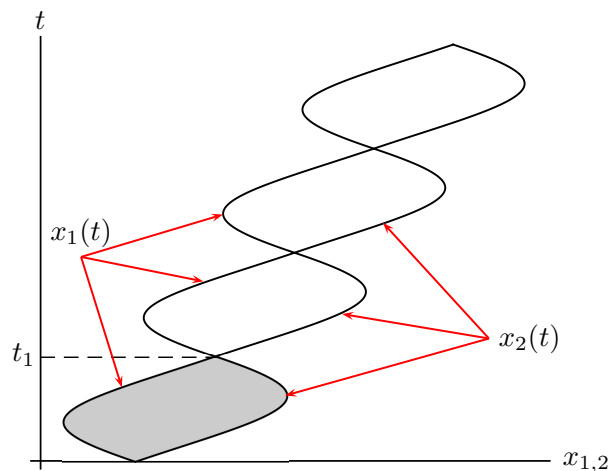


FIG. 8: World paths  $x_1(t)$  and  $x_2(t)$  of two particles for their classical evolution determined by equation (172), (178).

by the staggered longitudinal field, which are given by the semiclassical and low-energy expansions, are numerically very close to each other. The high efficiency of the semiclassical expansions for prediction of the energies of lightest mesons in several other models exhibiting confinement were also noticed in papers [17, 42–44], in which the meson energies were studied by direct numerical methods. By this reason, only the semiclassical quantization procedure will be considered in the present work.

It is easy to show [18], that if two particles behave as free fermions at  $f = 0$ , application of the Bohr-Sommerfeld rule [40] to their classical dynamics determined by equations (178) with  $f > 0$  leads to the quantization of the area  $S_n$  of the dashed region shown in Figure 8:

$$f S_n = 2\pi \left( n - \frac{1}{4} \right), \quad (180)$$

where  $n \gg 1$  is the number of the semiclassical energy level.

If the two Fermi-particles are not free, but strongly interact at short distances, formula (180) requires only a minor modification. Really, the short-range interaction between two particles induces their elastic scattering. Suppose, that the latter can be characterized at  $f = 0$  by the commutation relation

$$|p_1 p_2\rangle = -\exp[i\theta(p_1, p_2)] |p_2 p_1\rangle, \quad (181)$$

where  $p_1 > p_2$  are the momenta of two colliding particles, and  $\theta(p_1, p_2)$  denotes their scattering phase. At  $f > 0$ , the semiclassical evolution of two particles can be viewed as a combination of the classical movement along the world paths  $x_1(t), x_2(t)$  shown in Figure 8 with their quantum scattering at their meeting points, to which they arrive having the momenta  $p_1 = P/2 + p_a$ , and

$p_2 = P/2 - p_a$ . The elastic quantum scattering of two particles must be taken into account in the semiclassical quantization condition (180) by adding the scattering phase  $\theta(p_1, p_2)$  to its left-hand side:

$$f S_n + \theta(P/2 + p_a, -P/2 - p_a) = 2\pi \left( n - \frac{1}{4} \right). \quad (182)$$

This semiclassical quantization condition can be rewritten in the explicit form:

$$2E_n(P) p_a - \int_{-p_a}^{p_a} dp \epsilon(p|P) = \quad (183)$$

$$f [2\pi (n - 1/4) - \theta(P/2 + p_a, P/2 - p_a)].$$

In the above heuristic analysis based on the Hamiltonian (170), the kinks were treated as the spinless particles. However, the one-kink Bloch states  $|K_{ab}(p)\rangle_s$  of the unperturbed XXZ model, which are defined by equations (91), carry the spin index  $s = \pm 1/2$ . Accordingly, the two-particle scattering of such kinks is determined at zero magnetic field by three scattering phases  $\theta_\iota(p_1, p_2)$ , which are distinguished by the parity index  $\iota = 0, \pm$ , and explicitly given by equations (A6) in Appendix A. Then, one gets instead of (183) three quantization conditions:

$$2E_{\iota,n}(P) p_a - \int_{-p_a}^{p_a} dp \epsilon(p|P) = \quad (184)$$

$$f [2\pi (n - 1/4) - \theta_\iota(P/2 + p_a, P/2 - p_a)],$$

which determine the energies  $E_{\iota,n}(P)$  of the meson modes with  $\iota = 0, \pm$ .

The result (184) for the semiclassical meson energy spectra in the XXZ model (16)-(18) in the presence of a weak staggered longitudinal magnetic field  $h_z$  was obtained in [11, 12] and validated in [11] by the alternative derivation in the frame of the more rigorous and systematic approach exploiting the Bethe-Salpeter equation.

Now let us switch on the transverse magnetic field  $\mathbf{h}_t = h_2 \mathbf{e}_x + h_1 \mathbf{e}_y$  in the XXZ model Hamiltonian (16)-(18), and address the main question of our interest: how tuning the transverse magnetic field effects the meson energies in the weak confinement regime, which takes place in the presence of a weak staggered longitudinal field  $h_z > 0$ ? In order to clarify this issue, we intend to apply the heuristic semiclassical technique outlined above. To this end, three quantities characterising the model (16)-(18) at  $\mathbf{h}_t \neq 0$  are required.

1. The dispersion laws  $\Omega_{\mu\nu}(p|\mathbf{h}_t)$  of the kink topological excitations  $|\mathbb{K}_{\mu\nu}(p|\mathbf{h}_t)\rangle$  in the deconfined phase at  $h_z = 0$ . To the first order in  $\mathbf{h}_t$ , these dispersion laws are given by equations (118), (119) derived in section V.
2. The string tension

$$\mathfrak{f} = 2h_z \langle \sigma_0^z \rangle + O(h_z^3), \quad (185)$$

that determines the attractive force between two kinks at large distances in the weak confinement

regime at  $h_z > 0$ . Here  $\langle \sigma_0^z \rangle$  is the given by (152) staggered spontaneous magnetization in the presence of the transverse magnetic field  $\mathbf{h}_t$  at  $h_z = 0$ .

3. The two-kink scattering matrix in the deconfined phase  $h_z = 0$ , which at nonzero transverse magnetic field is determined by the commutation relation (132). At  $\mathbf{h}_t = 0$ , this commutation relation reduces to (126).

Note, that the one-kink Bloch states  $|\mathbb{K}_{\mu\nu}(p|\mathbf{h}_t)\rangle$  determined by equations (112), (117) describe spinless topological excitations, and their energies  $\Omega_{\mu\nu}(p|\mathbf{h}_t)$  are the  $2\pi$ -periodical functions of the quasimomentum  $p$ .

Following our previous strategy, we treat the two kinks as classical particles moving in the line and attracting one another with a linear potential. Their effective Hamiltonian will be taken in the form, which is analogous to (170):

$$H_{tr}(x_1, x_2, p_1, p_2) = \Omega_{10}(p_1|\mathbf{h}_t) + \Omega_{01}(p_2|\mathbf{h}_t) + \mathfrak{f} \cdot (x_2 - x_1), \quad (186)$$

where the particle spatial coordinates  $x_1, x_2$  satisfy (171).

At  $h_z = 0$ , the string tension  $\mathfrak{f}$  vanishes, and the right-hand side of (188) reduces to the energy

$$\Omega_{10}(p_1|\mathbf{h}_t) + \Omega_{01}(p_2|\mathbf{h}_t) \quad (187)$$

of the two-kink Bloch state  $|\mathbb{K}_{10}(p_1|\mathbf{h}_t)\mathbb{K}_{01}(p_2|\mathbf{h}_t)\rangle$ , in agreement with (122b).

Analysis of classical dynamics of two particles determined by the Hamiltonian (188) is straightforward. After the canonical transformation (172), the latter takes the form

$$H_{tr}(x, p|P) = \mathcal{E}(p|P, \mathbf{h}_t) - \mathfrak{f} x, \quad (188)$$

where  $\mathcal{E}(p|P, \mathbf{h}_t)$  is given by (149), and  $x < 0$ . The canonical equations of motion (178) now modify to:

$$\dot{X}(t) = \frac{\partial \mathcal{E}(p|P, \mathbf{h}_t)}{\partial P}, \quad (189a)$$

$$\dot{P}(t) = 0, \quad (189b)$$

$$\dot{x}(t) = \frac{\partial \mathcal{E}(p|P, \mathbf{h}_t)}{\partial p}, \quad (189c)$$

$$\dot{p}(t) = \mathfrak{f}. \quad (189d)$$

At  $\mathbf{h}_t = 0$  the effective kinetic energy  $\mathcal{E}(p|P, \mathbf{h}_t)$  reduces to the function  $\mathcal{E}(p|P, \mathbf{0}) = \epsilon(p|P)$ , which is even and  $\pi$ -periodical in the  $p$ -variable. These symmetries are broken at  $\mathbf{h}_t \neq 0$ , though the function  $\mathcal{E}(p|P, \mathbf{h}_t)$  remains  $2\pi$ -periodical in  $p$  at any  $\mathbf{h}_t$  and  $P$ .

Figures 9a and 9b illustrate the profiles of the effective kinetic energy (149) at  $P = 0$  in the cases  $\mathbf{h}_t = 0$  and  $\mathbf{h}_t \neq 0$ , respectively. Two kinematically allowed lacunas in the  $p$ -variable, which are determined by the inequality

$$\mathcal{E}(p|P, \mathbf{h}_t) < E, \quad (190)$$

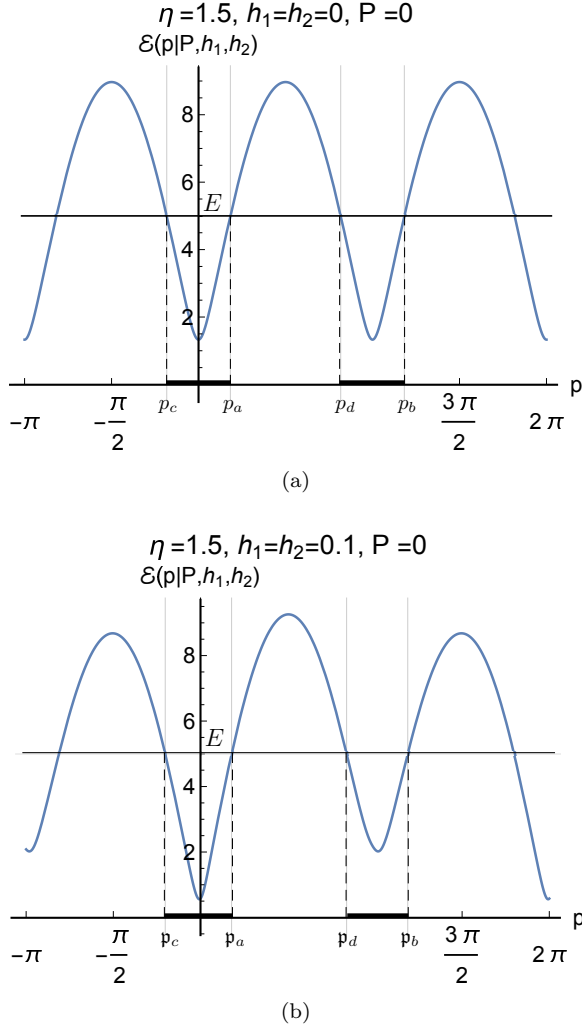


FIG. 9: Effective kinetic energy profile  $\mathcal{E}(p|P, \mathbf{h}_t)$  given by (149) at  $\eta = 1.5$ ,  $P = 0$  at  $h_1 = h_2 = 0$  (a); and at  $h_1 = h_2 = 0.1$  (b).

are also shown in these figures. Accordingly, for a given energy  $E$  of two particles, the canonical equations of motion (189) admit two periodical phase trajectories, in which the momentum  $p$  varies in the left, and in the right lacuna, respectively. In the case  $\mathbf{h}_t = 0$  illustrated in Figure 9a, these two phase trajectories being shifted one with respect to another by  $\pi$  in the  $p$ -variable, describe, in fact, the same physical dynamics. In contrast, at  $\mathbf{h}_t \neq 0$  the  $\pi$ -periodicity in the  $p$ -variable of the function  $\mathcal{E}(p|P, \mathbf{h}_t)$  is broken, and the phase trajectories corresponding to the lacunas  $(p_c, p_a)$  and  $(p_d, p_b)$  shown in Figure 9b, describe slightly different dynamics.

Existence of two non-equivalent periodical phase trajectories, which contributions interfere in the quantum state of the system, strongly effects the semiclassical quantization of the two-kink dynamics in the presence of the transverse magnetic field  $\mathbf{h}_t \neq 0$ . The energy spectrum of the two-kink bound states cannot be determined

in this case by means of the standard Bohr-Sommerfeld quantization rule. Instead, we will adopt to this end the well-known procedure, which was developed for calculation of the energy spectra of conducting electrons in normal metals in the regime of the magnetic breakdown, see e.g. [45, 46].

According to this procedure, the wave function of two kinks should be written as a linear combination of two semiclassical exponents, which correspond to the classical phase trajectories associated with the left and right lacunas in Figure 9b. This wave function describes the quantum state of two kinks at large enough separations  $|x| = x_2 - x_1$  between them. When two kinks meet together in the real space, they undergo the elastic two-channel quantum scattering, which, roughly speaking, induce the quantum jumps of the phase point from one lacuna to another. Sewing at small  $x_2 - x_1$  the semiclassical wave function by means of the scattering matrix yields the secular equation, which determines the semiclassical energy spectrum of the two-kink bound states.

The outlined above procedure of calculation of the semiclassical meson energy spectrum in the presence of the transverse magnetic field will be described in much details in the next section.

## IX. QUANTITATIVE ANALYSIS OF THE KINK CONFINEMENT AT A WEAK $h_z > 0$

Let us introduce the Fourier coefficients  $\psi_n(j|P)$  of the  $2\pi$ -periodical reduced wave function  $\phi_n(p|P)$  determined by equation (146):

$$\phi_n(p|P) = \sum_{j=-\infty}^{\infty} e^{-ipj} \psi_n(j|P), \quad (191)$$

$$\psi_n(j|P) = \int_0^{2\pi} \frac{dp}{2\pi} e^{ipj} \phi_n(p|P). \quad (192)$$

For negative  $j$ ,  $\psi_n(j|P)$  can be viewed as the reduced wave function of two kinks forming a meson, in the spatial coordinate representation. The integer variable  $-j = j_2 - j_1$  at  $j < 0$  has the physical meaning of the distance between two kinks "located near the points"  $j_1$  and  $j_2$ , respectively, with  $j_1 < j_2$ . Of course, if  $\eta$  is not too large, these kinks are not well localized, but instead are spread along the spin chain over the widths of order  $2\xi_c(\eta)$ , where

$$\xi_c(\eta) = \frac{m(\eta)^{-1}}{2} \quad (193)$$

is the correlation length, and

$$m(\eta) = \frac{k'(\eta)}{k(\eta)} \quad (194)$$

is the kink mass.

At large negative  $j < 0$ , such that  $|j| \gg 2\xi_c(\eta)$ , the kinks forming a meson interact one with another only by

the linear attractive potential  $f(j_2 - j_1) = -fj$ , where  $f$  is the string tension (185) in the presence of the transverse magnetic field  $\mathbf{h}_t$ . Accordingly, the wave function  $\psi(j|P)$  should satisfy at large negative  $j$  the following equation:

$$\hat{\mathcal{E}} \psi(j|P) - fj \psi(j|P) = E(P) \psi(j|P), \quad (195)$$

where  $\hat{\mathcal{E}}$  is the integral convolution operator of the "kinetic energy of two kinks":

$$\hat{\mathcal{E}} \psi(j) = \sum_{j'=-\infty}^{\infty} \psi(j') \int_0^{2\pi} \frac{dp}{2\pi} e^{ip(j-j')} \mathcal{E}(p|P). \quad (196)$$

The kernel of this integral operator exponentially decays  $\sim \exp\{-|j - j'|/[2\xi_c(\eta)]\}$  at large distances  $|j - j'| \gg 2\xi_c(\eta)$ .

The function  $\mathcal{E}(p|P)$  that stands in the right-hand side of (196) is the familiar effective kinetic energy of two kinks (149), which properties were discussed in the previous section.

At a small enough  $P \in (0, P_c(\eta))$  with  $P_c(\eta)$  given by (175), and at a fixed  $E \in (\epsilon(0|P), \epsilon(\pi/2|P))$ , equation

$$\epsilon(p|P) = E, \quad (197)$$

has in the interval  $-\pi/2 < p < 3/2\pi$  four solutions  $p_c(E), p_a(E), p_d(E), p_b(E)$ , which are shown in Figure 9a. Due to the symmetry relations (153), we get:

$$p_c = -p_a, \quad p_b = p_a + \pi, \quad p_d = \pi - p_a. \quad (198)$$

Accordingly, the two classically allowed intervals  $(p_c, p_a)$  and  $(p_d, p_b)$  for the momentum  $p$  have the same widths in this case.

Application of the weak transverse magnetic field  $\mathbf{h}_t$  deforms the kinetic energy profile, as it is shown in Figure 9b. As the result, the four solutions  $\mathbf{p}_c, \mathbf{p}_a, \mathbf{p}_d, \mathbf{p}_b$ , of the equation

$$\mathcal{E}(p|P, \mathbf{h}_t) = E \quad (199)$$

become slightly shifted with respect to their positions at  $\mathbf{h}_t = 0$ . To the first order in  $|\mathbf{h}_t|$ , we get from (199), (149):

$$\begin{aligned} \mathbf{p}_a(\mathbf{h}_t) &= p_a - \frac{\delta\mathcal{E}(p_a|P, \mathbf{h}_t)}{\epsilon'(p_a|P)} + O(|\mathbf{h}_t|^2), \\ \mathbf{p}_c(\mathbf{h}_t) &= p_c + \frac{\delta\mathcal{E}(-p_a|P, \mathbf{h}_t)}{\epsilon'(p_a|P)} + O(|\mathbf{h}_t|^2), \\ \mathbf{p}_b(\mathbf{h}_t) &= p_b + \frac{\delta\mathcal{E}(p_a|P, \mathbf{h}_t)}{\epsilon'(p_a|P)} + O(|\mathbf{h}_t|^2), \\ \mathbf{p}_d(\mathbf{h}_t) &= p_d - \frac{\delta\mathcal{E}(-p_a|P, \mathbf{h}_t)}{\epsilon'(p_a|P)} + O(|\mathbf{h}_t|^2). \end{aligned} \quad (200)$$

The widths of two kinematically allowed intervals  $(\mathbf{p}_c, \mathbf{p}_a)$ , and  $(\mathbf{p}_d, \mathbf{p}_b)$  become different at  $\mathbf{h}_t \neq \mathbf{0}$ .

At a small  $f > 0$ , the approximate semiclassical solution of equation (195) can be written as

$$\psi(j|P) = C_1 \psi^{(1)}(j|P) + C_2 \psi^{(2)}(j|P), \quad (201)$$

where

$$\psi^{(1)}(j|P) = \int_{-\pi/2}^{\pi/2} \frac{dp}{2\pi} e^{ipj - iF_1(p, E|\mathbf{h}_t)/f}, \quad (202a)$$

$$\psi^{(2)}(j|P) = \int_{\pi/2}^{3\pi/2} \frac{dp}{2\pi} e^{ipj - iF_2(p, E|\mathbf{h}_t)/f}, \quad (202b)$$

and

$$F_1(p, E|\mathbf{h}_t) = \int_0^p dp' [\mathcal{E}(p'|P, \mathbf{h}_t) - E], \quad (203a)$$

$$F_2(p, E|\mathbf{h}_t) = \int_\pi^p dp' [\mathcal{E}(p'|P, \mathbf{h}_t) - E]. \quad (203b)$$

The integrals in (202) are determined at small  $f$  by their saddle-points asymptotics. Close to the scattering region at  $-j \sim 2\xi_c(\eta)$ , this yields to the leading order in  $f > 0$ :

$$\psi(j|P) = B_{in,1} e^{i\mathbf{p}_a j} + B_{in,2} e^{i\mathbf{p}_b j} + B_{out,1} e^{i\mathbf{p}_c j} + B_{out,2} e^{i\mathbf{p}_d j}, \quad (204)$$

and

$$C_1 = B_{in,1} \sqrt{\frac{2\pi\mathcal{E}'(\mathbf{p}_a|P, \mathbf{h}_t)}{f}} e^{iF_1(\mathbf{p}_a, E|\mathbf{h}_t)/f + i\pi/4} \quad (205)$$

$$= B_{out,1} \sqrt{-\frac{2\pi\mathcal{E}'(\mathbf{p}_c|P, \mathbf{h}_t)}{f}} e^{iF_1(\mathbf{p}_c, E|\mathbf{h}_t)/f - i\pi/4},$$

$$C_2 = B_{in,2} \sqrt{\frac{2\pi\mathcal{E}'(\mathbf{p}_b|P, \mathbf{h}_t)}{f}} e^{iF_2(\mathbf{p}_b, E|\mathbf{h}_t)/f + i\pi/4}$$

$$= B_{out,2} \sqrt{-\frac{2\pi\mathcal{E}'(\mathbf{p}_d|P, \mathbf{h}_t)}{f}} e^{iF_2(\mathbf{p}_d, E|\mathbf{h}_t)/f - i\pi/4}.$$

On the other hand, the amplitudes of out- and in- plane waves at  $-j \gtrsim 2\xi_c(\eta)$  in equation (204) must be related by the scattering condition. Neglecting the effect of the weak longitudinal staggered magnetic field  $h_z$  on the two-kink scattering at small distances, we obtain from (132):

$$B_{out,1} = W_1^1(E, P|\mathbf{h}_t) B_{in,1} + W_1^2(E, P|\mathbf{h}_t) B_{in,2} + O(h_z), \quad (206)$$

$$B_{out,2} = W_2^1(E, P|\mathbf{h}_t) B_{in,1} + W_2^2(E, P|\mathbf{h}_t) B_{in,2} + O(h_z).$$

Combining (206) with (205), we arrive to the system of two uniform linear equations on the amplitudes  $B_{in,1}, B_{in,2}$ :

$$\begin{aligned} & B_{in,1} \sqrt{\mathcal{E}'(\mathbf{p}_a|P, \mathbf{h}_t)} e^{iF_1(\mathbf{p}_a, E|\mathbf{h}_t)/f + i\pi/4} \\ &= [W_1^1(E, P|\mathbf{h}_t) B_{in,1} + W_1^2(E, P|\mathbf{h}_t) B_{in,2}] \\ &\times \sqrt{-\mathcal{E}'(\mathbf{p}_c|P, \mathbf{h}_t)} e^{iF_1(\mathbf{p}_c, E|\mathbf{h}_t)/f - i\pi/4}, \\ & B_{in,2} \sqrt{\mathcal{E}'(\mathbf{p}_b|P, \mathbf{h}_t)} e^{iF_2(\mathbf{p}_b, E|\mathbf{h}_t)/f + i\pi/4} \\ &= [W_2^1(E, P|\mathbf{h}_t) B_{in,1} + W_2^2(E, P|\mathbf{h}_t) B_{in,2}] \\ &\times \sqrt{-\mathcal{E}'(\mathbf{p}_d|P, \mathbf{h}_t)} e^{iF_2(\mathbf{p}_d, E|\mathbf{h}_t)/f - i\pi/4}. \end{aligned} \quad (207)$$

Equating the determinant of these equations to zero leads to the secular equation, which determines the meson energy spectrum  $E_n(P|\mathbf{h}_t, h_z)$ .

In the analysis described above, we did not require, that the components  $h_1, h_2$  of the transverse magnetic field are infinitesimally small. Now let us treat  $h_1, h_2$  as small parameters and simplify the secular equation in two steps.

On the first step, we replace in (207) the scattering matrix  $W_i^j(E, P|\mathbf{h}_t)$  by the zero-order term in its expansions in  $\mathbf{h}_t$ :

$$\begin{aligned} W_1^1(E, P|\mathbf{h}_t) &= \frac{w_0 + w_+}{2} + O(\mathbf{h}_t), \\ W_1^2(E, P|\mathbf{h}_t) &= \frac{-w_0 + w_+}{2} + O(\mathbf{h}_t), \\ W_2^1(E, P|\mathbf{h}_t) &= \frac{-w_0 + w_+}{2} + O(\mathbf{h}_t), \\ W_2^2(E, P|\mathbf{h}_t) &= \frac{w_0 + w_+}{2} + O(\mathbf{h}_t), \end{aligned} \quad (208)$$

where

$$\begin{aligned} w_0 &= w_0(P/2 + p_a, P/2 - p_a), \\ w_+ &= w_+(P/2 + p_a, P/2 - p_a). \end{aligned} \quad (209)$$

We also replace the string tension  $\mathfrak{f} = 2h_z \langle \sigma_0^z \rangle$  by its value  $f = 2h_z \bar{\sigma}$  at  $\mathbf{h}_t = 0$ , taking into account that the linear in  $\mathbf{h}_t$  term in the expansion of  $\langle \sigma_0^z \rangle$  vanishes:  $\langle \sigma_0^z \rangle = \bar{\sigma} + O(|\mathbf{h}_t|^2)$ . As the result, the secular equation takes the form:

$$\det \mathbf{D} = 0, \quad (210)$$

where  $\mathbf{D}$  is the  $2 \times 2$ -matrix with the following entries:

$$\begin{aligned} D_{11} &= \frac{w_0 + w_+}{2} \\ &- i \sqrt{\frac{\mathcal{E}'(\mathbf{p}_a|P, \mathbf{h}_t)}{|\mathcal{E}'(\mathbf{p}_c|P, \mathbf{h}_t)|}} e^{i[F_1(\mathbf{p}_a, E|\mathbf{h}_t)] - F_1(\mathbf{p}_c, E|\mathbf{h}_t)]/f}, \\ D_{12} &= D_{21} = \frac{-w_0 + w_+}{2}, \\ D_{22} &= \frac{w_0 + w_+}{2} \\ &- i \sqrt{\frac{\mathcal{E}'(\mathbf{p}_b|P, \mathbf{h}_t)}{|\mathcal{E}'(\mathbf{p}_d|P, \mathbf{h}_t)|}} e^{i[F_2(\mathbf{p}_b, E|\mathbf{h}_t)] - F_2(\mathbf{p}_d, E|\mathbf{h}_t)]/f}. \end{aligned} \quad (211)$$

At the second step, we hold the linear terms in  $\mathbf{h}_t$  in

the functions  $F_{1,2}(\mathbf{p}_j, E|\mathbf{h}_t)$ ,  $j = a, b, c, d$ :

$$\begin{aligned} F_1(\mathbf{p}_a, E|\mathbf{h}_t) &= F_1(p_a, E|0) \\ &+ \int_0^{p_a} dp \delta\mathcal{E}(p|P, \mathbf{h}_t) + O(|\mathbf{h}_t|^2), \\ F_1(\mathbf{p}_c, E|\mathbf{h}_t) &= -F_1(p_a, E|0) \\ &- \int_{-p_a}^0 dp \delta\mathcal{E}(p|P, \mathbf{h}_t) + O(|\mathbf{h}_t|^2), \\ F_2(\mathbf{p}_b, E|\mathbf{h}_t) &= F_1(p_a, E|0) \\ &- \int_0^{p_a} dp \delta\mathcal{E}(p|P, \mathbf{h}_t) + O(|\mathbf{h}_t|^2), \\ F_2(\mathbf{p}_d, E|\mathbf{h}_t) &= -F_1(p_a, E|0) \\ &+ \int_{-p_a}^0 dp \delta\mathcal{E}(p|P, \mathbf{h}_t) + O(|\mathbf{h}_t|^2), \end{aligned} \quad (212)$$

since these functions are divided by the small parameter  $f \sim h_z$  in the exponent factors in (211). In the functions under the square roots in the right-hand side of (211), we put  $\mathbf{h}_t = 0$ :

$$\begin{aligned} \mathcal{E}'(p_a|P, \mathbf{h}_t) &= \epsilon'(p_a^{(0)}|P) + O(\mathbf{h}_t), \\ \mathcal{E}'(p_c|P, \mathbf{h}_t) &= -\epsilon'(p_a^{(0)}|P) + O(\mathbf{h}_t), \\ \mathcal{E}'(p_b|P, \mathbf{h}_t) &= \epsilon'(p_a^{(0)}|P) + O(\mathbf{h}_t), \\ \mathcal{E}'(p_d|P, \mathbf{h}_t) &= -\epsilon'(p_a^{(0)}|P) + O(\mathbf{h}_t). \end{aligned} \quad (213)$$

Upon substitutions (208), (212), and (213), equations (207) reduce to the form:

$$\begin{aligned} B_{in,1} \frac{w_0 + w_+}{2} + B_{in,2} \frac{-w_0 + w_+}{2} &= B_{in,1} e^{i\Lambda_0} Z_0, \\ B_{in,1} \frac{-w_0 + w_+}{2} + B_{in,2} \frac{w_0 + w_+}{2} &= B_{in,2} e^{-i\Lambda_0} Z_0, \end{aligned} \quad (214)$$

where

$$\begin{aligned} Z_0(E, P) &= \exp[2iF_1(p_a, E|0)/f + i\pi/2] \\ &= \exp\left\{\frac{2i}{f} \int_0^{p_a} dp [\epsilon(p|P) - E] + \frac{i\pi}{2}\right\}, \\ \Lambda_0(E, P) &= \frac{1}{f} \int_{-p_a}^{p_a} dp \delta\mathcal{E}(p|P, \mathbf{h}_t). \end{aligned} \quad (216)$$

Using equations (151), (119), the integral in the right-hand side of (216) can be rewritten in the explicit form, yielding:

$$\Lambda_0(E, P) = -\frac{2 \sinh \eta}{f} A_+ h_2 \int_{p_2}^{p_1} dp \frac{\cos p}{\omega(p)}, \quad (217)$$

where  $p_{1,2}$  are the solutions of the equations

$$p_1 + p_2 = P, \quad \omega(p_1) + \omega(p_2) = E, \quad (218)$$

such that  $-\pi/2 < p_2 < p_1 < \pi/2$ . Note, that parameter  $\Lambda_0$  does not depend on the  $y$ -component of the transverse magnetic field  $h_1$ , as one can see from (217).

Equating the determinant of the system (214) to zero

yields the secular equation

$$Z_0^2 - (w_0 + w_+)Z_0 \cos \Lambda_0 + w_0 w_+ = 0, \quad (219)$$

that determines the meson energies  $E_n(P)$ . This equation can be rewritten in the more symmetric form, which is convenient for numerical calculations:

$$\sin \left[ \frac{2F_1(p_a, E|0)}{f} - \frac{\theta_0(P/2 + p_a, P/2 - p_a) + \theta_+(P/2 + p_a, P/2 - p_a)}{2} \right] - \cos \left[ \frac{\theta_+(P/2 + p_a, P/2 - p_a) - \theta_0(P/2 + p_a, P/2 - p_a)}{2} \right] \cos \Lambda_0 = 0. \quad (220)$$

For the ratio  $B_{in,2}/B_{in,1}$ , we get from (214):

$$\frac{B_{in,2}}{B_{in,1}} = \frac{2Z_0 \exp(i\Lambda_0) - w_+ - w_0}{w_+ - w_0}. \quad (221)$$

The absolute value of the coefficient  $B_{in,1}$  can be fixed from the normalization condition (147), as it is described in Appendix B. The final result reads:

$$|B_{in,1}|^2 = \frac{f}{2p_a \epsilon'(p_a)(1 + |B_{in,2}/B_{in,1}|^2)}. \quad (222)$$

At zero transverse magnetic field  $\mathbf{h}_t = 0$ , parameter  $\Lambda_0$  vanishes, and equation (219) has two solutions:

$$Z_0 = w_0, \quad \text{and} \quad Z_0 = w_+. \quad (223)$$

The first one leads to the equation

$$\exp[2iF_1(p_a, E|0)/f + i\pi/2] = w_0, \quad (224)$$

which determines in the first semiclassical regime the energy spectrum of the so-called *transverse meson modes* (T) with spin  $s = \pm 1$ . In the explicit form, the above equation reduced to the semiclassical quantization condition (184) with  $\iota = 0$ , in agreement with equation (172) in [11].

The second solution in (223) leads to the equation

$$\exp[2iF_1(p_a, E|0)/f + i\pi/2] = w_+. \quad (225)$$

Its explicit form is given by equation (184) for the *longitudinal meson modes* (L) with  $s = 0$  and parity  $\iota = +$ , in agreement with [11].

The meson states in equation (184) are enumerated by the natural number  $n = 1, 2, \dots$ . Note, that two equations (224), and (225) can be joined into the single one, that can be obtained from equation (220) by putting  $\Lambda_0 = 0$  in the latter. Solutions  $E_n(P)$  of equation (220) at  $\Lambda_0 = 0$  determine the spectra of the meson modes in the first semiclassical regime at  $\mathbf{h}_t = 0$ , and  $P \in (-P_c(\eta), P_c(\eta))$ . The solutions  $E_n(P)$  with odd

$n$  correspond to the transverse meson modes with spin  $s = \pm 1$ , while solutions with even  $n$  represent the longitudinal meson modes with spin  $s = 0$ :

$$E_n(P) = \begin{cases} E_{0,(n+1)/2}(P), & n \text{ odd,} \\ E_{+,n/2}(P), & n \text{ even,} \end{cases} \quad (226)$$

where  $n = 1, 2, \dots$ , and  $E_{0,n}(P)$ ,  $E_{+,n}(P)$  are given by (184). At  $\mathbf{h}_t \neq 0$ , the factor  $\cos \Lambda_0$  in the right-hand side of (220) leads to the mixing of the transverse and longitudinal meson modes.

Figures 10 display the variation of the left-hand side of the secular equation (220) with the energy of two kinks  $E$  for  $P = 0$  at three different values  $h_1 = 0, 0.05, 0.01$  of the  $y$ -component of the transverse magnetic field. The the  $x$ -component of the transverse magnetic field is taken by  $h_2 = 0.4h_1$  in all three cases. Two other parameters of the Hamiltonian (16) are taken at the fixed values  $\eta = 1.25$ , and  $h_z = 0.02$ . The meson energies  $E_n(P)$ ,  $n = 1, 2, \dots$  in model (16) at small enough  $h_z, h_1, h_2$  are given in the semiclassical approximation by zeroes of equation (220).

At  $h_1 = h_2 = 0$ , the parameter  $\Lambda_0$  in the secular equation (220) vanishes, and  $\cos \Lambda_0 = 1$ . Figure 10a displays the energy dependence of the left-hand side of (220) in the latter case. This oscillating function is defined in the interval between the minimal and maximal values of the two-kink effective kinetic energy  $\epsilon(p|P, \eta)$ , which are indicated by vertical lines in Figure 10a. The zeroes of this function are located at the energies  $E_n(P)$  of the transverse and longitudinal meson modes, which are given by equation (184) with  $\iota = 0$ , and  $\iota = +$ , respectively.

Application of the transverse magnetic field  $\mathbf{h}_t$  breaks the symmetry between the left and right classically allowed lacunas  $\mathfrak{P}^{(1)} = (\mathfrak{p}_c, \mathfrak{p}_a)$  and  $\mathfrak{P}^{(2)} = (\mathfrak{p}_d, \mathfrak{p}_b)$  in the  $p$ -variable, which are shown in Figure 9b. As the result, the wave functions  $\psi^{(1)}(j|P)$  and  $\psi^{(2)}(j|P)$  defined by (202), which correspond to the semiclassical evolution  $\langle x(t), p(t) \rangle$  of two kinks with  $p(t)$  in the lacunas  $p(t) \in \mathfrak{P}^{(1)}$  and  $p(t) \in \mathfrak{P}^{(2)}$ , respectively, become different. The quantum scattering of two kinks upon their

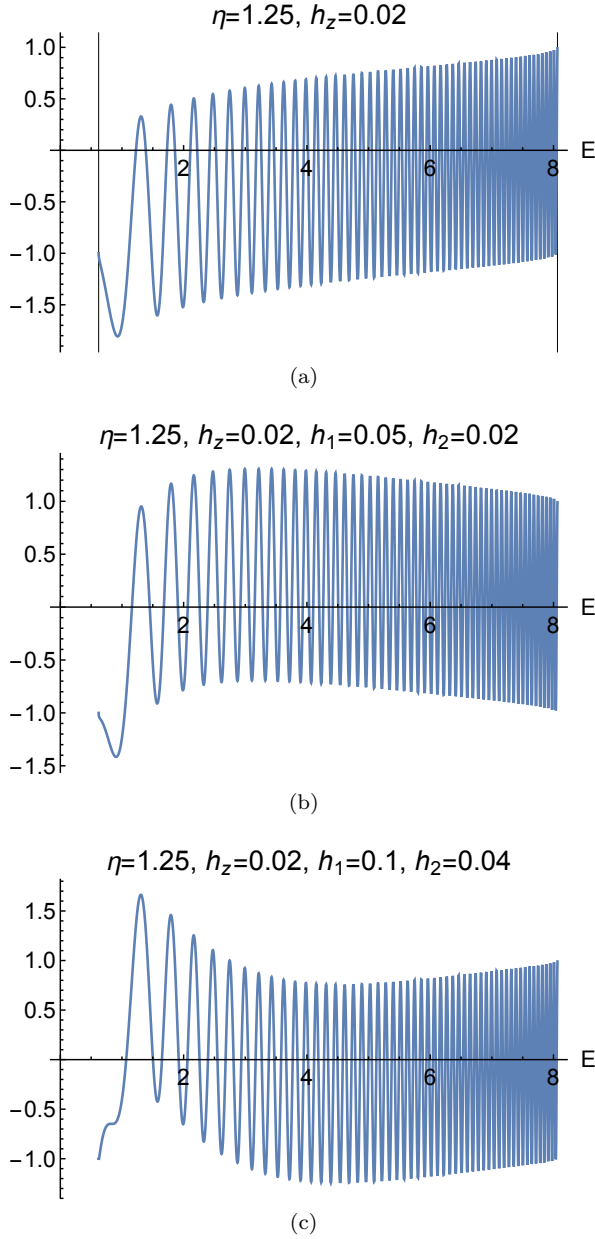


FIG. 10: Plot of the left-hand side of (220) versus the energy  $E$  of two kinks for  $\eta = 1.25$ ,  $h_z = 0.02$ , and  $P = 0$  at three values of the transverse magnetic field  $y$ -component  $h_1$ : (a)  $h_1 = 0$ ; (b)  $h_1 = 0.05$ ; (c)  $h_1 = 0.1$ . The  $x$ -component  $h_2$  of the transverse magnetic fields is taken  $h_2 = 0.4h_1$  in all cases.

collisions at  $|x| \lesssim \xi_c(\eta)$  provides the effective “hopping” of the two-kink classical phase point from one lacuna to another. This leads to the interference of two semiclassical wave functions  $\psi^{(1)}(j|P)$  and  $\psi^{(2)}(j|P)$ , which, in turn, causes the  $\mathbf{h}_t$ -dependent modulation of the function in the left-hand of the secular equation (220) shown in Figures 10b, 10c.

Figure 11 shows the dependences of energies  $E_n(P|\mathbf{h}_t, h_z)$  of four lightest meson modes at  $P = 0$

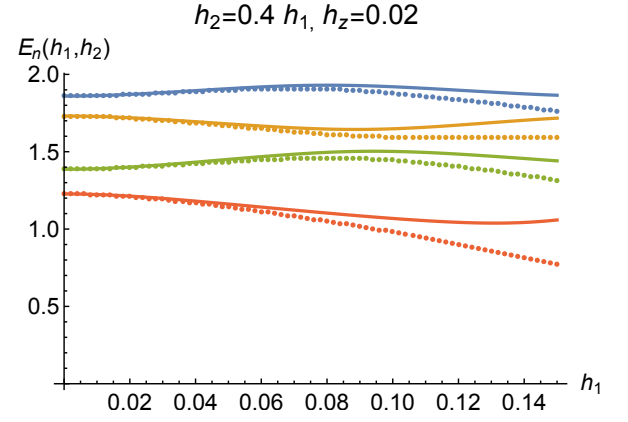


FIG. 11: Dependences of energies  $E_n$  of four lowest meson modes on the  $y$ -component  $h_1$  of the transverse magnetic field at  $\eta = 1.25$ ,  $P = 0$ ,  $h_z = 0.02$ ,  $h_2 = 0.4h_1$  according to (220) (solid curves), and (210) (dotted curves), respectively.

on the  $y$ -component  $h_1$  of the transverse magnetic field  $\mathbf{h}_t$ . Three other parameters of the Hamiltonian (16) are taken the same as in Figure 10:  $\eta = 1.25$ ,  $h_2 = 0.4h_1$ ,  $h_z = 0.02$ . The solid lines in Figure 11 represent the meson energies obtained from the secular equation (220). The dotted curves display the meson energies, that were obtained from the secular equation (210), which we expect to be slightly more accurate.

Comparison of solid and dotted curves in Figure 11 allows one to estimate the accuracy of the described above calculations of the meson energy spectra. One can conclude from Figure 11, that the perturbative in  $\mathbf{h}_t$  calculations of the meson energies are rather accurate at  $0 < h_1 \lesssim 0.1$  for chosen values of other parameters, but the accuracy rapidly decreases at larger  $h_1 \gtrsim 0.12$ .

As it was noticed above, at  $\mathbf{h}_t = 0$ , the states  $|\tilde{\pi}_n(P)\rangle$  with odd  $n = 1, 3, \dots$  represent the transverse meson modes characterized by the spin polarization  $s = \pm 1$ , while the states with  $n = 2, 4, \dots$  correspond to the longitudinal meson modes with  $s = 0$ . Application of the transverse magnetic field  $\mathbf{h}_t \neq 0$  leads to the hybridization of the transverse and longitudinal meson modes. At very weak transverse magnetic fields  $\mathbf{h}_t$ , the energies of the mesons with odd  $n$  exhibit an downward variation with increasing  $|\mathbf{h}_t|$ , while the energies of the modes with even  $n$  increase together with  $|\mathbf{h}_t|$ . Upon further increase of the transverse magnetic field, the avoided crossing of the energies of the modes with  $n = 2m$  and  $n = 2m + 1$  takes place. As one can see in Figure 11, for the second and third meson modes, this avoided crossing takes place at  $h_1 \approx 0.1$ , at chosen values of other parameters.

Let us turn now to the energy spectra of mesons with momenta  $P$  close to  $\pi$ . Perturbative calculations of these energy spectra can be performed by means of the described above heuristic semiclassical technique. The central role in this calculation plays the effective kinetic energy of two kinks  $\mathcal{E}(p|P, \mathbf{h}_t)$  defined by (149). Due to



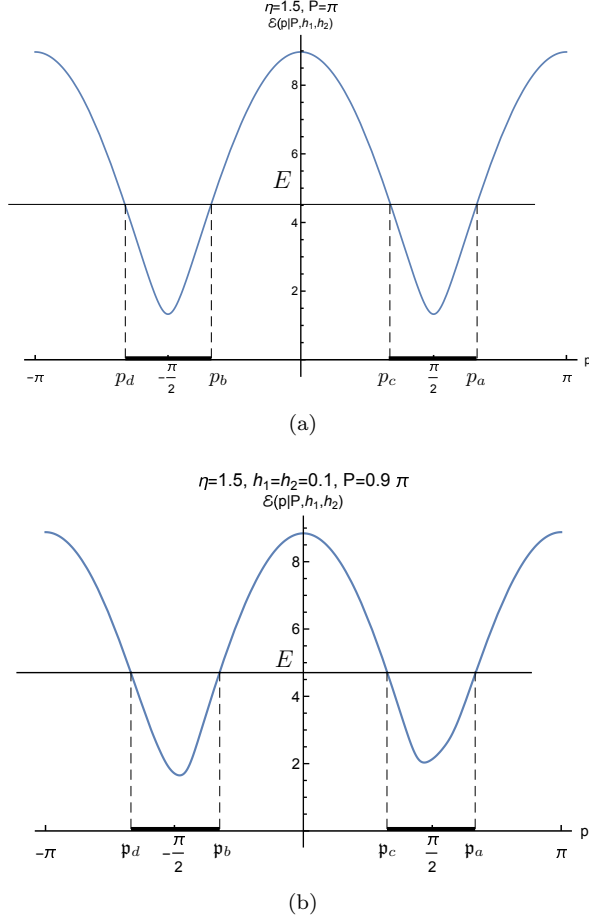


FIG. 12: Effective kinetic energy profile  $\mathcal{E}(p|P, \mathbf{h}_t)$  given by (149) at  $\eta = 1.5$ , and (a)  $P = \pi$  and arbitrary  $h_1, h_2$ ; (b)  $P = 0.9\pi$  and  $h_1 = h_2 = 0.1$ .

(157), the first variation with  $\mathbf{h}_t$  of this function vanishes at  $P = \pi$ :

$$\mathcal{E}(p|\pi, \mathbf{h}_t) = \epsilon(p|\pi) + O(|\mathbf{h}_t|^2). \quad (227)$$

Figure 12a displays the plot of the function  $\epsilon(p|\pi)$  at  $\eta = 1.5$ . At a given  $E \in (\epsilon(\pi/2|\pi), \epsilon(0|\pi))$ , equation  $\epsilon(p|\pi) = E$  has in the interval  $(-\pi/2, \pi/2)$  four solutions  $p_i$ ,  $i = a, b, c, d$ , shown in this figure. It follows from the symmetry properties (153) of the function  $\epsilon(p|P)$ , that:

$$p_c = \pi - p_a, \quad p_b = p_a - \pi, \quad p_d = -p_a. \quad (228)$$

Figure 12b illustrates the plot of the function  $\mathcal{E}(p|P, \mathbf{h}_t)$  at  $P = 0.9\pi$ ,  $h_1 = h_2 = 0.1$ , and  $\eta = 1.5$ . The four solutions  $\mathbf{p}_i$ ,  $i = a, b, c, d$  of the equation  $\mathcal{E}(p|P, \mathbf{h}_t) = E$  shown in this figure are slightly shifted from their positions at  $P = \pi$ , and the widths of the lacunas  $(\mathbf{p}_d, \mathbf{p}_b)$  and  $(\mathbf{p}_c, \mathbf{p}_a)$  become different.

Subsequent calculations of the meson energy spectra at  $P$  close to  $\pi$  are very similar to the performed above calculations at small  $P$ . We define by (192) the reduced wave function  $\psi_n(j|P)$  of two kinks in the spatial coordinate representation. At large negative  $j$ , this function

must satisfy the integral equation (195) with the convolution operator (196). We again write the approximate semiclassical solution of equation (195) in the form (201), but now

$$\psi^{(1)}(j|P) = \int_0^\pi \frac{dp}{2\pi} e^{ipj - iF_1(p, E|\mathbf{h}_t)/f}, \quad (229a)$$

$$\psi^{(2)}(j|P) = \int_{-\pi}^0 \frac{dp}{2\pi} e^{ipj - iF_2(p, E|\mathbf{h}_t)/f}, \quad (229b)$$

and

$$F_1(p, E|\mathbf{h}_t) = \int_{\pi/2}^p dp' [\mathcal{E}(p'|P, \mathbf{h}_t) - E], \quad (230a)$$

$$F_2(p, E|\mathbf{h}_t) = \int_{-\pi/2}^p dp' [\mathcal{E}(p'|P, \mathbf{h}_t) - E]. \quad (230b)$$

Formula (204) still gives us the saddle-point asymptotics of the wave function  $\psi(j|P)$  at  $-j \sim \xi_c(\eta)$ , but now the four solutions of equation (199) are ordered as it is shown in Figure 12b:

$$-\pi < \mathbf{p}_d < \mathbf{p}_b < 0 < \mathbf{p}_c < \mathbf{p}_a < \pi. \quad (231)$$

To the leading order in  $|\mathbf{h}_t|$ , the coefficients  $B_{in,i}$ , and  $B_{out,i}$ ,  $i = 1, 2$ , in equation (204) must satisfy two linear equations, which are analogous to (214):

$$B_{in,1} \frac{-w_0 + w_+}{2} + B_{in,2} \frac{w_0 + w_+}{2} = B_{in,1} e^{i\Lambda\pi} Z_\pi, \quad (232)$$

$$B_{in,1} \frac{w_0 + w_+}{2} + B_{in,2} \frac{-w_0 + w_+}{2} = B_{in,2} e^{-i\Lambda\pi} Z_\pi,$$

where

$$Z_\pi(E, P) = \exp \left\{ \frac{2i}{f} \int_{\pi/2}^{p_a} dp [\epsilon(p|P) - E] + \frac{i\pi}{2} \right\}, \quad (233)$$

$$\Lambda_\pi(E, P) = \frac{1}{f} \int_{\pi-p_a}^{p_a} dp \delta\mathcal{E}(p|P, \mathbf{h}_t), \quad (234)$$

and  $w_0, w_+$  are the scattering amplitudes given by (209). Note, that

$$Z_\pi(E, P) = Z_0(E, P - \pi). \quad (235)$$

For the ratio  $B_{in,2}/B_{in,1}$ , we get from (232):

$$\frac{B_{in,2}}{B_{in,1}} = \frac{2Z_\pi \exp(i\Lambda_\pi) - w_+ + w_0}{w_+ + w_0}. \quad (236)$$

The normalization condition (147) leads now to the following formula for the absolute value of the coefficient  $B_{in,1}$ :

$$|B_{in,1}|^2 = \frac{f}{2(p_a - \pi/2)\epsilon'(p_a)(1 + |B_{in,2}/B_{in,1}|^2)}. \quad (237)$$

We skip derivation of this formula, since it similar to the described in Appendix B derivation of formula (222).

The analogous to (219) secular equation following from (232) reads:

$$Z_\pi^2 - (-w_0 + w_+)Z_\pi \cos \Lambda_\pi - w_0 w_+ = 0. \quad (238)$$

Using equations (151), (119), the integral in the right-hand side of (234) can be simplified to the form:

$$\Lambda_\pi(E, P) = -\frac{2 \sinh \eta}{f} A_- h_1 \int_{p_2}^{p_1} dp \frac{\sin p}{\omega(p)}, \quad (239)$$

where  $p_{1,2}$  are the solutions of the equations

$$p_1 + p_2 = P - \pi, \quad \omega(p_1) + \omega(p_2) = E, \quad (240)$$

such that  $-\pi/2 < p_2 < p_1 < \pi/2$ . The parameter  $\Lambda_\pi$  does not depend on the  $x$ -component of the transverse magnetic field  $h_2$ , as one can see from (239). It is clear also from (239), (240), that the parameter  $\Lambda_\pi$  vanishes in two cases: (i) at  $h_1 = 0$ , and (ii) at  $P = \pi$ . If any of these conditions is satisfied, equation (238) has two solutions:

$$Z_\pi = -w_0, \quad \text{and} \quad Z_\pi = w_+. \quad (241)$$

Solutions of the first equation determine the spectrum of the meson modes with  $s = \pm 1$ . At  $\mathbf{h}_t = 0$  and  $P \in (\pi - P_c(\eta), \pi + P_c(\eta))$ , their energies are determined by equation (184), which can be extended in  $P$  from the its original interval  $(-P_c(\eta), P_c(\eta))$  to the interval  $(\pi - P_c(\eta), \pi + P_c(\eta))$  due to the periodicity relation [11]:  $E_{0,n}(P) = E_{0,n}(P + \pi)$ .

Solutions of the second equation in (241) determine at  $\mathbf{h}_t = 0$  and  $P \in (\pi - P_c(\eta), \pi + P_c(\eta))$  the energies  $E_{+,n}(P)$  of the meson modes with spin  $s = 0$  and parity  $\iota = +$ . It was shown in [11], that the energy spectra of mesons with  $s = 0$  and parities  $\iota = \pm$  are connected by the relation  $E_{+,n}(P) = E_{-,n}(P \pm \pi)$ , see equation (131) in [11].

The solutions  $E_n(P)$  of the secular equation (238) at  $h_1 = 0$  and  $P \in (\pi - P_c(\eta), \pi + P_c(\eta))$  correspond to transverse ( $s = \pm 1$ ) and longitudinal ( $s = 0$ ) meson modes at odd, and even  $n$ , respectively:

$$E_n(P) = \begin{cases} E_{0,(n+1)/2}(P - \pi), & n \text{ odd}, \\ E_{-,n/2}(P - \pi), & n \text{ even}, \end{cases} \quad (242)$$

and the functions  $E_{\iota,n}(P - \pi)$  are given by (184).

If  $P \neq \pi$ , the application of the transverse magnetic field with nonzero  $y$ -component  $h_1$  gains a nonzero value to the parameter  $\Lambda_\pi$  and induces hybridization of transverse and longitudinal meson modes due to the term  $\sim \cos \Lambda_\pi$  in the secular equation (238).

However, at any fixed value of  $h_1$ , the parameter  $\Lambda_\pi$  given by (239) decreases in absolute value as  $P$  approaches to  $\pi$ , and finally vanishes at  $P = \pi$ . Therefore, the meson energies  $E_n(P)$  at  $P = \pi$  in presence of the transverse magnetic field  $\mathbf{h}_t$  are still described by equation (242). This means, in particular, that the application of the transverse magnetic field  $\mathbf{h}_t$  does not lead to

hybridisation of transverse and longitudinal meson modes with  $P = \pi$ , and the energies  $E_n(\pi)$  of these mesons do not depend on  $\mathbf{h}_t$ . Of course, this result holds only in the adopted approximation corresponding to the leading order in the weak transverse magnetic field  $\mathbf{h}_t$ .

## X. DYNAMICAL STRUCTURE FACTORS OF SPIN OPERATORS

In this section we study the effect of the mutually orthogonal staggered and uniform transverse magnetic fields on the DSF of the local spin operators in the XXZ spin chain in the weak confinement regime. In the thermodynamic limit, this structure factor can be defined as follows:

$$S^{\mathbf{a}\mathbf{b}}(\mathbf{k}, \omega) = \frac{1}{8} \sum_{j=-\infty}^{\infty} e^{-ikj} \int_{-\infty}^{\infty} dt e^{i\omega t} \quad (243)$$

$$\times \left[ \langle {}^{(1)}\text{Vac}(\mathbf{h}_t, h_z) | e^{i\mathcal{H}t} \sigma_j^{\mathbf{a}} e^{-i\mathcal{H}t} \sigma_0^{\mathbf{b}} | \text{Vac}(\mathbf{h}_t, h_z) \rangle^{(1)} + \langle {}^{(1)}\text{Vac}(\mathbf{h}_t, h_z) | e^{i\mathcal{H}t} \sigma_{j+1}^{\mathbf{a}} e^{-i\mathcal{H}t} \sigma_1^{\mathbf{b}} | \text{Vac}(\mathbf{h}_t, h_z) \rangle^{(1)} \right],$$

where  $\mathbf{a}, \mathbf{b} = x, y, z$ ,  $\mathcal{H}$  is the Hamiltonian given by (16),  $|\text{Vac}(\mathbf{h}_t, h_z)\rangle^{(1)}$  is its ground-state. Exploiting equations (26d), (134), and (135), formula (243) can be simplified to the form

$$S^{\mathbf{a}\mathbf{b}}(\mathbf{k}, \omega) = \frac{\delta_{d_{\mathbf{a}}, d_{\mathbf{b}}}}{4} \sum_{j=-\infty}^{\infty} e^{-ikj} \int_{-\infty}^{\infty} dt e^{i\omega t} \quad (244)$$

$$\times \langle {}^{(1)}\text{Vac}(\mathbf{h}_t, h_z) | e^{i\mathcal{H}t} \sigma_j^{\mathbf{a}} e^{-i\mathcal{H}t} \sigma_0^{\mathbf{b}} | \text{Vac}(\mathbf{h}_t, h_z) \rangle^{(1)},$$

where  $d_x = 0$ ,  $d_y = d_z = 1$ . Note, that due to the Kronecker-delta  $\delta_{d_{\mathbf{a}}, d_{\mathbf{b}}}$  in the right-hand of (244), only two non-diagonal components  $S^{yz}(\mathbf{k}, \omega)$ , and  $S^{zy}(\mathbf{k}, \omega)$  of the DSF tensor (244) are non-zero.

As in [11], we will use two approximations in calculation of the structure factors (244). First, the analysis will be limited to the leading order in the weak staggered longitudinal magnetic fields  $h_z$ . This allows us to replace the vacuum state  $|\text{Vac}(\mathbf{h}_t, h_z)\rangle^{(1)}$  of the Hamiltonian (16) in equation (244) by its counterpart at  $h_z = 0$ :

$$|\text{Vac}(\mathbf{h}_t)\rangle^{(1)} = \lim_{h_z \rightarrow +0} |\text{Vac}(\mathbf{h}_t, h_z)\rangle^{(1)}.$$

Second, our analysis will be restricted solely to the two-spinon contribution  $S_{(2)}^{\mathbf{a}\mathbf{b}}(\mathbf{k}, \omega)$  to the structure factor. To the leading order in  $h_z$ , the latter is defined by the equation:

$$S_{(2)}^{\mathbf{a}\mathbf{b}}(\mathbf{k}, \omega) = \frac{\delta_{d_{\mathbf{a}}, d_{\mathbf{b}}}}{4} \sum_{j=-\infty}^{\infty} e^{-ikj} \int_{-\infty}^{\infty} dt e^{i\omega t} \quad (245)$$

$$\times \langle {}^{(1)}\text{Vac}(\mathbf{h}_t) | e^{i\mathcal{H}^{(2)}t} \sigma_j^{\mathbf{a}} e^{-i\mathcal{H}^{(2)}t} \mathcal{P}_{11}^{(2)}(\mathbf{h}_t) \sigma_0^{\mathbf{b}} | \text{Vac}(\mathbf{h}_t) \rangle^{(1)},$$

where  $\mathcal{P}_{11}^{(2)}(\mathbf{h}_t)$  is the projector operator (143) onto the two-spinon subspace  $\mathcal{L}_{11}^{(2)}(\mathbf{h}_t)$ , and  $\mathcal{H}^{(2)}$  is given by (141).

After substitution of (143) into (245) and straightforward calculations following the lines described in section III of [11], the dynamical structure factor (245) can be represented in the compact form:

$$S_{(2)}^{\text{ab}}(\mathbf{k}, \omega) = \delta_{d_a, d_b} \sum_{n=1}^{\infty} \delta[\omega - \tilde{E}_n(\mathbf{k} + \pi d_a)] I_n^{\text{ab}}(\mathbf{k} + \pi d_a), \quad (246)$$

where

$$I_n^{\text{ab}}(P) = \frac{\pi}{2} \langle \text{Vac}(\mathbf{h}_t) | \sigma_0^{\text{a}} | \tilde{\pi}_n(P) \rangle \times \langle \tilde{\pi}_n(P) | \sigma_0^{\text{b}} | \text{Vac}(\mathbf{h}_t) \rangle^{(1)} \quad (247)$$

is the intensity of the  $n$ th meson mode, and  $\tilde{E}_n(P)$  is the meson energy in the two-kink approximation. Following our practice noticed by the end of Section VII, we will neglect the difference (169), and identify  $\tilde{E}_n(P)$  with  $E_n(P)$ .

The matrix element of the  $\sigma_0^{\text{a}}$  operator in the right-hand side of (247) can be expressed in terms of the reduced wave function  $\phi_n(p|P, \mathbf{h}_t, h_z)$ , which is defined by equation (146) and normalized due to (147):

$$\langle \text{Vac}(\mathbf{h}_t) | \sigma_0^{\text{a}} | \tilde{\pi}_n(P) \rangle = \int_{-\pi}^{\pi} \frac{dp}{4\pi} \phi_n(p|P, \mathbf{h}_t, h_z) \times \langle \text{Vac}(\mathbf{h}_t) | \sigma_0^{\text{a}} | \mathbb{K}_{10}(P/2 + p|\mathbf{h}_t) \mathbb{K}_{01}(P/2 - p|\mathbf{h}_t) \rangle. \quad (248)$$

We replace the matrix element in the second line of the above formula by the zero-order term of its expansion in  $\mathbf{h}_t$ :

$$\langle \text{Vac}(\mathbf{h}_t) | \sigma_0^{\text{a}} | \mathbb{K}_{10}(p_1|\mathbf{h}_t) \mathbb{K}_{01}(p_2|\mathbf{h}_t) \rangle = \langle \text{vac} | \sigma_0^{\text{a}} | K_{10}(p_1) K_{01}(p_2) \rangle + O(|\mathbf{h}_t|), \quad (249)$$

where  $\langle \text{vac} |$  and  $|K_{10}(p_1) K_{01}(p_2)\rangle$  are defined by equations (27a), (27b), and (123), respectively. The matrix element in the right-hand side can be represented in terms of the two-kink states  $|\mathcal{K}_{10}(\xi_1) \mathcal{K}_{01}(\xi_2)\rangle$  parametrized by the multiplicative spectral parameters  $\xi_{1,2}$ :

$$\langle \text{vac} | \sigma_0^{\text{a}} | K_{10}(p_1) K_{01}(p_2) \rangle = \frac{\sinh \eta}{\sqrt{\omega(p_1) \omega(p_2)}} \times \langle \text{vac} | \sigma_0^{\text{a}} | \mathcal{K}_{10}(\xi_1) \mathcal{K}_{01}(\xi_2) \rangle, \quad (250)$$

where  $\xi_{1,2} = -ie^{i\alpha_{1,2}}$ , the rapidities  $\alpha_{1,2}$  are related with momenta  $p_{1,2}$  due to (83), and

$$|\mathcal{K}_{10}(\xi_1) \mathcal{K}_{01}(\xi_2)\rangle = \sqrt{2} |\mathcal{K}_{10}(\xi_1) \mathcal{K}_{01}(\xi_2)\rangle_+ + |\mathcal{K}_{10}(\xi_1) \mathcal{K}_{01}(\xi_2)\rangle_{1/2, 1/2} + |\mathcal{K}_{10}(\xi_1) \mathcal{K}_{01}(\xi_2)\rangle_{-1/2, -1/2}. \quad (251)$$

The two-kink states in the right-hand side of (251) are defined by equations (A7) and (A8) in Appendix A.

Using (251) and (A9), the matrix elements  $\langle \text{vac} | \sigma_0^{\text{a}} | \mathcal{K}_{10}(\xi_1) \mathcal{K}_{01}(\xi_2) \rangle$  in the right-hand side

of (250) can be written in the explicit form:

$$\langle \text{vac} | \sigma_0^x | \mathcal{K}_{10}(\xi_1) \mathcal{K}_{01}(\xi_2) \rangle \quad (252)$$

$$= X^0(\xi_1, \xi_2) + X^1(\xi_1, \xi_2),$$

$$\langle \text{vac} | \sigma_0^y | \mathcal{K}_{10}(\xi_1) \mathcal{K}_{01}(\xi_2) \rangle \quad (253)$$

$$= i[X^0(\xi_1, \xi_2) - X^1(\xi_1, \xi_2)],$$

$$\langle \text{vac} | \sigma_0^z | \mathcal{K}_{10}(\xi_1) \mathcal{K}_{01}(\xi_2) \rangle = \sqrt{2} X_{\pm}^z(\xi_1, \xi_2), \quad (254)$$

where the functions  $X^j(\xi_1, \xi_2)$  and  $X_{\pm}^z(\xi_1, \xi_2)$  are determined by equations (A10).

In order to complete calculation of the intensities (247), it remains to obtain the explicit expression for the wave function  $\phi_n(p|P, \mathbf{h}_t, h_z)$ , that stays in the integrand in the right-hand side of (248). In principle, this can be achieved by the perturbative solution of the Bethe-Salpeter equation (148), as it was done in [11] in the case  $\mathbf{h}_t = 0$ . Here we shall use a more simple and less rigorous procedure exploiting the heuristic semiclassical solutions obtained above in two cases  $P \in (-P_c(\eta), P_c(\eta))$ , and  $P \in (\pi - P_c(\eta), \pi + P_c(\eta))$ .

In the first case  $P \in (-P_c(\eta), P_c(\eta))$ , the wave function  $\phi_n(p|P, \mathbf{h}_t, h_z)$  in the semiclassical approximation can be written in the form:

$$\phi_n(p|P, \mathbf{h}_t, h_z) = 2\pi [B_{in,1} \delta(p - p_a) + B_{in,2} \delta(p - p_b) + B_{out,1} \delta(p - p_c) + B_{out,2} \delta(p - p_d)]. \quad (255)$$

Indeed, the result of substitution of the right-hand side into the integrand in (192) reproduces (to the zero order in  $|\mathbf{h}_t|$ ) formula (204). The coefficients  $B_{in,i}$ ,  $B_{out,i}$ , with  $i = 1, 2$ , are known due to (206), (208), (221), (222).

Combing(247)-(255), we obtain finally:

$$I_n^{xx}(P) = \frac{\Delta E_n}{2\epsilon'(p_a)} \frac{\sinh^2 \eta}{\omega(p_1)\omega(p_2)} \quad (256a)$$

$$\times |X^0(\xi_1, \xi_2) + X^1(\xi_1, \xi_2)|^2 \frac{|1 - B_{in,2}/B_{in,1}|^2}{2(1 + |B_{in,2}/B_{in,1}|^2)},$$

$$I_n^{yy}(P) = \frac{\Delta E_n}{2\epsilon'(p_a)} \frac{\sinh^2 \eta}{\omega(p_1)\omega(p_2)} \quad (256b)$$

$$\times |X^0(\xi_1, \xi_2) - X^1(\xi_1, \xi_2)|^2 \frac{|1 - B_{in,2}/B_{in,1}|^2}{2(1 + |B_{in,2}/B_{in,1}|^2)},$$

$$I_n^{zz}(P) = \frac{\Delta E_n}{2\epsilon'(p_a)} \frac{\sinh^2 \eta}{\omega(p_1)\omega(p_2)} \quad (256c)$$

$$\times 2|X_+^z(\xi_1, \xi_2)|^2 \frac{|1 + B_{in,2}/B_{in,1}|^2}{2(1 + |B_{in,2}/B_{in,1}|^2)},$$

$$I_n^{xz}(P) = \frac{\sqrt{2} \Delta E_n}{2\epsilon'(p_a)} \frac{\sinh^2 \eta}{\omega(p_1)\omega(p_2)} \quad (256d)$$

$$\times [X^0(\xi_1, \xi_2)^* + X^1(\xi_1, \xi_2)^*] X_+^z(\xi_1, \xi_2)$$

$$\times \frac{(1 - B_{in,2}^*/B_{in,1}^*)(1 + B_{in,2}/B_{in,1})}{2(1 + |B_{in,2}/B_{in,1}|^2)},$$

$$I_n^{yz}(P) = \frac{-i\sqrt{2} \Delta E_n}{2\epsilon'(p_a)} \frac{\sinh^2 \eta}{\omega(p_1)\omega(p_2)} \quad (256e)$$

$$\times [X^0(\xi_1, \xi_2)^* - X^1(\xi_1, \xi_2)^*] X_+^z(\xi_1, \xi_2)$$

$$\times \frac{(1 - B_{in,2}^*/B_{in,1}^*)(1 + B_{in,2}/B_{in,1})}{2(1 + |B_{in,2}/B_{in,1}|^2)},$$

$$I_n^{zx}(P) = I_n^{xz}(P)^*, \quad I_n^{zy}(P) = I_n^{yz}(P)^*. \quad (256f)$$

Here  $p_a$  is the solution of equation (197) shown in Figure 9a,  $p_1 = P/2 + p_a$ ,  $p_2 = P/2 - p_a$ ,  $\alpha_{1,2}$  are the rapidities corresponding to the momenta  $p_{1,2}$ , and

$$\Delta E_n = \frac{\pi f}{p_a} \quad (257)$$

is the small interval between the energies of  $n$ th and  $(n + 2)$ th meson modes at given  $P \in (-P_c, P_c)$  and  $\mathbf{h}_t = 0$ .

Obtained results (256) for the intensities of the meson modes are illustrated for the case  $P = 0$  in Figures 13a, 13b. The dotted curves in these figures are identical with those in Figure 11, and display the dependencies of the energies  $E_n(0|\mathbf{h}_t, h_z)$  on the magnetic field  $h_1$  at  $h_2 = 0.4h_1$ , and  $\eta = 1.25$ ,  $h_z = 0.02$ . The darknesses of dots in Figures 13a, and Figure 13b, characterize the intensities  $I_n^{xx}(P)$ , and  $I_n^{zz}(P)$ , respectively, of the presented four lightest meson modes at  $P = 0$ . We did not show the intensity  $I_n^{yy}(P)$  determined by equation (256b), since it is very small for the mesons with zero momentum  $P = 0$  at the chosen value  $\eta = 1.25$  of the anisotropy parameter. As one can see from Figure 13, application of the transverse magnetic field causes the effective hybridization of transverse and longitudinal meson modes at  $P = 0$ .

In the second case  $P \in (\pi - P_c(\eta), \pi + P_c(\eta))$ , we can again use formula (255) for the wave function

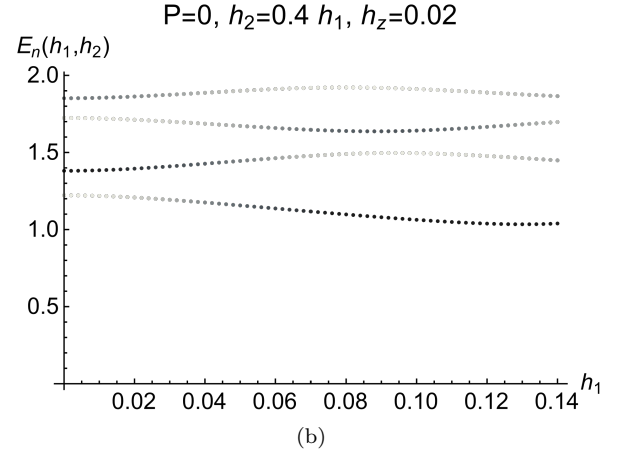
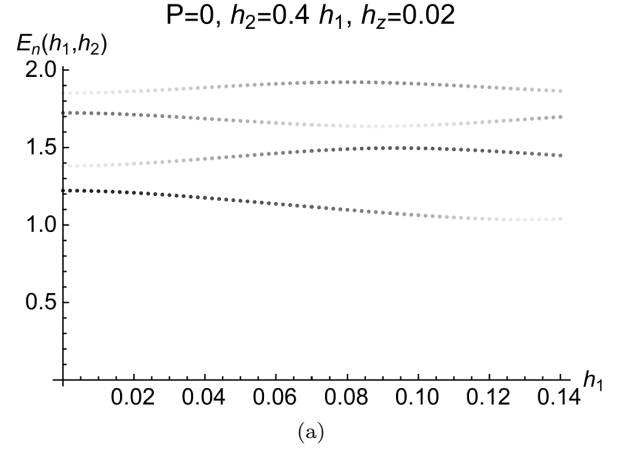


FIG. 13: Dependences of energies  $E_n$  of four lowest meson modes on the  $y$ -component  $h_1$  of the transverse magnetic field at  $\eta = 1.25$ ,  $P = 0$ ,  $h_z = 0.02$ ,  $h_2 = 0.4h_1$ , according to (220). Darkness of the dots in Figures (a), and (b) characterizes the intensities  $I_n^{xx}(0)$ , and  $I_n^{zz}(0)$ , respectively, which are given by (256).

$\phi_n(p|P, \mathbf{h}_t, h_z)$ . However, the momenta  $\mathbf{p}_a, \mathbf{p}_b, \mathbf{p}_c, \mathbf{p}_d$  in this formula now are ordered in accordance with (231), and the in- and out-amplitudes in (255) are different from those in the first case. In particular, the in-amplitudes solve equations (232), and satisfy equalities (236) and (237). It turns out, that formulas (256) can still describe the intensities  $I_n^{ab}(P)$  at  $P \in (\pi - P_c(\eta), \pi + P_c(\eta))$ , upon the following minor modifications: (i) the momentum  $p_a$  solving equation (197) lies now in the interval  $p_a \in (\pi/2, \pi)$ , see Figure 12a, (ii) the ratio  $B_{in,2}/B_{in,1}$  is determined by formula (236), instead of (221), (iii) the parameter  $\Delta E_n$  in (256) now denotes the ratio:

$$\Delta E_n = \frac{\pi f}{p_a - \pi/2}. \quad (258)$$

In particular, the intensities  $I_n^{ab}(P = \pi)$  do not depend on  $h_1, h_2$  in the adopted approximation, and coincide with their values at  $h_1 = h_2 = 0$ .

## XI. COMPARISON WITH EXPERIMENT

In previous sections we followed the convention used in the algebraic approach [33] by choosing the “−” sign in front of the right-hand side of the Hamiltonian (4). This choice corresponds to the ferromagnetic nearest-neighbor exchange coupling in the  $xy$ -plane of the XXZ spin-chain. In the experimental research papers, however, the different and more physically relevant form of the XXZ model Hamiltonian is commonly used with the antiferromagnetic exchange in the  $xy$ -plane. These two forms of the XXZ model Hamiltonian are simply related by a certain unitary transform, which we will recall below in order to facilitate comparison of our theoretical predictions with the results of already published and future experiments and computer simulations.

Let us start from the finite-size version  $\mathcal{H}_N(\Delta, \mathbf{h}_t, h_z)$  of the Hamiltonian (16) defined on the spin-chain having  $N$ -sites. The periodic boundary conditions are implied, and the number of sites is a multiple of eight,  $N \bmod 8 = 0$ . The appropriate unitary transform  $U_N$  is the rotation by  $\pi$  around the  $z$ -axis of all spins at odd sites of the chain:

$$U_N = \otimes_{m=-N/4}^{N/4-1} \sigma_{2m+1}^z. \quad (259)$$

Operators  $\mathcal{H}_N(\Delta, \mathbf{h}_t, h_z)$  and  $\tilde{T}_1 = T_1 \mathbb{C}$  modify upon the action of this transform to:

$$\check{\mathcal{H}}_N(\check{\Delta}, \mathbf{h}_t, h_z) = U_N \mathcal{H}_N(\Delta, \mathbf{h}_t, h_z) U_N^{-1}, \quad (260)$$

$$\check{T}_1 = U_N \tilde{T}_1 U_N^{-1}, \quad (261)$$

where  $\check{\Delta} = -\Delta = \cosh \eta$ , and  $\check{T}_1$  is given by (22). The explicit form of the resulting Hamiltonian in the thermodynamic limit  $N \rightarrow \infty$  reads:

$$\begin{aligned} \check{\mathcal{H}}(\check{\Delta}, \mathbf{h}_t, h_z) &= \lim_{N \rightarrow \infty} \check{\mathcal{H}}_N(\check{\Delta}, \mathbf{h}_t, h_z) \quad (262) \\ &= \frac{1}{2} \sum_{j=-\infty}^{\infty} \left( \sigma_j^x \sigma_{j+1}^x + \sigma_j^y \sigma_{j+1}^y + \check{\Delta} \sigma_j^z \sigma_{j+1}^z \right) \\ &\quad - \sum_{j=-\infty}^{\infty} [(-1)^j h_2 \sigma_j^x + h_1 \sigma_j^y + (-1)^j h_z \sigma_j^z]. \end{aligned}$$

We shall use the notation  $U$  for the thermodynamic limit of the transform operator (259):

$$U = \lim_{N \rightarrow \infty} U_N. \quad (263)$$

Note, that the unitary transform (263) permutes the staggered and uniform transverse magnetic fields, as one can see by comparison of (262) with (17). Note also, that operators  $\check{\mathcal{H}}(\check{\Delta}, \mathbf{h}_t, h_z)$  and  $\check{T}_1$  commute:

$$[\check{\mathcal{H}}(\check{\Delta}, \mathbf{h}_t, h_z), \check{T}_1] = 0. \quad (264)$$

The vacuum and meson states in the new representation are determined by relations:

$$|\check{V}ac(\mathbf{h}_t, h_z)\rangle^{(1)} = U |Vac(\mathbf{h}_t, h_z)\rangle^{(1)}, \quad (265)$$

$$|\check{\pi}_n(P|\mathbf{h}_t, h_z)\rangle = U |\pi_n(P|\mathbf{h}_t, h_z)\rangle. \quad (266)$$

It follows from (135), (261), (263), (265) that:

$$\check{T}_1 |\check{V}ac(\mathbf{h}_t, h_z)\rangle^{(1)} = |\check{V}ac(\mathbf{h}_t, h_z)\rangle^{(1)}. \quad (267)$$

Due to (260)-(263), (136), the meson states (266) satisfy equalities:

$$\check{T}_1 |\check{\pi}_n(P|\mathbf{h}_t, h_z)\rangle = e^{iP} |\check{\pi}_n(P|\mathbf{h}_t, h_z)\rangle, \quad (268a)$$

$$(\check{\mathcal{H}} + C) |\check{\pi}_n(P|\mathbf{h}_t, h_z)\rangle = E_n(P|\mathbf{h}_t, h_z) |\check{\pi}_n(P|\mathbf{h}_t, h_z)\rangle. \quad (268b)$$

The meson dispersion laws  $E_n(P|\mathbf{h}_t, h_z)$  and the constant  $C$  in equations (136b) and (268b) are the same.

The dynamical structure factor  $\check{S}^{ab}(\mathbf{k}, \omega)$  corresponding to the Hamiltonian (260) is defined by the formula

$$\begin{aligned} \check{S}^{ab}(\mathbf{k}, \omega) &= \frac{1}{8} \sum_{j=-\infty}^{\infty} e^{-ikj} \int_{-\infty}^{\infty} dt e^{i\omega t} \quad (269) \\ &\times \left[ {}^{(1)}\langle \check{V}ac(\mathbf{h}_t, h_z) | e^{i\check{\mathcal{H}}t} \sigma_j^a e^{-i\check{\mathcal{H}}t} \sigma_0^b | \check{V}ac(\mathbf{h}_t, h_z) \rangle^{(1)} + \right. \\ &\left. {}^{(1)}\langle \check{V}ac(\mathbf{h}_t, h_z) | e^{i\check{\mathcal{H}}t} \sigma_{j+1}^a e^{-i\check{\mathcal{H}}t} \sigma_1^b | \check{V}ac(\mathbf{h}_t, h_z) \rangle^{(1)} \right], \end{aligned}$$

which is analogous to (243). Exploiting equations (22), (264), and (267), formula (269) can be simplified to the form:

$$\begin{aligned} \check{S}^{ab}(\mathbf{k}, \omega) &= \frac{\delta_{\check{d}_a, \check{d}_b}}{4} \sum_{j=-\infty}^{\infty} e^{-ikj} \int_{-\infty}^{\infty} dt e^{i\omega t} \quad (270) \\ &\times {}^{(1)}\langle \check{V}ac(\mathbf{h}_t, h_z) | e^{i\check{\mathcal{H}}t} \sigma_j^a e^{-i\check{\mathcal{H}}t} \sigma_0^b | \check{V}ac(\mathbf{h}_t, h_z) \rangle^{(1)}. \end{aligned}$$

Due to (259), (260), (263), and (265), this formula can be further rewritten as

$$\begin{aligned} \check{S}^{ab}(\mathbf{k}, \omega) &= \frac{\delta_{\check{d}_a, \check{d}_b}}{4} \sum_{j=-\infty}^{\infty} e^{-ikj} \int_{-\infty}^{\infty} dt e^{i\omega t} \quad (271) \\ &\times {}^{(1)}\langle Vac(\mathbf{h}_t, h_z) | e^{i\mathcal{H}t} \sigma_j^a e^{-i\mathcal{H}t} \sigma_0^b | Vac(\mathbf{h}_t, h_z) \rangle^{(1)}, \end{aligned}$$

where the Hamiltonian  $\mathcal{H}$  is given by (16),  $|Vac(\mathbf{h}_t, h_z)\rangle^{(1)}$  is its ground state, and

$$\check{\sigma}_j^a = U^{-1} \sigma_j^a U = \begin{cases} (-1)^j \sigma_j^a, & \text{if } \mathbf{a} = x, y, \\ \sigma_j^z, & \text{if } \mathbf{a} = z \end{cases}. \quad (272)$$

This leads to the following simple exact relations between the diagonal matrix elements of the DSF tensors  $\check{S}^{ab}(\mathbf{k}, \omega)$  and  $S^{ab}(\mathbf{k}, \omega)$ :

$$\begin{aligned} \check{S}^{xx}(\mathbf{k}, \omega) &= S^{xx}(\mathbf{k} + \pi, \omega), \\ \check{S}^{yy}(\mathbf{k}, \omega) &= S^{yy}(\mathbf{k} + \pi, \omega), \\ \check{S}^{zz}(\mathbf{k}, \omega) &= S^{zz}(\mathbf{k}, \omega). \end{aligned}$$

On the other hand, the non-diagonal matrix elements of the DSF tensors  $S^{ab}(\mathbf{k}, \omega)$  and  $\check{S}^{ab}(\mathbf{k}, \omega)$  are different: the only non-vanishing non-diagonal components of the later are  $\check{S}^{xz}(\mathbf{k}, \omega)$  and  $\check{S}^{zx}(\mathbf{k}, \omega)$ , while the non-vanishing

non-diagonal components of  $S^{\text{ab}}(\mathbf{k}, \omega)$  are  $S^{yz}(\mathbf{k}, \omega)$  and  $S^{zy}(\mathbf{k}, \omega)$ , see equation (244).

For the non-zero matrix elements  $\check{S}_{(2)}^{\text{ab}}(\mathbf{k}, \omega)$  of the DSF (270) in the two-kink approximation we get finally:

$$\check{S}_{(2)}^{xx}(\mathbf{k}, \omega) = \sum_{n=1}^{\infty} \delta[\omega - E_n(\mathbf{k} + \pi)] I_n^{xx}(\mathbf{k} + \pi), \quad (274a)$$

$$\check{S}_{(2)}^{yy}(\mathbf{k}, \omega) = \sum_{n=1}^{\infty} \delta[\omega - E_n(\mathbf{k})] I_n^{yy}(\mathbf{k}), \quad (274b)$$

$$\check{S}_{(2)}^{zz}(\mathbf{k}, \omega) = \sum_{n=1}^{\infty} \delta[\omega - E_n(\mathbf{k} + \pi)] I_n^{zz}(\mathbf{k} + \pi), \quad (274c)$$

$$\check{S}_{(2)}^{xz}(\mathbf{k}, \omega) = \sum_{n=1}^{\infty} \delta[\omega - E_n(\mathbf{k} + \pi)] I_n^{xz}(\mathbf{k} + \pi), \quad (274d)$$

$$\check{S}_{(2)}^{zx}(\mathbf{k}, \omega) = \sum_{n=1}^{\infty} \delta[\omega - E_n(\mathbf{k} + \pi)] I_n^{zx}(\mathbf{k} + \pi). \quad (274e)$$

The intensities  $I_n^{\text{ab}}(P)$  in the right-hand sides of these relations are given by (256).

Figures 14a, 14b display the density plots in the plane  $\langle h_1, \omega \rangle$  of the DSF  $\check{S}_{(2)}^{\text{aa}}(\mathbf{k} = \pi, \omega)$  with  $\mathbf{a} = x, y, z$ , which are determined by equations (274a)-(274c). The other parameters are taken at the same values, as in Figure 13:  $h_2 = 0.4h_1$ ,  $\eta = 1.25$ ,  $h_z = 0.02$ .

The density plot of the longitudinal DSF  $\check{S}_{(2)}^{zz}(\pi, \omega)$  is shown in Figure 14a. Due to the  $\delta$ -functions in the right-hand side of (274c), it is located along the dispersion curves of the mesons with zero quasimomentum:

$$\omega(h_1) = E_n(P = 0 | h_1, h_2 = 0.4h_1), \quad n = 1, 2, \dots, \quad (275)$$

which were depicted previously in Figure 13. The corresponding intensities  $I_n^{zz}(\mathbf{k} = 0)$  display substantial variation with increasing  $h_1$  in accordance with equation (256c).

The transverse  $\check{S}_{(2)}^{xx}(\pi, \omega)$  component of the DSF tensor shown in Figure 14b is located in the plane  $\langle h_1, \omega \rangle$  along the same curves (275), and corresponding intensities  $I_n^{xx}(\mathbf{k} = 0)$  also strongly depend on  $h_1$  due to (256a).

The two remaining horizontal dotted lines in Figure 14b represent the density plot of the transverse component  $\check{S}_{(2)}^{yy}(\pi, \omega)$  of the DSF tensor, which is given by equation (274b). It is located along the dispersion curves of mesons having the quasimomentum  $P = \pi$ :

$$\omega(h_1) = E_n(P = \pi | h_1, h_2 = 0.4h_1). \quad (276)$$

It was shown in Section IX, that the energies of such mesons do not depend on  $h_1, h_2$ :

$$E_n(P = \pi | h_1, h_2) = E_n(P = \pi | 0, 0),$$

to the leading order in  $h_1, h_2$ . Furthermore, the intensities  $I_n^{yy}(\mathbf{k} = \pi)$  that stay in the right-hand side of (274b) also do not depend on  $h_1, h_2$ :

$$I_n^{yy}(\mathbf{k} = \pi | h_1, h_2) = I_n^{yy}(\mathbf{k} = \pi | 0, 0),$$

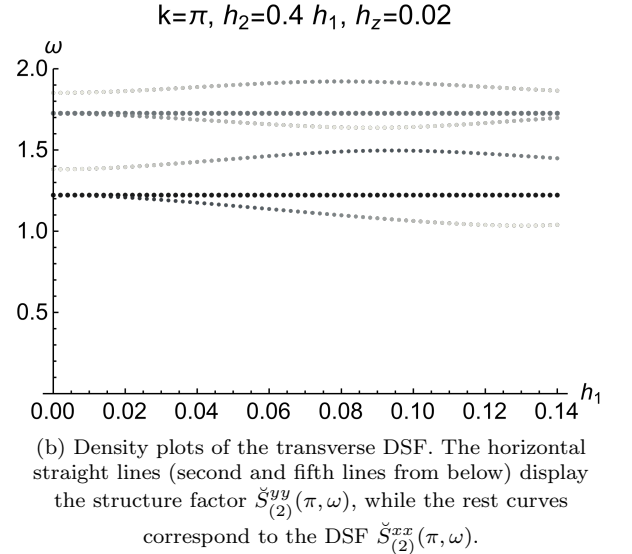
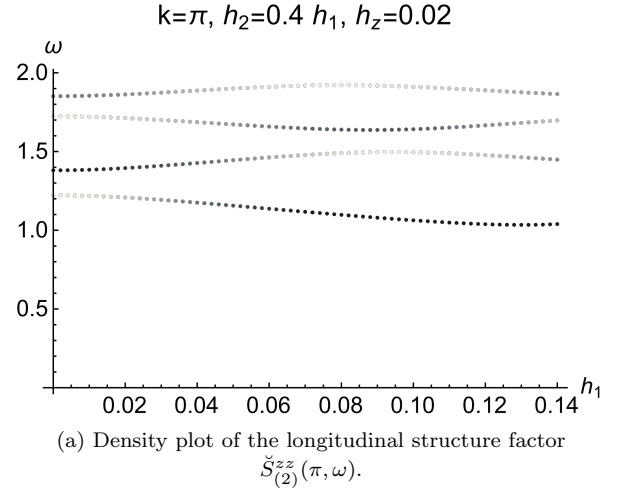


FIG. 14: Density plots in the plane  $\langle h_1, \omega \rangle$  of the structure factors  $\check{S}_{(2)}^{\text{aa}}(\mathbf{k} = \pi, \omega)$  due to (274) at  $h_2 = 0.4h_1$ ,  $\eta = 1.25$ ,  $h_z = 0.02$ . Darkness of the dots characterizes intensities  $I_n^{\text{aa}}(\pi\delta_{y,a})$  of the meson modes with  $n = 1, 2, 3, 4$ , and energies  $E_n(\pi\delta_{y,a}) = \omega$ .

as it was mentioned by the end of Section X. These intensities vanish for all even  $n = 2, 4, \dots$ , since the meson modes with even  $n$  carry zero spin  $s = 0$  at  $\mathbf{h}_t = 0$  and do not contribute to the transverse DSF, as it was explained in Section IX, see equation (226). On the other hand, the following equalities hold for the transverse meson modes with odd  $n = 1, 3, \dots$  at  $\mathbf{h}_t = 0$ :

$$E_n(P = \pi | 0, 0) = E_n(P = 0 | 0, 0),$$

$$I_n^{yy}(\mathbf{k} = \pi | 0, 0) = I_n^{xx}(\mathbf{k} = 0 | 0, 0).$$

The resulting pattern of the transverse DSF in the  $\langle h_1, \omega \rangle$ -plane at the antiferromagnetic point  $\mathbf{k} = \pi$ , which is shown in Figure 14b, looks at  $h_1 = 0$  like a set of transverse meson modes. Each of these modes splits upon application of the transverse magnetic field  $h_1 > 0$  into two

branches. The energy of the lower branch has a strong non-linear  $h_1$ -dependence, while the energy of the upper branch does not depend on  $h_1$ . The lower branch of the split modes becomes polarized in the  $\langle x, z \rangle$ -plane, whereas the upper branch has the linear polarization along the  $y$  direction, that does not change with increase of  $h_1$ .

The described above rather peculiar evolution of the DSF with increasing transverse magnetic field was indeed observed by Faure *et al.* [10], who studied in the inelastic neutron scattering experiments the effect of the transverse magnetic field on the magnetic excitation energy spectra in the antiferromagnetic crystal  $\text{BaCo}_2\text{V}_2\text{O}_8$  at low temperatures.

For interpretation of their experimental results, the authors of [10] have used the following effective spin-chain Hamiltonian:

$$\begin{aligned} \mathbb{H} = & \frac{J}{4} \sum_{j=-\infty}^{\infty} \left[ \varepsilon(\sigma_j^x \sigma_{j+1}^x + \sigma_j^y \sigma_{j+1}^y) + \sigma_j^z \sigma_{j+1}^z \right] \quad (277) \\ & - \frac{\mu_B}{2} \sum_{j=-\infty}^{\infty} \left[ g_{zz} h^{\text{eff}} (-1)^j \sigma_j^z + (-1)^j g_{yx} H \sigma_j^x \right. \\ & \left. + g_{yy} H \sigma_j^y + \cos[(2j+1)\pi/4] g_{yz} H \sigma_j^z \right], \end{aligned}$$

which was introduced earlier by Kimura *et al.* [22] for description of the quasi-1D magnetic structure of  $\text{BaCo}_2\text{V}_2\text{O}_8$ .

In the effective Hamiltonian (277),  $J > 0$  is the anti-ferromagnetic intra-chain interaction,  $\varepsilon$  is the anisotropy parameter,  $H$  denotes the strength of the uniform magnetic field (in Tesla) applied in the  $y$ -direction,  $h^{\text{eff}}$  is the effective staggered longitudinal magnetic field, that mimics in the mean-field approximation the weak interchain interaction in the 3D-ordered antiferromagnetic phase,  $g_{ab}$  are the components of the Landé tensor, and  $\mu_B = 5.788 \times 10^{-5} \text{eV/T}$  is the Bohr magneton.

According to [22], the effective magnetic field  $\cos[(2j+1)\pi/4]g_{yz}H$  in the  $z$ -direction having the four-step periodicity arises in (277) due to the combination of the anisotropy of the Landé  $g$ -tensor, with the specific screw structure of the  $\text{Co}^{2+}$  magnetic ion chains in the compound  $\text{BaCo}_2\text{V}_2\text{O}_8$ . Note also, that the effective spin-chain Hamiltonian (277) can be used to describe the magnetic structure of this crystal only if the external uniform magnetic field is applied along the  $\mathbf{b}$  (or  $\mathbf{a}$ ) crystallographic axis [22].

Comparing (262) and (277), one can see that the simplified version of the Hamiltonian  $\mathbb{H}$  with  $g_{yz} = 0$  is proportional to  $\check{\mathcal{H}}(\tilde{\Delta}, \mathbf{h}_t, h_z)$ :

$$\mathbb{H} \Big|_{g_{yz}=0} = \frac{J\varepsilon}{2} \check{\mathcal{H}}(\tilde{\Delta}, \mathbf{h}_t, h_z), \quad (278)$$

and parameters of the Hamiltonians  $\check{\mathcal{H}}$  and  $\mathbb{H}$  are simply

related:

$$\begin{aligned} \tilde{\Delta} &= \frac{1}{\varepsilon}, & h_z &= \frac{\mu_B}{J\varepsilon} g_{zz} h^{\text{eff}}, \quad (279) \\ h_1 &= \frac{\mu_B}{J\varepsilon} g_{yy} H, & h_2 &= \frac{\mu_B}{J\varepsilon} g_{yx} H. \end{aligned}$$

The following numerical values have been used in [10] for the parameters in the Hamiltonian (277):

$$J = 5.8 \text{ meV}, \quad \varepsilon = 0.53, \quad g_{zz} \mu_B h^{\text{eff}} = 0.06 \text{ meV}, \quad (280)$$

$$g_{zz} = 6.07, \quad g_{yy} = 2.35, \quad g_{yx}/g_{yy} = 0.4, \quad g_{yz}/g_{yy} = 0.14.$$

For these numerical values, we get from (279):

$$h_1(H) \approx 0.0443H, \quad h_2(H) \approx 0.0177H, \quad \check{\mathcal{H}} \approx 651\mathbb{H}, \quad (281)$$

where the magnetic field  $H$  and the energy  $\mathbb{H}$  in the right-hand sides are measured in Tesla and electron-volt, respectively.

Note, that Kimura *et al.* [22], and Grenier *et al.* [6, 47] used slightly different from (280) values for the parameters of the effective Hamiltonian (277).

The values of parameters  $\eta = 1.25$ ,  $h_z = 0.02$ ,  $h_2 = 0.4h_1$  of the Hamiltonian (16), which we have chosen for illustration of our results in Figures 10, 11, 13, are close to those determined by equations (279), (280).

The evolution of the static magnetic structure of  $\text{BaCo}_2\text{V}_2\text{O}_8$  in the low-temperature phase with the applied in the  $y$ -direction uniform magnetic field  $H$  is displayed in Figure 2 of [10]. It is shown, in particular, in Figure 2b, that the staggered magnetization  $m_c(H)$  in the  $z$ -direction monotonically decreases from its maximal value at  $H = 0$  to the zero value at the critical field  $H_c \approx 10\text{T}$ . As one can see from this figure, the staggered magnetization  $m_c(H)$  remains close to its zero-field value  $m_c(0)$  at weak enough magnetic fields in the interval  $0 < H \lesssim 3\text{T}$ . It is natural to expect, that our perturbative treatment of the effect of the transverse magnetic field is appropriate in this interval.

The dependences of the inelastic neutron scattering intensities on the transverse magnetic field  $H$  at three different neutron scattering vectors  $\mathbf{Q} = (2, 0, 1)$ ,  $\mathbf{Q} = (0, 0, 2)$ , and  $\mathbf{Q} = (3, 0, 1)$  are shown in [10] in Figures 3 a,b, and c, respectively. Note, that the components of the vector  $\mathbf{Q}$  are written here in terms of the crystallographic lattice spacings. This means, in particular, that the 1D momentum transfer  $k$ , that stands in equations (274), is proportional to  $Q_z$ :

$$k = \frac{2\pi Q_z}{c/c'}, \quad (282)$$

where  $c$  is the crystallographic lattice spacing in the  $z$ -direction, and  $c'$  is the spacing (along the  $z$ -direction) between the  $\text{Co}^{2+}$  ions in the magnetic chains. Since each magnetic chain contains four  $\text{Co}^{2+}$  ions in the crystallographic cell [10, 22], the denominator in (282) equals

four, and

$$\mathbf{k} = \frac{\pi Q_z}{2}. \quad (283)$$

It is well known [10], further, that neutron scattering experiments probe only the spin fluctuations perpendicular to the scattering vector  $\mathbf{Q}$ .

The arguments listed above allow us to expect, that our analytical perturbative results (274a), (274b) for the transverse structure factors  $\check{S}_{(2)}^{xx}(\mathbf{k}, \omega)$ ,  $\check{S}_{(2)}^{yy}(\mathbf{k}, \omega)$  at  $\mathbf{k} = \pi$  for the model (262), which are illustrated in Figure 14b, can be directly applied to the interpretation of the results of the neutron scattering intensity measurements for  $\mathbf{Q} = (0, 0, 2)$  shown in Figure 3b in [10].

Figures 3a and 3c in [10] display the measured by Faure *et al.* neutron scattering intensities at the scattering vectors  $\mathbf{Q}$  with  $Q_z = 1$ , which correspond due to (283) to the 1D momentum transfer  $k = \pi/2$ . As one can see, the energies of the meson excitation modes in these two figures are close to those in Figure 3b, the only difference is in their intensities. This experimental result cannot be explained in the frame of the theory based on the spin-chain Hamiltonian (262). Really, the energy of the lightest meson with zero momentum in the absence of the transverse magnetic field is well below the two-spinon threshold  $2\omega(\pi/4)$  at their total momentum  $P = \pi/2$ :

$$E_1(P, h_1, h_2) \Big|_{P=0, h_1=h_2=0} < \min_p [\omega(P + p/2) + \omega(P - p/2)] \Big|_{P=\pi/2} = 2\omega(\pi/4).$$

The natural and well-known [6–8, 28, 48] way to overcome this difficulty is to perturb the Hamiltonian (262) with a term  $\lambda V_1$

$$\check{\mathcal{H}}(\check{\Delta}, \mathbf{h}_t, h_z) \rightarrow \check{\mathcal{H}}(\check{\Delta}, \mathbf{h}_t, h_z) + \lambda V_1, \quad (284)$$

having the four-site periodicity. Note, that such a term proportional to the small parameter  $g_{yz}$  is already present in the Hamiltonian (277). Further additional terms of this kind refining this effective Hamiltonian were introduced in [28, 48]. The symmetry-breaking perturbation  $\lambda V_1$  reduces the Brillouin zone  $P \in (-\pi, \pi)$  by the factor of four, and should lead at small  $\lambda$  to folding of the meson modes:

$$E_n(P, h_1, h_2) \rightarrow E_n(P + l\pi/2, h_1, h_2), \quad \text{with } l = 0, 1, 2, 3. \quad (285)$$

It is reasonable to expect, that the small deformation (284) of the Hamiltonian (262) would give rise also to the weighted sum of four “copies” of the structure factors, which are shifted in  $\mathbf{k}$  with respect to one another by  $\pi/2$ :

$$\check{S}_{(2)}^{ab}(\mathbf{k}, \omega) \rightarrow \check{S}_{(2)}^{ab}(\mathbf{k}, \omega|\lambda) \simeq \sum_{l=0}^3 A_l(\lambda) \check{S}_{(2)}^{ab}(\mathbf{k} + \pi l/2, \omega). \quad (286)$$

where the weight coefficients  $A_l(\lambda)$  do not depend on  $\mathbf{h}_t, h_z$ , and  $A_l(0) = \delta_{l,0}$ . In the case of  $\mathbf{h}_t = 0$ , a similar

assumption was used by Bera *et al.*, see equation (7) in [7]. Accordingly, we will use the  $l = 1$  term in the right-hand side of (286) at  $\mathbf{k} = \pi/2$  in order to interpret the inelastic neutron scattering intensities shown in Figures 3a, and 3c of [10].

So, there are good reasons to expect, that in the region of weak transverse magnetic fields  $0 < H \lesssim 3T$ , the experimental inelastic neutron scattering patterns shown in Figures 3 a,b,c of [10], can be, at least, qualitatively described by our perturbative results (274), (256) for the DSF at  $\mathbf{k} = \pi$ , which are illustrated in Figure 14. We will show below, that this is really the case.

1. The lowest mode in Figures 3, which is called the *spin-flip* (SF) mode in [10], exhibits a strong non-linear monotonic downward variation upon increase of the transverse field in the interval  $0 < H < 10T$ . The inelastic neutron scattering measurements using polarized neutrons allow authors of [10] to conclude, that this SF mode remains polarized in the  $xz$ -plane in the whole range of variation of the transverse field  $H$ . At  $H = 0$ , this mode is polarized purely in the  $x$ -direction. Upon increase of the magnetic field  $H$ , the transverse polarization in the  $x$ -direction decreases, while longitudinal polarization along the  $z$ -axis increases. All listed above qualitative features of the evolution of the lowest mode upon increase of the transverse field  $H$  are in agreement with our theoretical predictions (274a), (274c) on the contribution of the meson mode with  $n = 1$  and  $P = 0$  into the diagonal DSF components  $\check{S}_{(2)}^{xx}(\pi, \omega)$ ,  $\check{S}_{(2)}^{zz}(\pi, \omega)$ , which are illustrated in Figures 14a,b.
2. The second in energy mode in Figures 3 in [10] is called there the *non-spin-flip* (NSF) mode. At  $H = 0$ , the energies of the NSF and SF modes are the same. The NSF mode exhibits a small upward variation upon increase of the magnetic field in the interval  $0 < H \lesssim 3T$ . The NSF is polarized along the  $y$ -direction at the magnetic fields  $H$  inside this interval. The NSF mode observed in the neutron scattering experiments should be identified with the meson mode with  $n = 1$  and  $P = \pi$ , which contributes to the DSF  $\check{S}_{(2)}^{yy}(\pi, \omega)$ , according to (274b). In the adopted approximation, the energy and polarization of this mode do not depend on the transverse magnetic field.
3. The third and the fourth modes in Figures 3 of [10] are polarized at  $H = 0$  along the  $z$ - and  $x$ -axes, respectively. Their energies approach one another upon increase of  $H$  up to about  $3T$ , where the avoided crossing of two modes occurs. These two modes can be identified with the meson modes  $n = 2$  and  $n = 3$  at  $P = 0$  in our classification. Evolution of energies and polarizations of these two meson modes with increasing magnetic field  $h_1 \sim H$ ,



which is illustrated in Figures 14, is similar to those of the third and fourth modes in Figures 3 of [10].

4. Contributions of two subsequent  $n = 3$ ,  $P = \pi$ , and  $n = 4$ ,  $P = 0$  meson modes into the DSF, which are shown in Figures 14, are also clearly seen in Figures 3 a,b,c of [10].

To summarise, the observed in the inelastic neutron scattering experiments [10] evolution of the meson energies and spin polarizations in  $\text{BaCo}_2\text{V}_2\text{O}_8$  with the increase of the transverse magnetic field are in a good qualitative agreement in the small-field region with our theoretical predictions obtained by the perturbative analysis of the XXZ spin-chain model (16). Furthermore, using equations (281) one can see, that the evolution of the DSF with the transverse magnetic field  $h_1$  displayed in Figure 14 is also in a reasonable quantitative agreement with the experimental data shown in Figure 3 of [10].

Recently, the evolution of the energies of magnetic excitations upon increase of the transverse magnetic field was experimentally studied by Amelin *et al.* [27] in the quasi-one-dimensional Ising-like ferromagnet  $\text{CoNb}_2\text{O}_6$  and antiferromagnet  $\text{BaCo}_2\text{V}_2\text{O}_8$  by means of the high-resolution terahertz spectroscopy. The presented in Figure 2 in [27] the magnetic-field dependence of the THz absorption spectrum of  $\text{BaCo}_2\text{V}_2\text{O}_8$  has a lot of similarities with the inelastic neutron scattering patterns for the same compound displayed in Figure 3 of [10] by Faure *et al.* However, for the reliable identification of different meson modes contributing into the THz absorption spectrum shown in Figure 2 in [27], the detailed information on the polarizations of the corresponding spin fluctuations is still required.

## XII. CONCLUSIONS

In this paper we present a perturbative analysis of the effect of mutually orthogonal uniform and staggered transverse magnetic fields  $h_1, h_2$  on the confinement of spinons in the Heisenberg XXZ spin-1/2 chain (16), (4). The spinon confinement in this model in the massive antiferromagnetic regime is induced by the staggered longitudinal magnetic field  $h_z$ . The energy spectra of the two-kink bound states in model (16), (4) are calculated perturbatively in two asymptotic regimes: (i) in the extreme anisotropic limit  $-\Delta \rightarrow \infty$ , and (ii) for generic  $\Delta < -1$  at weak transverse  $h_1, h_2$ , and staggered longitudinal  $h_z$  magnetic fields. In the second regime, the perturbative calculations have been performed in two steps. First, in the de-confinement regime at  $h_z = 0$ , the effect of the weak transverse uniform and staggered magnetic fields on the ground states and kink excitations of the XXZ spin chain are calculated by means the Rayleigh-Schrödinger perturbation expansion in small  $h_1, h_2$ . Then on top of that, the weak staggered longitudinal magnetic field  $h_z > 0$  is switched on. It induces confinement of kinks

into the “mesons” - the two-kink bound states. Their energy spectra and the dynamical structure factors of local spin operators for the momenta close to the points 0 and  $\pi$  are calculated in the second regime by means of the properly modified semiclassical perturbative technique, which was developed previously in [11, 12].

It is shown, that the superposition of the semiclassical wave-functions corresponding to different classical trajectories of two kinks forming a meson can be very sensitive to the strength of the transverse magnetic fields  $h_1, h_2$ . This leads to the oscillatory interference patterns in the transverse magnetic field dependencies of the energies of mesons, and of the DSF of local spin operators. Our theoretical predictions on the evolution of these quantities with increasing transverse magnetic field are in good qualitative and reasonable quantitative agreement with the results reported by Faure *et al.* [10] on the inelastic neutron scattering experiments in the quasi-1D antiferromagnetic compound  $\text{BaCo}_2\text{V}_2\text{O}_8$ . For a detailed quantitative comparison of the obtained theoretical results with experiment, the values of the parameters in the effective Hamiltonian (277) should be reliably refined, preferable not from fitting the experimentally observed meson energy spectra, but from some independent measurements.

There are several directions for further study. Our analysis in this paper was based on the XXZ spin-chain Hamiltonian (16), which is equivalent to (262). The obtained by Kimura *et al.* effective Hamiltonian (277) differs from (262) by an extra term  $\cos[(2j+1)\pi/4]g_{yz}H$ . We expect, that this term is responsible, at least partly, for the folding of the meson modes and DSF according to equations (285), and (286), respectively. It would be interesting to account for this term perturbatively in small  $g_{yz}$ , and to explicitly determine the coefficients  $A_l$  in equation (286). On the other hand, it would be also interesting to perform direct numerical calculations of the DSF of local spin operators for the model (262), and to compare the results with our analytical perturbative formulas (274), (256) for these DSF. On the experimental side, further detailed measurements of the meson energy spectra in the quasi-1D antiferromagnets  $\text{BaCo}_2\text{V}_2\text{O}_8$  and  $\text{SrCo}_2\text{V}_2\text{O}_8$  in different regimes are desirable.

## ACKNOWLEDGMENTS

I am thankful to Frank Göhmann for many fruitful discussions. This work was supported by Deutsche Forschungsgemeinschaft (DFG) via Grant BO 3401/7-1.

### Appendix A: Two-kink scattering and form factors for the XXZ spin chain (4)

In this Appendix we collect some well-known results about the two-kink scattering phases and form factors of spin operators for the antiferromagnetic XXZ spin chain

at zero magnetic field, which Hamiltonian is given by (4). More details can be found in [11].

The two-kink Bloch states  $|K_{\mu\nu}(p_1)K_{\nu\mu}(p_2)\rangle_{s_1s_2}$  at zero magnetic field are characterized by the quasimomenta  $p_1, p_2$ , and  $z$ -projections  $s_1, s_2$  of the spins of particular kinks. The defining equations for these states read:

$$\tilde{T}_1|K_{\mu\nu}(p_1)K_{\nu\mu}(p_2)\rangle_{s_1s_2} = e^{i(p_1+p_2)} \quad (\text{A1a})$$

$$\times |K_{\mu\nu}(p_1)K_{\nu\mu}(p_2)\rangle_{-s_1, -s_2},$$

$$S^z|K_{\mu\nu}(p_1)K_{\nu\mu}(p_2)\rangle_{s_1s_2} = (s_1 + s_2) \quad (\text{A1b})$$

$$\times |K_{\mu\nu}(p_1)K_{\nu\mu}(p_2)\rangle_{s_1s_2},$$

$$(\mathcal{H}_0 - E_{vac}^{(0)})|K_{\mu\nu}(p_1)K_{\nu\mu}(p_2)\rangle_{s_1s_2} \quad (\text{A1c})$$

$$= [\omega(p_1) + \omega(p_2)]|K_{\mu\nu}(p_1)K_{\nu\mu}(p_2)\rangle_{s_1s_2},$$

where  $\mathcal{H}_0$  is the Hamiltonian (4),  $E_{vac}^{(0)}$  is its ground-state energy, and  $\omega(p)$  is the kink dispersion law (77). The Bloch states  $|K_{\mu\nu}(p_1)K_{\nu\mu}(p_2)\rangle_{s_1s_2}$  with  $0 < p_2 < p_1 < \pi$  and  $s_{1,2} = \pm 1/2$  form the basis in the two-kink subspace  $\mathcal{L}^{(2)}$ . They are normalized by the condition:

$${}_{s_2s_1}\langle K_{\mu\nu}(p_2)K_{\nu\mu}(p_1) | K_{\mu'\nu'}(p'_1)K_{\nu\mu}(p'_2) \rangle_{s'_1s'_2} \quad (\text{A2})$$

$$= \pi^2 \delta_{\mu\mu'} \delta_{\nu\nu'} \delta_{s_1s'_1} \delta_{s_2s'_2} \delta(p_1 - p'_1) \delta(p_2 - p'_2),$$

where  $0 < p_2 < p_1 < \pi$ ,  $0 < p'_2 < p'_1 < \pi$ , and  $\mu \neq \nu$ .

The following equalities hold [11]:

$$|K_{\mu\nu}(p_1)K_{\nu\mu}(p_2)\rangle_{s_1s_2} = \quad (\text{A3})$$

$$\varkappa(\mu, s_1)|K_{\mu\nu}(p_1 + \pi)K_{\nu\mu}(p_2)\rangle_{s_1s_2}$$

$$= \varkappa(\nu, s_2)|K_{\mu\nu}(p_1)K_{\nu\mu}(p_2 + \pi)\rangle_{s_1s_2},$$

where  $\varkappa(\nu, s)$  is defined in the in-line formulas below equation (92).

It is useful to define an alternative basis in the subspace of two-kink states with zero total spin  $S^z = 0$ :

$$|K_{\mu\nu}(p_1)K_{\nu\mu}(p_2)\rangle_{\pm} \equiv \frac{1}{\sqrt{2}} \left( |K_{\mu\nu}(p_1)K_{\nu\mu}(p_2)\rangle_{1/2, -1/2} \right.$$

$$\left. \pm |K_{\mu\nu}(p_1)K_{\nu\mu}(p_2)\rangle_{-1/2, 1/2} \right). \quad (\text{A4})$$

The two-kink scattering can be described by the Faddeev-Zamolodchikov commutation relations:

$$|K_{\mu\nu}(p_1)K_{\nu\mu}(p_2)\rangle_{ss} = w_0(p_1, p_2)|K_{\mu\nu}(p_2)K_{\nu\mu}(p_1)\rangle_{ss}, \quad (\text{A5a})$$

$$|K_{\mu\nu}(p_1)K_{\nu\mu}(p_2)\rangle_{\pm} = w_{\pm}(p_1, p_2)|K_{\mu\nu}(p_2)K_{\nu\mu}(p_1)\rangle_{\pm}. \quad (\text{A5b})$$

The three scattering amplitudes  $w_{\iota}(p_1, p_2)$ , with  $\iota = 0, \pm$ ,

can be parametrized by the rapidity variable  $\alpha$ ,

$$w_{\iota}(p_1, p_2) = \exp[-i\pi + i\theta_{\iota}(p_1, p_2)], \quad (\text{A6a})$$

$$\theta_{\iota}(p_1, p_2) = \Theta_{\iota}(\alpha_1 - \alpha_2), \quad (\text{A6b})$$

$$\Theta_0(\alpha) = \alpha + \sum_{n=1}^{\infty} \frac{e^{-n\eta} \sin(2\alpha n)}{n \cosh(n\eta)}, \quad (\text{A6c})$$

$$\Theta_{\pm}(\alpha) = \Theta_0(\alpha) + \chi_{\pm}(\alpha), \quad (\text{A6d})$$

$$\chi_{+}(\alpha) = -i \ln \left( -\frac{\sin[(\alpha + i\eta)/2]}{\sin[(\alpha - i\eta)/2]} \right), \quad (\text{A6e})$$

$$\chi_{-}(\alpha) = -i \ln \left( \frac{\cos[(\alpha + i\eta)/2]}{\cos[(\alpha - i\eta)/2]} \right), \quad (\text{A6f})$$

where  $p_j = p(\alpha_j)$ ,  $j = 1, 2$ , and  $\Theta_{\iota}(\alpha)$  are the scattering phases. The scattering amplitude  $w_0(p_1, p_2)$  was found by Zabrodin [49], and the whole two-kink scattering matrix was determined by Davies *et al.* [50].

The two-kink states  $|\mathcal{K}_{\mu\nu}(\xi_1)\mathcal{K}_{\nu\mu}(\xi_2)\rangle_{s_1s_2}$  parametrized by the multiplicative spectral parameters  $\xi_{1,2} = -ie^{i\alpha_{1,2}}$  are simply related with  $|K_{\mu\nu}(p_1)K_{\nu\mu}(p_2)\rangle_{s_1s_2}$ :

$$|\mathcal{K}_{\mu\nu}(\xi_1)\mathcal{K}_{\nu\mu}(\xi_2)\rangle_{s_1s_2} = \quad (\text{A7})$$

$$\frac{\sqrt{\omega(p_1)\omega(p_2)}}{\sinh \eta} |K_{\mu\nu}(p_1)K_{\nu\mu}(p_2)\rangle_{s_1s_2}.$$

The states  $|\mathcal{K}_{\mu\nu}(\xi_1)\mathcal{K}_{\nu\mu}(\xi_2)\rangle_{\pm}$  are related in the same way with  $|K_{\mu\nu}(p_1)K_{\nu\mu}(p_2)\rangle_{\pm}$ :

$$|\mathcal{K}_{\mu\nu}(\xi_1)\mathcal{K}_{\nu\mu}(\xi_2)\rangle_{\pm} = \quad (\text{A8})$$

$$\frac{\sqrt{\omega(p_1)\omega(p_2)}}{\sinh \eta} |K_{\mu\nu}(p_1)K_{\nu\mu}(p_2)\rangle_{\pm}.$$

All non-vanishing two-particle form factors of the spin operators  $\sigma_0^{\pm}, \sigma_0^z$  can be expressed in terms of four functions  $X^1(\xi_1, \xi_2)$ ,  $X^0(\xi_1, \xi_2)$ , and  $X_{\pm}^z(\xi_1, \xi_2)$ :

$$X^1(\xi_1, \xi_2) = {}^{(1)}\langle vac | \sigma_0^+ | \mathcal{K}_{10}(\xi_1)\mathcal{K}_{01}(\xi_2) \rangle_{-1/2, -1/2} =$$

$${}^{(0)}\langle vac | \sigma_0^- | \mathcal{K}_{01}(\xi_1)\mathcal{K}_{10}(\xi_2) \rangle_{1/2, 1/2}, \quad (\text{A9a})$$

$$X^0(\xi_1, \xi_2) = {}^{(1)}\langle vac | \sigma_0^- | \mathcal{K}_{10}(\xi_1)\mathcal{K}_{01}(\xi_2) \rangle_{1/2, 1/2} =$$

$${}^{(0)}\langle vac | \sigma_0^+ | \mathcal{K}_{01}(\xi_1)\mathcal{K}_{10}(\xi_2) \rangle_{-1/2, -1/2}, \quad (\text{A9b})$$

$$X_+^z(\xi_1, \xi_2) = {}^{(1)}\langle vac | \sigma_0^z | \mathcal{K}_{10}(\xi_1)\mathcal{K}_{01}(\xi_2) \rangle_+ =$$

$$- {}^{(0)}\langle vac | \sigma_0^z | \mathcal{K}_{01}(\xi_1)\mathcal{K}_{10}(\xi_2) \rangle_+, \quad (\text{A9c})$$

$$X_-^z(\xi_1, \xi_2) = {}^{(1)}\langle vac | \sigma_0^z | \mathcal{K}_{10}(\xi_1)\mathcal{K}_{01}(\xi_2) \rangle_- =$$

$${}^{(0)}\langle vac | \sigma_0^z | \mathcal{K}_{01}(\xi_1)\mathcal{K}_{10}(\xi_2) \rangle_-. \quad (\text{A9d})$$

The functions  $X^j(\xi_1, \xi_2)$  and  $X_{\pm}^z(\xi_1, \xi_2)$  admit the fol-

lowing explicit representations:

$$X^j(\xi_1, \xi_2) = \rho^2 \frac{(q^4; q^4)^2}{(q^2; q^2)^3}. \quad (\text{A10a})$$

$$\frac{(-q\xi_1\xi_2)^{1-j}\xi_2 \gamma(\xi_2^2/\xi_1^2) \theta_{q^8}(-\xi_1^{-2}\xi_2^{-2}q^{4j})}{\theta_{q^4}(\xi_1^{-2}q^3) \theta_{q^4}(\xi_2^{-2}q^3)},$$

$$X_+^z(\xi_1, \xi_2) = \frac{\sqrt{2} e^{-\eta/4} g(\alpha_1 + \alpha_2, \eta)}{\sin[(\alpha_1 - \alpha_2 - i\eta)/2]} X^0(\xi_1, \xi_2), \quad (\text{A10b})$$

$$X_-^z(\xi_1, \xi_2) = -X_+^z(-\xi_1, \xi_2), \quad (\text{A10c})$$

where

$$\gamma(\xi) \equiv \frac{(q^4\xi; q^4; q^4)(\xi^{-1}; q^4; q^4)}{(q^6\xi; q^4; q^4)(q^2\xi^{-1}; q^4; q^4)}, \quad (\text{A11})$$

$$\rho \equiv (q^2; q^2)^2 \frac{(q^4; q^4; q^4)}{(q^6; q^4; q^4)}, \quad (\text{A12})$$

$$(x; y) \equiv \prod_{n=0}^{\infty} (1 - xy^n), \quad (\text{A13})$$

$$(x; y; z) \equiv \prod_{m,n=0}^{\infty} (1 - x y^n z^m), \quad (\text{A14})$$

$$\theta_x(y) = (x; x)(y; x)(xy^{-1}; x), \quad (\text{A15})$$

$$g(\alpha, \eta) = \frac{\vartheta_1\left(\frac{\alpha}{2i\eta} | e^{-\pi^2/\eta}\right)}{\vartheta_4\left(\frac{\alpha}{4i\eta} | e^{-\pi^2/(4\eta)}\right)}. \quad (\text{A16})$$

Here  $\vartheta_i(u|p)$  denote the elliptic theta-functions:

$$\vartheta_1(u|p) = 2p^{1/4} \sin(\pi u). \quad (\text{A17})$$

$$\prod_{n=1}^{\infty} (1 - p^{2n}) (1 - 2p^{2n} \cos(2\pi u) + p^{4n}),$$

$$\vartheta_4(u|p) = \prod_{n=1}^{\infty} (1 - p^{2n}) (1 - 2p^{2n-1} \cos(2\pi u) + p^{2(2n-1)}),$$

$$\vartheta_2(u|p) = \vartheta_1(u + 1/2|p), \quad \vartheta_3(u|p) = \vartheta_4(u + 1/2|p).$$

The two-kink form factors of the  $\sigma_0^\pm$  operators were determined by means of the vertex-operator formalism by Jimbo and Miwa [33]. The explicit formulas for the form factors of the  $\sigma_0^\pm$  operator in the XYZ spin-1/2 chain were obtained by Lashkevich [51]. The XXZ limit of these formulas used in (A10b) and (A10c) can be found in [52].

## Appendix B: Derivation of equation (222)

In this Appendix we describe calculation of the absolute value of the normalization constant  $B_{in,1}$ , which was introduced in equation (204).

Let us start from the normalization condition (147) for the reduced wave functions  $\phi_n(p|P, \mathbf{h}_t, h_z)$  describing the relative motion of two kinks forming a meson. For  $n = n'$ , this normalization condition takes the form

$$\int_{-\pi}^{\pi} \frac{dp}{2\pi} |\phi_n(p|P)|^2 = 2. \quad (\text{B1})$$

Here we have skipped parameters  $\mathbf{h}_t, h_z$  in the wave function  $\phi_n(p|P, \mathbf{h}_t, h_z)$ . The normalization condition (B1) can be rewritten in terms of the Fourier coefficients (192) of the reduced wave function:

$$\sum_{j=-\infty}^{\infty} |\psi_n(j|P)|^2 = 2. \quad (\text{B2})$$

One can easily show using (192), (160), that the following equality holds at  $\mathbf{h}_t = 0$ :

$$\sum_{j=0}^{-\infty} |\psi_n(j|P)|^2 = \sum_{j=0}^{\infty} |\psi_n(j|P)|^2.$$

Accordingly, the normalization condition (B2) reduces in this case to the form:

$$-\frac{1}{2} |\psi_0(j|P)|^2 + \sum_{j=0}^{-\infty} |\psi_n(j|P)|^2 = 1. \quad (\text{B3})$$

At a small string tension  $f \sim h_z$ , the main contribution into the sum in the left-hand side comes from the terms with large enough negative  $j$ , such that  $|j| \gg 2\xi_c(\eta)$ , where  $\xi_c(\eta)$  is the correlation length (193). By this reason, to the leading order in  $f$ , we can neglect the first term in the left-hand side of (B3) and replace the functions  $\psi_n(j|P)$  in the sum by their semiclassical asymptotics (201). This yields:

$$\sum_{j=0}^{-\infty} \left\{ |C_1|^2 |\psi_n^{(1)}(j|P)|^2 + |C_2|^2 |\psi_n^{(2)}(j|P)|^2 + 2 \operatorname{Re}[C_1 C_2^* \psi_n^{(1)}(j|P) \psi_n^{(2)}(j|P)^*] \right\} = 1. \quad (\text{B4})$$

For the coefficients  $\psi_n^{(1,2)}(j|P)$  in the left-hand side, we obtained in Section IX the asymptotical formulas (202), that hold at small  $f > 0$ . To the leading order in  $f$ , these formulas reduce to the form:

$$\psi^{(1)}(j|P) = \int_{-\pi/2}^{\pi/2} \frac{dp}{2\pi} e^{ipj - iF_1(p, E|0)/f} [1 + O(f)], \quad (\text{B5a})$$

$$\psi^{(2)}(j|P) = (-1)^j \psi^{(1)}(j|P) [1 + O(f)]. \quad (\text{B5b})$$

The integral in the right-hand side of (B5a) is mainly determined at small  $f > 0$  by the contributions of the vicinity of the saddle points  $\pm p(j)$ , where  $p(j)$  is the solution of the equation:

$$E + fj = \epsilon(p(j)|P). \quad (\text{B6})$$

For  $j \in (j_{min}, 0)$ , with  $j_{min} = [\epsilon(0|P) - E]/f < 0$ , the solution of saddle-point equation (B6) is real and lies in the interval  $p(j) \in (0, p_a)$  in the left kinematically allowed region shown in Figure 9a. In this case, the saddle

point asymptotics of the integral (B5a) reads:

$$\psi^{(i)}(j|P) = 2i \sqrt{\frac{f}{2\pi\epsilon'(p|P)}} \Big|_{p=p(j)} \quad (\text{B7})$$

$$\times \sin \left[ p(j) - \frac{F_1(p(j), E|0)}{f} - \frac{\pi}{4} \right] [1 + O(f)].$$

After substitution of (B7), (B5b) into the left-hand side of equation (B4), one can see, that the highly oscillating third term in the curly brackets under the sum sign can be dropped. As the result, the normalization condition

(B4) reduces to the form:

$$1 = \frac{|C_1|^2 + |C_2|^2}{\pi} \quad (\text{B8})$$

$$\times \sum_{j=j_{min}}^0 \Delta p(j) \{1 - \sin [2p - 2F_1(p(j), E|0)/f]\},$$

where  $\Delta p(j) = f/\epsilon'(p|P)|_{p=p(j)}$ .

After dropping the oscillation sin-term in the curly brackets in the second line of (B8) and replacement the summation in  $j$  by the integration in  $p$

$$\sum_{j=j_{min}}^0 \Delta p(j) \dots \rightarrow \int_0^{p_a} dp \dots,$$

we find from (B8):

$$|C_1|^2 + |C_2|^2 = \pi/p_a.$$

Combining this result with (205), (213), and (221), we arrive to the final expression (222) for the absolute value of the normalization constant  $B_{in,1}$ .

- 
- [1] S. Narison, *QCD as a Theory of Hadrons* (Cambridge University Press, Cambridge, 2004).
- [2] K. G. Wilson, Confinement of quarks, *Phys. Rev. D* **10**, 2445 (1974).
- [3] G. 't Hooft, A two-dimensional model for mesons, *Nucl. Phys. B* **75**, 461 (1974).
- [4] B. M. McCoy and T. T. Wu, Two dimensional Ising field theory in a magnetic field: Breakup of the cut in the two-point function, *Phys. Rev. D* **18**, 1259 (1978).
- [5] H. Shiba, Quantization of magnetic excitation continuum due to interchain coupling in nearly one-dimensional Ising-like antiferromagnets, *Progress of Theoretical Physics* **64**, 466 (1980).
- [6] B. Grenier, S. Petit, V. Simonet, E. Canévet, L.-P. Regnault, S. Raymond, B. Canals, C. Berthier, and P. Lejay, Longitudinal and transverse Zeeman ladders in the Ising-like chain antiferromagnet BaCo<sub>2</sub>V<sub>2</sub>O<sub>8</sub>, *Phys. Rev. Lett.* **114**, 017201 (2015).
- [7] A. K. Bera, B. Lake, F. H. L. Essler, L. Vanderstraeten, C. Hubig, U. Schollwöck, A. T. M. N. Islam, A. Schneidewind, and D. L. Quintero-Castro, Spinon confinement in a quasi-one-dimensional anisotropic Heisenberg magnet, *Phys. Rev. B* **96**, 054423 (2017).
- [8] Z. Wang, M. Schmidt, A. K. Bera, A. T. M. N. Islam, B. Lake, A. Loidl, and J. Deisenhofer, Spinon confinement in the one-dimensional Ising-like antiferromagnet SrCo<sub>2</sub>V<sub>2</sub>O<sub>8</sub>, *Phys. Rev. B* **91**, 140404 (2015).
- [9] Z. Wang, M. Schmidt, A. Loidl, J. Wu, H. Zou, W. Yang, C. Dong, Y. Kohama, K. Kindo, D. I. Gorbunov, S. Niesen, O. Breunig, J. Engelmayr, and T. Lorenz, Quantum critical dynamics of a Heisenberg-Ising chain in a longitudinal field: Many-body strings versus fractional excitations, *Phys. Rev. Lett.* **123**, 067202 (2019).
- [10] Q. Faure, S. Takayoshi, S. Petit, V. Simonet, S. Raymond, L.-P. Regnault, M. Boehm, J. S. White, M. Månsson, C. Rüegg, P. Lejay, B. Canals, T. Lorenz, S. C. Furuya, T. Giamarchi, and B. Grenier, Topological quantum phase transition in the Ising-like antiferromagnetic spin chain BaCo<sub>2</sub>V<sub>2</sub>O<sub>8</sub>, *Nature Physics* **14**, 716 (2018).
- [11] S. B. Rutkevich, Spinon confinement in the gapped antiferromagnetic XXZ spin- $\frac{1}{2}$  chain, *Phys. Rev. B* **106**, 134405 (2022).
- [12] S. B. Rutkevich, Kink confinement in the antiferromagnetic XXZ spin-(1/2) chain in a weak staggered magnetic field, *EPL (Europhysics Letters)* **121**, 37001 (2018).
- [13] P. Fonseca and A. B. Zamolodchikov, Ising field theory in a magnetic field: Analytic properties of the free energy, *J. Stat. Phys.* **110**, 527 (2003).
- [14] P. Fonseca and A. B. Zamolodchikov, Ising spectroscopy I: Mesons at  $T < T_c$  (2006), arXiv:0612304 [hep-th].
- [15] S. B. Rutkevich, Large- $n$  excitations in the ferromagnetic Ising field theory in a weak magnetic field: Mass spectrum and decay widths, *Phys. Rev. Lett.* **95**, 250601 (2005).
- [16] S. B. Rutkevich, Two-kink bound states in the magnetically perturbed Potts field theory at  $T < T_c$ , *J. Phys. A* **43**, 235004 (2010).
- [17] M. Lencsés, G. Mussardo, and G. Takács, Confinement in the tricritical Ising model, *Physics Letters B* **828**, 137008 (2022).
- [18] S. B. Rutkevich, Energy spectrum of bound-spinons in the quantum Ising spin-chain ferromagnet, *J. Stat. Phys.* **131**, 917 (2008).
- [19] G. Lagnese, F. M. Surace, M. Kormos, and P. Calabrese, Quenches and confinement in a Heisenberg-Ising spin ladder, *Journal of Physics A: Mathematical and Theoretical* **55**, 124003 (2022).

- [20] F. B. Ramos, M. Lencsés, J. C. Xavier, and R. G. Pereira, Confinement and bound states of bound states in a transverse-field two-leg Ising ladder, *Phys. Rev. B* **102**, 014426 (2020).
- [21] S. B. Rutkevich, Soliton confinement in the double sine-Gordon model (2023), arXiv:2311.07303 [hep-th].
- [22] S. Kimura, K. Okunishi, M. Hagiwara, K. Kindo, Z. He, T. Taniyama, M. Itoh, K. Koyama, and K. Watanabe, Collapse of magnetic order of the quasi one-dimensional Ising-like antiferromagnet  $\text{BaCo}_2\text{V}_2\text{O}_8$  in transverse fields, *Journal of the Physical Society of Japan* **82**, 033706 (2013).
- [23] S. Kimura, T. Takeuchi, K. Okunishi, M. Hagiwara, Z. He, K. Kindo, T. Taniyama, and M. Itoh, Novel ordering of an  $s = 1/2$  quasi-1d Ising-like antiferromagnet in magnetic field, *Phys. Rev. Lett.* **100**, 057202 (2008).
- [24] Q. Faure, S. Takayoshi, B. Grenier, S. Petit, S. Raymond, M. Boehm, P. Lejay, T. Giamarchi, and V. Simonet, Solitonic excitations in the Ising anisotropic chain  $\text{BaCo}_2\text{V}_2\text{O}_8$  under large transverse magnetic field, *Phys. Rev. Research* **3**, 043227 (2021).
- [25] Z. Wang, J. Wu, S. Xu, W. Yang, C. Wu, A. K. Bera, A. T. M. N. Islam, B. Lake, D. Kamenskyi, P. Gogoi, H. Engelkamp, N. Wang, J. Deisenhofer, and A. Loidl, From confined spinons to emergent fermions: Observation of elementary magnetic excitations in a transverse-field Ising chain, *Phys. Rev. B* **94**, 125130 (2016).
- [26] H. Zou, Y. Cui, X. Wang, Z. Zhang, J. Yang, G. Xu, A. Okutani, M. Hagiwara, M. Matsuda, G. Wang, G. Mussardo, K. Hódsági, M. Kormos, Z. He, S. Kimura, R. Yu, W. Yu, J. Ma, and J. Wu,  $E_8$  spectra of quasi-one-dimensional antiferromagnet  $\text{BaCo}_2\text{V}_2\text{O}_8$  under transverse field, *Phys. Rev. Lett.* **127**, 077201 (2021).
- [27] K. Amelin, J. Viirik, U. Nagel, T. Rööm, J. Engelmayer, T. Dey, A. A. Nugroho, T. Lorenz, and Z. Wang, Quantum spin dynamics of quasi-one-dimensional Heisenberg-Ising magnets in a transverse field: confined spinons,  $E_8$  spectrum, and quantum phase transitions, *Journal of Physics A: Mathematical and Theoretical* **55**, 484005 (2022).
- [28] S. Takayoshi, Q. Faure, V. Simonet, B. Grenier, S. Petit, J. Ollivier, P. Lejay, and T. Giamarchi, Phase transitions and spin dynamics of the quasi-one dimensional Ising-like antiferromagnet  $\text{BaCo}_2\text{V}_2\text{O}_8$  in a longitudinal magnetic field, *Phys. Rev. Res.* **5**, 023205 (2023).
- [29] D. V. Dmitriev, V. Y. Krivnov, A. A. Ovchinnikov, and A. Langari, One-dimensional anisotropic Heisenberg model in the transverse magnetic field, *JETP* **95**, 538 (2002).
- [30] S. Takayoshi, S. C. Furuya, and T. Giamarchi, Topological transition between competing orders in quantum spin chains, *Phys. Rev. B* **98**, 184429 (2018).
- [31] A. Okutani, H. Onishi, S. Kimura, T. Takeuchi, T. Kida, M. Mori, A. Miyake, M. Tokunaga, K. Kindo, and M. Hagiwara, Spin excitations of the  $s = 1/2$  one-dimensional Ising-like antiferromagnet  $\text{BaCo}_2\text{V}_2\text{O}_8$  in transverse magnetic fields, *Journal of the Physical Society of Japan* **90**, 044704 (2021).
- [32] C.-M. Halati, Z. Wang, T. Lorenz, C. Kollath, and J.-S. Bernier, Repulsively bound magnon excitations of a spin- $\frac{1}{2}$  xxz chain in a staggered transverse field, *Phys. Rev. B* **108**, 224429 (2023).
- [33] M. Jimbo and T. Miwa, *Algebraic Analysis of Solvable Lattice Models*, Conference Board of the Mathematical Sciences No. 85 (American Mathematical Soc., 1995).
- [34] S. Lukyanov and V. Terras, Long-distance asymptotics of spin-spin correlation functions for the XXZ spin chain, *Nuclear Physics B* **654**, 323 (2003).
- [35] R. J. Baxter, Spontaneous staggered polarization of the F-model, *Journal of Statistical Physics* **9**, 145 (1973).
- [36] R. J. Baxter, Corner transfer matrices of the eight-vertex model. I. Low-temperature expansions and conjectured properties, *Journal of Statistical Physics* **15**, 485 (1976).
- [37] A. G. Izergin, N. Kitanine, J. M. Maillet, and V. Terras, Spontaneous magnetization of the XXZ Heisenberg spin- $1/2$  chain, *Nuclear Physics B* **554**, 679 (1999).
- [38] N. Ishimura and H. Shiba, Dynamical correlation functions of one-dimensional anisotropic Heisenberg model with spin  $1/2$ . I: Ising-like antiferromagnets, *Progress of Theoretical Physics* **63**, 743 (1980).
- [39] G. Teschl, *Jacobi Operators and Completely Integrable Nonlinear Lattices*, Mathematical surveys and monographs (American Mathematical Society, 2000).
- [40] L. D. Landau and E. M. Lifshitz, *Quantum Mechanics: Non-Relativistic Theory*, Course of Theoretical Physics (Elsevier Science, 1981).
- [41] J. D. Johnson, S. Krinsky, and B. M. McCoy, Vertical-arrow correlation length in the eight-vertex model and the low-lying excitations of the  $X-Y-Z$  Hamiltonian, *Phys. Rev. A* **8**, 2526 (1973).
- [42] M. Lencsés and G. Takács, Excited state TBA and renormalized TCSA in the scaling Potts model, *Journal of High Energy Physics* **2014**, 52 (2014).
- [43] M. Kormos, M. Collura, G. Takács, and P. Calabrese, Real-time confinement following a quantum quench to a non-integrable model, *Nat. Phys.* **13**, 246 (2017).
- [44] G. Lagnese, F. M. Surace, M. Kormos, and P. Calabrese, Confinement in the spectrum of a Heisenberg-Ising spin ladder, *Journal of Statistical Mechanics: Theory and Experiment* **2020**, 093106 (2020).
- [45] A. M. Kadigrobov and A. A. Slutskin, Influence of magnetic breakdown on low-frequency conductivity and weak damping electromagnetic waves in metals, *Journal of Low Temp. Phys.* **6**, 69 (1972).
- [46] A. A. Abrikosov, *Fundamentals of the Theory of Metals* (Dover Publications Inc., 2017).
- [47] B. Grenier, S. Petit, V. Simonet, E. Canévet, L.-P. Regnault, S. Raymond, B. Canals, C. Berthier, and P. Lejay, Erratum: Longitudinal and transverse Zeeman ladders in the Ising-like chain antiferromagnet  $\text{BaCo}_2\text{V}_2\text{O}_8$  [*Phys. Rev. Lett.* **114**, 017201 (2015)], *Phys. Rev. Lett.* **115**, 119902 (2015).
- [48] S. Kimura, H. Onishi, A. Okutani, M. Akaki, Y. Narumi, M. Hagiwara, K. Okunishi, K. Kindo, Z. He, T. Taniyama, and M. Itoh, Optical selection rules of the magnetic excitation in the  $S = \frac{1}{2}$  one-dimensional Ising-like antiferromagnet  $\text{BaCo}_2\text{V}_2\text{O}_8$ , *Phys. Rev. B* **105**, 014417 (2022).
- [49] A. Zabrodin, Integrable models of field theory and scattering on quantum hyperboloids, *Modern Physics Letters A* **07**, 441 (1992).
- [50] B. Davies, O. Foda, M. Jimbo, T. Miwa, and A. Nakayashiki, Diagonalization of the  $XXZ$  Hamiltonian by vertex operators, *Commun. Math. Phys.* **151**, 89 (1993).
- [51] M. Lashkevich, Free field construction for the eight-vertex model: representation for form factors, *Nuclear Physics B* **621**, 587 (2002).

[52] M. Dugave, F. Göhmann, K. K. Kozłowski, and J. Suzuki, On form-factor expansions for the  $XXZ$  chain

in the massive regime, *Journal of Statistical Mechanics: Theory and Experiment* **2015**, P05037 (2015).